THE UNIVERSITY OF QUEENSLAND

AUSTRALIA

Fundamentals for the Fire Design of Cross Laminated Timber Buildings

Richard Lawrence Emberley

Bachelor of Science (Civil Engineering)

Master of Science (Civil Engineering)

Master of Science (Fire Protection Engineering)

A thesis submitted for the degree of Doctor of Philosophy at

The University of Queensland in 2017

School of Civil Engineering

Abstract

A timber renaissance has occurred in the built environment in an effort for architectural freedom and increased sustainable construction. Current building codes place limits on the extent to which timber can be exposed. Overall building heights and floor areas are capped due the perception that timber burns continuously. Original fire resistance requirements were derived on the concept of complete burnout of the fuel within a compartment. Whether non-combustible or combustible materials are used, materials must be capable of withstanding a certain fire load until burnout at which point flaming combustion of the material must cease. If not, then the fire resistance framework loses its meaning and the concepts used in the design process need to be re-evaluated. This study focuses on the underpinning behavior of timber exposed to a fire in an attempt to extract meaning processes that enable an adequate assessment of the structural performance of timber as a construction material. The focus is on cross laminated timber (CLT) as an example of relevant engineered wood products but the concepts presented in this work could be applied to any other timber product.

The first aspect researched in this study was the self-extinction characteristics of CLT. Self-extinction is an unavoidable starting point since it is the critical process that defines the relevance of fire resistance as an assessment methodology for structural performance. CLT samples were exposed to a range of heat fluxes (6-100 kW/m^2). Samples were heated by an external heat flux until either flaming or smoldering combustion occurred. Exposure continued throughout the transient stage of burning until steady-state was achieved. After a pre-established heating period the heat flux was completely removed. In every case tested, flaming combustion ceased. A series of tests were then conducted to determine the critical heat flux and mass loss rate for extinction. The tests were repeated except, instead of removing the heat flux completely, the heat flux was gradually decreased until flaming combustion ceased. The experiments showed that for all conditions studied an almost constant critical mass loss rate was measured at extinction. However, in some cases, flaming combustion continued due to debonding of the timber plies. Where cracks and gaps opened at the bond line, re-ignition of flaming combustion would occur. The test allowed the threshold for self-extinction to be quantified and showed that careful detailing in the design and construction process is likely to be necessary in order for self-extinction to be predictable.

Once self-extinction of flaming combustion of timber was confirmed, the relevant mechanics that influence debonding were studied. To quantify the effects of temperature between timber plies, series of tests were conducted to investigate thermal penetration and thermal profiles within the CLT. The samples were exposed to a range of heat fluxes (6-100kW/m^2) and the results showed that above

30kW/m^2 the thermal profiles were approximately the same. The only difference between the heat fluxes was the speed at which the pyrolysis front moves through the material.

Once the thermal profiles had been measured, a single-lap shear test was performed using a range of temperatures (20-150°C). The samples were heated to the target temperature and then a tensile force was applied to the joint until failure. Digital image correlation was used to capture the displacement and strains of the adhesive bond. The results showed that the strain experienced by the bond was greater as the sample increased in load and temperature. The interfacial stresses (normal and shear) were compared and the normal stresses in the bonded joint at areas of discontinuity were shown to be orders of magnitude greater than the shearing stresses. The study found that the mechanics of the debonding were primarily governed by the normal forces creating a separation at the local discontinuities and then unzipping the bond until failure.

Following the small scale tests, a larger scale testing program was executed to identify whether the behaviors observed in the single-lap shear test could be observed in industrial CLT. CLT beams both at ambient and elevated temperature were loaded in a three-point bend test until failure. Differences in the bond performance between the two tests were not observed as the primary failure mode was rolling shear. In each case, debonding occurred but was initiated at cracks formed by the rolling shear. Once the local discontinuities appeared on the bond line, the increased normal forces proceeded to unzip the bond until failure. Failure occurred due to insufficient effective bond length.

This work develops methodologies and provides quantification for many of the fundamental parameters required for analyzing the performance of CLT structures in fire. Designing timber structures for fire conditions was concluded to be possible but the need for further research is evident. Self-extinction of flaming combustion is required for any fire safety strategy to be valid but self-extinction is not only a combustion problem, but it is also a problem that is intimately related to the mechanical behavior of the bonds in engineered timber. Thus, a detailed understanding of the combined thermos-mechanical behavior is necessary before timber (and timber structural systems) can be engineered to deliver adequate fire performance.

Declaration by author

This thesis is composed of my original work, and contains no material previously published or written by another person except where due reference has been made in the text. I have clearly stated the contribution by others to jointly-authored works that I have included in my thesis.

I have clearly stated the contribution of others to my thesis as a whole, including statistical assistance, survey design, data analysis, significant technical procedures, professional editorial advice, and any other original research work used or reported in my thesis. The content of my thesis is the result of work I have carried out since the commencement of my research higher degree candidature and does not include a substantial part of work that has been submitted to qualify for the award of any other degree or diploma in any university or other tertiary institution. I have clearly stated which parts of my thesis, if any, have been submitted to qualify for another award.

I acknowledge that an electronic copy of my thesis must be lodged with the University Library and, subject to the policy and procedures of The University of Queensland, the thesis be made available for research and study in accordance with the Copyright Act 1968 unless a period of embargo has been approved by the Dean of the Graduate School.

I acknowledge that copyright of all material contained in my thesis resides with the copyright holder(s) of that material. Where appropriate I have obtained copyright permission from the copyright holder to reproduce material in this thesis.

Publications during candidature

Peer-review papers:

Shaw, T., Gibson, T., J. Karlovsek, R. Emberley, and J.L. Torero. Experimental evaluation of the heat flux induced by tunnel fires. Tunnelling and Underground Space Technology, 2016. 60: p. 49-55.

Emberley, R., A. Inghelbrecht, Z. Yu, J.L. Torero, *Self-Extinction of Timber*, Proceedings of the Combustion Institute, v. 36, 2016

Conference papers:

Emberley, R., A. Inghelbrecht, N. Doyle, J.L. Torero, *Components and Consequences of Cross-Laminated Timber Delamination*, in *The 10th Asia-Oceania Symposium on Fire Science and Technology*. 2015: Tsukuba, Japan.

Doyle, N., R. Emberley, and J.L. Torero, *Fire Behavior of Cross Laminated Timber (CLT) Slabs: Two-way Action*, in *The 10th Asia-Oceania Symposium on Fire Science and Technology*. 2015: Tsukuba, Japan.

Emberley, R., and J.L. Torero, *Cross-Laminated Timber Failure Modes for Fire Conditions*, in *Second International Conference on Performance-based and Life-cycle Structural Engineering*, 2015: Brisbane, Australia.

Gibson, T., T. Shaw, J. Karlovsek, R. Emberley, J.L. Torero, *Experimental Quantification of Tunnel Fire Heat Flux*, World Tunneling Congress. 2016: San Francisco, California, USA.

Emberley, R., A. Nicolaidis, D. Fernando, J.L. Torero, *Changing Failure Modes of Cross-Laminated Timber*, 9th International Conference on Structures in Fire. 2016: Princeton, New Jersey, USA.

Emberley, R., Z. Yu, D. Fernando, J.L. Torero, *Delamination Occurrence in Engineered Mass Timber Products at Elevated Temperatures*, World Conference on Timber Engineering. 2016: Vienna, Austria.

Nicolaidis, A., R. Emberley, D. Fernando, J.L. Torero, *Thermally Driven Failure Mode Changes in Bonded Timber Joints*, World Conference on Timber Engineering. 2016: Vienna, Austria.

Lawton, A., R. Emberley, J.L. Torero, *Heat Transfer through Mass Timber Connections,* World Conference on Timber Engineering. 2016: Vienna, Austria.

Publications included in this thesis

No publications included.

Contributions by others to the thesis

No contributions by others.

Statement of parts of the thesis submitted to qualify for the award of another degree

None.

Acknowledgements

Innumerable people have helped me physically, mentally, and spiritually along this journey. While I have named a few specific people, naming all is next to impossible. So, to everyone, no matter how small the role, thank you for all you have done for me.

To my primary advisor, Professor José L. Torero, thank you for taking me on and allowing me to be part of the start of fire safety engineering at The University of Queensland. I have thoroughly enjoyed every minute of conversation with you about fire, engineering, education, music, politics, etc. Thank you for it all. I still have much to learn.

To my secondary advisors, Dr. Angus Law and Dr. Dilum Fernando, thank you both for your advice and help over the past two years. Getting to know you as an advisor and colleague has been a true pleasure. Office banter will never be better.

To my longtime friend and mentor, Dr. Jonathan Barnett, thank you for starting me down this road and directing me along the way. I would never have made it this far without you. In our very first meeting, you said something that has stuck with me all these years. "It's not about brains; it's about working hard." Thank you for that piece of advice. It has kept me going through all the late nights and early mornings.

To those I had the pleasure of working with on the experiments for this project, Alex, Tam, Jess, Zeyu, Arne, Nick, and Andrea, thank you for the great and sometimes late times in the lab and for all the hard work. You set the bar very high. Thursdays will never be the same.

To the fire research group, thanks for the wonderful memories and I look forward to future interactions with you wherever they may be. You're always welcome at my place. One of these days I will learn Spanish.

To those who took me in as part of their family and gave me a permanent seat in their vehicles, Tim and Gail Zerk, I have so much for which to be thankful and so many stories I could tell, but all I will say is this: I will truly miss not being the third wheel. Thank you.

To my incredible sisters, Stephanie and Elizabeth, who went before me in their doctoral degrees, thank you for your love and support over these past three years knowing what I going through. Thank you too for sacrificing yourselves to come visit me.

And finally and most importantly to my parents, Richard and Sarah Emberley, thank you for everything. I am eternally grateful for the sacrifices you have made over my entire life to bring me to this point and to set me up for an incredible future. That is something I will truly never be able to repay or forget. I know I would not have made it over these past three years without you. Thank you from the bottom of my heart. And, yes, I promise to finally get some sleep now. I didn't even get out of bed this morning.

Keywords

self-extinction, fire, cross laminated timber, debonding, thermal penetration depth, interfacial stresses, external incident heat flux, adhesive, rolling shear, crack propagation

Australian and New Zealand Standard Research Classifications (ANZSRC)

ANZSRC code: 090506, Structural Engineering, 80%

ANZSRC code: 120202, Building Science and Techniques, 20%

Fields of Research (FoR) Classification

FoR code: 0905, Civil Engineering, 80%

FoR code: 1202, Building, 20%

Table of Contents

Table of Figures

Table of Tables

Chapter 1: Introduction

The use of engineered timber in the built environment has increased dramatically over the past decade. The main drivers behind this trend include a desire for increased sustainability in construction, architectural freedom, and economical building designs. Advances in structural engineering and innovations in timber products have made this trend a reality. Engineered timber such as cross laminated timber (CLT), glue laminated timber (Glulam), and laminated veneer lumber (LVL) have seen increased usage. These engineered timber products have allowed structural engineering companies and architectural firms to push the boundaries of what is possible in timber design. The heights of new timber buildings increase every year with companies producing taller and taller buildings that have a primary structural frame comprised of timber. The current tallest timber building is 13 stories tall but designs are being produced which project even taller (42 stories) with some much taller (in excess of 300 meters) [1-7].

One of the main design limitations of using timber in the built environment is the combustible nature of the material. In the event of a compartment fire in a room with exposed timber the structural members will char—reducing the cross-section and the strength of the member. However, unlike steel and concrete which can on cooling regain a least a portion of their original strength, the charring of timber is an irreversible process. The charring of timber can be accounted for in design with the resulting timber member capable of withstanding the design load during and after the event of a fire.

The current perception of timber buildings is that once flaming combustion is ignited the material will continue to burn until no fuel remains. In a structural context, continued flaming combustion and charring means inevitable structural failure. This perception of timber is driven by the fire resistance requirements in building codes and standards. Building requirements require structural members to have a certain number of hours of fire resistance depending on the type of building and the occupancy classification. Building codes classify structures based on building type and occupancy. These classifications are then used to specify a period of fire resistance in accordance with the standard furnace test [8, 9]. Buildings are frequently limited in height and area if a combustible structural material is used [10]. When subjected to a standard furnace test, combustible materials continue to burn for the entire duration of the test and generally fail early in the testing regime. This provides a distinct disadvantage for combustible materials; current solutions are to protect the members by covering them with non-combustible materials in a process called encapsulation.

A disconnect, however, exists between the performance of timber in a standard fire resistance test and its performance in reality. In a real compartment fire scenario, the actual length of fire exposure on a structural member depends on the geometry, the ventilation conditions of the room, and the

amount of fuel. However, in the standard fire resistance test, the fire resistance time is an arbitrary time based on equivalent areas under time-temperature curves [11]. A specific numerical value of time in a standard furnace test is not actual time in a real fire.

Just as in the case of the burning duration of a compartment fire, the heat fluxes generated on the structural members and walls vary with the conditions of the room. The actual heat flux also varies over time in the course of a fire. Heat fluxes are generally low between ignition and flashover as well as in the decay stage of the fire. The highest heat fluxes in a compartment fire are post-flashover when the room is fully involved in the fire. Typical heat fluxes post-flashover can range between 30 and 80 kW/m^2 [12, 13]. Heat fluxes in a standard furnace, however, are initially higher and only continue to increase in intensity for the entire duration of a test of non-combustible materials. The heat transfer and heat fluxes in a furnace become more complicated when a combustible materials is tested which contributes to the energy supplied to the furnace. At the same time, thermal loading conditions differ between furnaces depending on variables such as material lining and geometry. These differing thermal loads make comparisons between tests in separate furnaces impossible as the test conditions are not the same.

The thermal load on a structural member is the intensity of the heat flux for the duration of the compartment fire. The structural member is required to withstand the thermal loading and remain structurally sound. In the compartment fire design scenario, a limit exists for the duration and exposure a timber member is required to endure. While many considerations are introduced when defining the required fire resistance, the only physical consideration is the expected time to burn-out of the predicted fuel load. As has already been described, in order for the timber to be used as viable structural material, the timber member has to withstand the thermal load and continue to support the applied load. In order for the timber to support the applied load, the material has to cease charring when the fire is extinguished and the heat flux is reduced. If the timber does not cease flaming combustion then the material will continue to deteriorate structurally leading to collapse. Compartment penetration will follow, leading to potentially very large fires that can affect surrounding structures. Furthermore, the inability of a timber member to self-extinguish may lead to increases in the burning duration as well as multiple instances of flashover [14]. Consequently, self-extinction of flaming combustion in timber is therefore necessary [15, 16] and all conditions that prevents self-extinction from occurring should be eliminated.

The objectives of this study focus on understanding the characteristics of self-extinction of flaming combustion of timber and the aspects that either allow or prevent self-extinction from occurring. One of the main aspects of engineered timber that prevents self-extinction is debonding of timber plies.

Debonding is driven by the increase in temperature of the adhesive which results in a decrease in strength. This decrease in strength potentially leads to the timber plies and protective char layer to debond during combustion. Various aspects behind structural debonding of CLT are analysed in this study.

In order to assess self-extinction and debonding, a review of the current state-or-the-art design methods needed to be detailed which was accomplished in Chapter 2. In Chapter 2, both the structural and fire design methods for CLT and timber are reviewed. Chapter 3 outlines the methodology used to study the characteristics of self-extinction of flaming combustion of timber as well as the physics behind self-extinction. Chapter 4 describes the test used to measure the thermal penetration profile in the unburned portion of timber. The methodology for both the single-lap shear and large CLT beam tests was outlined. The results from each of the tests and observation take were shown. Finally, Chapter 5 lists the conclusion from the entire study as well as outlines future work. Major design implications from the results of the study conclude the Chapter 5 and the thesis.

Chapter 2: Current Design Methods

Structural design methods for CLT encompass two scenarios: ambient temperature and fire conditions. Design for ambient conditions deals solely with the mechanics of the material while design of CLT for fire also relies on an understanding of timber pyrolysis and char formation.

2.1 Timber Engineering

Structural design with timber has historically faced limitations in design due to the inherent properties of the material. Timber grows naturally and thus is inhomogeneous. The structural strength of timber is highest against forces loaded parallel to the grain structure; however, timber is approximately thirty times weaker against forces loaded perpendicular to the grain. Wood also has defects caused by knots, decay, and weaker portions of the tree. As such, design of timber structures attempts to limit loading conditions that are perpendicular to the grain; timber sections are also carefully manufactured with proper strength grading of the raw timber. Height and size limitations for natural timber are obvious as cross-sectional areas of timber are limited by the dimensions of the tree.

In recent years, engineered timber has grown more popular due to advances in the manufacturing and innovations in the types of timber products delivered by the industry. Several different products are available but three main products have come to dominate the market: cross laminated timber (CLT), laminated veneer lumber (LVL) and glue laminated beams (Glulam).

In LVL, thin veneers of timber are cut to a thickness of 2.5-4.4mm. These veneers are then glued together with the grain structure of each timber veneer oriented parallel to each other. Glulam is based on the same principle as LVL except that instead of veneers glulam uses plies approximately 30-40mm thick. The grain direction of each of the plies is parallel. The grain orientation of both glulam and LVL limit the structural capability to one-way spanning members.

To increase the range of design applications, CLT makes use of the grain orientation to provide two-way spanning capabilities for the engineered product. The grain direction of each adjacent ply is positioned orthogonally (Figure 1). The perpendicular orientation creates a quasi-isotropic member with a high stiffness and the ability to span in two directions [17, 18]. The thickness of each timber ply can range from 10 to 45 mm with the overall CLT panel having three or more plies [19].

Figure 1: Five-layer CLT

The design principles and reasoning behind utilizing products such as LVL, Glulam, and CLT is to mitigate any defects, such as knots in the timber. Adhering multiple plies together homogenizes the strength variability and allows for a stronger section that has more consistency and reliability in the overall properties of the section. Moisture migration and creep are eliminated due to the glue and the various forms of layering. This reduces the uncertainties in the design of differential expansion of members. Each engineering product relies on composite action between two adjacent timber plies and the glue layer adhering them together.

2.2 Ambient Design

Design methods for CLT under ambient conditions are based on three methods derived from analytical and experimental solutions. These three methods are the most popular and can be found in current standards and codes as well as design guides for CLT [19, 20].

2.2.1 Mechanically Jointed Beams Theory

The Mechanically Jointed Beams Theory (Gamma Method) was originally developed for beams mechanically fastened by connections with a fixed stiffness K spaced s distance apart. The plies of the beam were oriented parallel with adjacent layers. The resulting beam had an effective stiffness of EI_{eff} which was dependent on the efficiency of the connection, γ (Eq. 1 and 2). Completely glued connections received a γ of one and non-glued connections had a γ equal to zero. This allowed the stiffness of the member to be dependent on the amount of slip in the connection [19]. This methodology for glued beams can be found in Annex B of EN 1995-1-1:2004 [21].

$$EI_{eff} = \sum_{i=1}^{n} (E_i I_i + \gamma_i E_i A_i a_i^2) \quad (1)$$

$$\gamma_i = [1 + \frac{\pi^2 E_i A_i s_i}{K_i l^2}]^{-1} \quad (2)$$

where:

i = layer number

E_i = Modulus of Elasticity

I_i = Moment of Inertia

A_i = Area

a_i = distance from centroid of each layer to the neutral axis of the cross section

l = span length

$0 \leq \gamma \leq 1$

Several corrections and assumptions were made to the Gamma Method due to the orthogonally oriented timber plies of CLT. The first assumption was that the layers oriented perpendicular to the direction of the span would carry no load. The perpendicular layers were accounted for as fasteners to the longitudinal layers and the rolling shear stiffness, G_R, would act as the fastener stiffness between load carrying layers (Eq.3).

$$\frac{s}{K_i} = \frac{\bar{h}_i}{G_R b} \quad (3)$$

where:

$\bar{h}_i$ =thickness of ply

G_R = Rolling shear stiffness

b = width of panel

The maximum bending stress (σ_{max}), ply 1, can therefore found by equating both the local and global bending stresses in Eq. 4. Other stresses such as axial and shear can be found as well.

$$\sigma_{max} = \frac{ME_1}{(EI)_{eff}} (\gamma_1 a_1 + 0.5 h_1) \quad (4)$$

where:

M = applied moment

2.2.2 Composite Theory

Similarly to the Gamma Method, the composite theory (otherwise known as the k-theory) uses an effective stiffness but in the form of composition factors which account for loading configurations and each individual layer's properties. The main assumptions are linear stress strain relationship and Bernoulli's hypothesis of plane sections. Each composition factor (Eq. 5) is multiplied with each strength value and compared with the maximum stress applied. A list of composition factors can be found in [19, 22]. Shear deformations are not accounted for in this method.

$$\sigma_{max} \leq f_{b,0}k \tag{5}$$

where:

$f_{b,0}$ = bending strength

k = composition factor

2.2.3 Shear Analogy Method

The shear analogy method accounts for shear deformations and is the most precise CLT design method according to Blass and Fellmoser [22]. The bending and shear stress both incorporate the properties of each layer. The rolling shear stiffness is incorporated in the maximum deflection of a CLT slab by the introduction of the second term in Eq. 6 [19].

$$u_{max} = \frac{5}{384} \cdot \frac{qL^4}{(EI)_{eff}} \cdot (1 + \frac{48(EI)_{eff}k}{5(GA)_{eff}L^3}) \tag{6}$$

where:

k = shear coefficient form factor

q = distributed load

L = span length

$(EI)_{eff}$ = effective bending stiffness

$(GA)_{eff}$ =effective shear stiffness

While each of the methods (besides the k-method), assume a degree of shear deformation, the shear is isolated in the plies themselves. All the methods assume complete bond adherence and no slip between the plies.

2.3 Design for Fire Conditions

Design of CLT for fire conditions relies on the predictability of uniform charring rates of timber exposed to a standard furnace fire in order to determine the residual capacity of the timber for a predetermined period of exposure. In addition, accounting for the increase in temperature beyond the pyrolysis front into the virgin timber and resultant degradation in material properties is necessary. This combined approach allows the residual capacity of the CLT member to be calculated. Most standards calculate charring rates in similar ways but the change in material properties in the heated (but uncharred) timber is calculated differently depending on the code. The methods listed in this section were created for use with the standard furnace test as the charring rates and strength compensating layers were all measured and derived using data from the standard furnace test. All these methods presume that degradation stops at the moment when external heating ends.

2.3.1 The Eurocode Approach

EN 1995-1-2 defines the charring depth in solid timber as the distance from the exposed surface of char to the char line, which is the boundary where timber pyrolysis occurs. The char line is usually taken as the 300°C isotherm. The charring depth ($d_{char,0}$) is defined in Eq. 7 for one-dimensional charring and Eq. 8 for corner rounding [23].

$$d_{char,0} = \beta t \tag{7}$$

where:

$\beta = \beta_0$ (one-dimensional charring rate under standard fire exposure) or β_n (notional charring rate accounting for corner rounding under standard fire exposure)

t = fire exposure time

To calculate the strength of a timber structural member, EN 1995-1-2 allows two calculation methods: the Reduced Properties Method (RPM) and the Reduced Cross-Section Method (RCSM). Both methods use the charring depth and assume the char contributes no strength to the structural capacity of the member. Both methods use a modification factor to account for the thermal penetration depth, the thickness of the member at temperatures above ambient but below the pyrolysis temperature. Where the methods differ is that the RPM modifies the modulus of elasticity and the bending, tensile, and compressive strength of timber in the overall structural calculations. The RCSM specifies a "zero-strength" layer to be added to the char layer. This increased char layer is termed the effective char depth (d_{ef}) and accounts for the reduction in structural properties by eliminating a portion of the

thermal penetration depth (Eq. 8). The remaining section is then used to calculate the strength of the member assuming ambient temperature strength.

$$d_{ef} = d_{char,n} + k_0 d_0 \quad (8)$$

where:

$d_0 = 7mm$

$$k_0 = \begin{cases} \frac{t}{20}; t < 20\ min \\ 1\ ; t \geq 20\ min \end{cases}$$

If the structural member protection (such as gypsum board) falls off, the charring rate doubles until the char layer re-increases to 25mm (Figure 2). The solid line in Figure 2 represents timber which chars at a constant rate. The dashed line represents a newly unprotected timber member which chars at double the rate until a charring depth of 25 mm is achieved. While EN 1995-1-2 only accounts for char and protection fall off, ply delamination of CLT acts in a similar manner [24-26]. However, temperature values or fall-off criterion are not given.

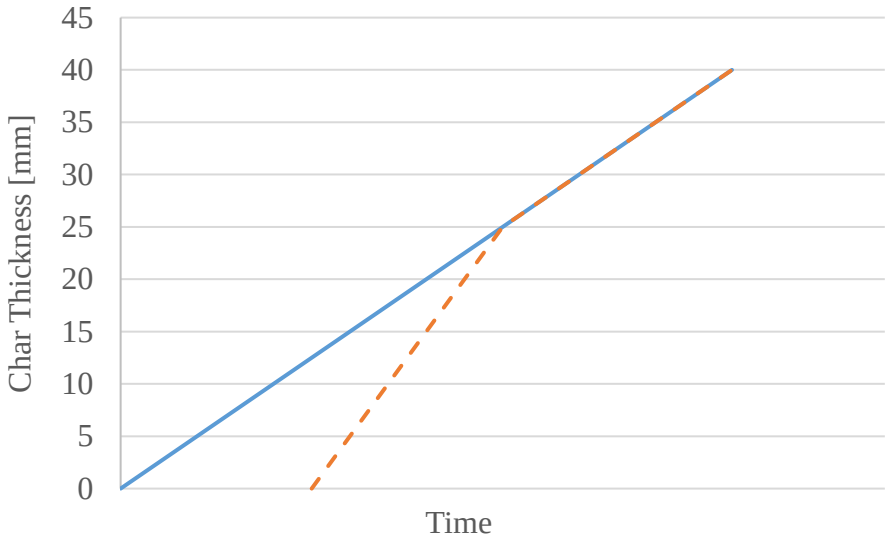

Figure 2: Normal charring (solid line) and increased charring due to protection fall-off (dashed) [23]

2.3.2 National Design Specification

The National Design Specification (NDS) methodology for structural performance of timber in fire uses an effective charring depth as specified in Eq. 9 [25].

$$d_{ef} = \frac{\beta_n t}{t^{0.187}} \quad (9)$$

where:

t = fire exposure

β_n = notional charring rate under standard fire exposure

NDS also uses zero-strength concept and adds twenty percent to Eq. 9 to determine the thickness of this layer. Unlike EN 1995-1-2, the zero-strength layer is variable and depends on the actual char depth. While the maximum zero-strength layer for EN 1995-1-2 is 7mm, the NDS zero strength layer is assumed to be 20% of the thickness of the char.

The NDS accounts for char and ply delamination by assuming the CLT layer falls off once the temperature of the adhesive reaches 300°C. Once the ply has fallen off, the char layer is assumed to grow again from zero thickness. Aguanno [27] recommended, based on medium and full-scale tests, that ply fall-off should be assumed to occur when the 300°C isotherm reached 12mm from the bond line.

2.3.3 SP Model

The last commonly used model to account for structural deterioration of timber and CLT due to fire is the SP Technical Research Institute of Sweden (SP) model [28]. The charring model recommends a thickness for the char layer and also includes an additional compensating layer for the thermal penetration depth into the uncharred portion of the cross section. The charring depth recommended is shown in Eq. 10 and is based on a compensating layer factor, s_o. The compensating layer is dependent on:

- Number of CLT plies,
- Overall member thickness,
- Stress orientation of fire-exposed side, and
- Thermal penetration temperature gradient.

$$d_{ef} = d_{char,n/0} + k_0 s_0 \quad (10)$$

where:

$d_{char,n/0}$ = notional or one-dimensional charring depth under standard fire exposure

$k_0 = \frac{t}{20}$ for unprotected members. Increases linearly from 0 to 1 then remains constant.

s_0 = compensating layer

Char and ply fall off are calculated the same manner as in the EN 1995-1-2 and NDS methods. Each of the methods described above accounts for structural deterioration of timber due to fire through the use of a charring method. The methods accounts for the thermal penetration depth through the use of a compensating factor. Char fall-off is assumed to occur at 300°C. To calculate the overall amount of char during the required fire resistance time, the progression of the char layer (300°C isotherm) is calculated. If the 300°C isotherm reaches the bond line during the exposure period, the layer is assumed to fall-off and the charring rate is doubled until 25mm of char is reached - at which point the charring rate reduces to normal values. The calculation is performed until the fire resistance period is reached. The amount of char that has been consumed plus the compensating layer is the portion of the timber section that provides no strength. The resulting timber section must maintain adequate structural capacity to resist the applied load.

2.3.4 Principles of the Thermal Compensating Layer

The thermal compensating layer was originally proposed by Schaffer [29-31]. The approach was devised to account for the decrease in strength properties of the timber due to an increase in the temperature. In the study, the temperature of the curve below the pyrolysis zone was modelling using Eq. 11. The equation below is the steady-state thermal profile after 20 minutes of exposure to a standard time-temperature curve in a standard furnace.

$$\frac{(T - T_o)}{(T_c - T_o)} = \exp\left(\frac{-\beta\delta}{\alpha}\right) \tag{11}$$

where:

T_c= pyrolysis temperature

T_o = ambient temperature

δ = depth into wood from pyrolysis layer

β = steady-state charring rate

α = thermal diffusivity

T = wood temperature at depth δ.

The temperature curve with depths was generated using a pyrolysis temperature of 288°C. Temperature values were then substituted for values of reductions in strength. A lower limit to the temperature curve was chosen as 50°C as this corresponded to approximately 90 percent of the strength for each of the types of strength as shown in Figure 3 [32]. The strength values were averaged over the entire zone. A thickness in timber for the amount of strength lost due to the average reduction was calculated. This thickness is the thermal compensating layer and was added to the amount of

timber that was removed from the cross section due to charring. The remaining timber cross section is used with ambient temperature strength values to calculate the residual capacity of the member. Current research has shown, however, that the 7mm thermal compensation layer should be increased [25, 28, 33].

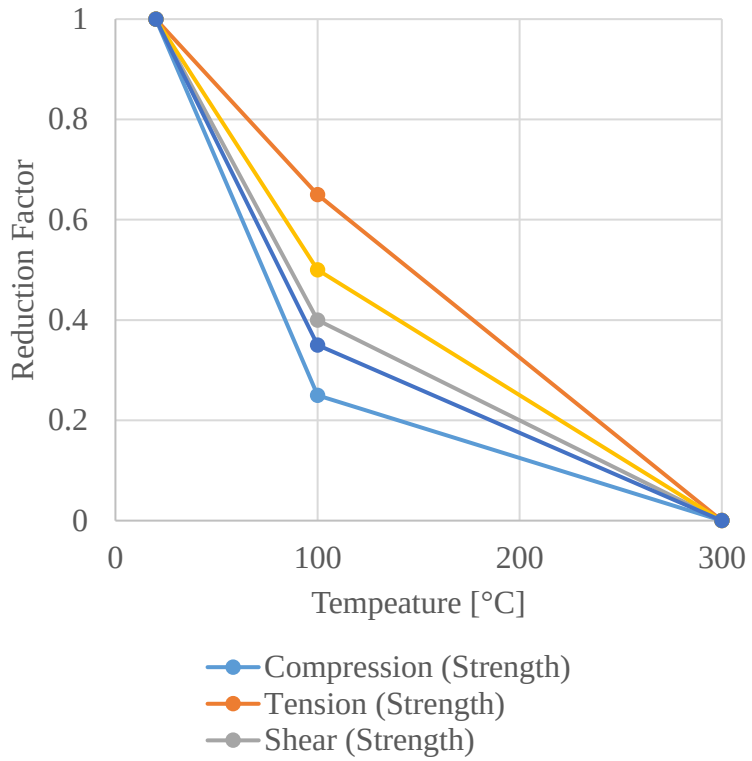

Figure 3: Eurocode 1995-1-2:2005 timber strength reduction factors [23]

2.3.5 Summary

The current design for timber structures is to design for a given fire resistance period which is defined by a given amount of time in a standard furnace. Because of the resulting heat flux provided by the furnace, charring is relatively constant over the entire fire resistance period, whether the time is 30 minutes or 4 hours. The concept of self-extinction of timber is not included in the design process and thus timber members have to be designed with large cross-sectional areas in order to account of the area reduction due to charring. Furthermore, past the required fire resistance time, the timber is assumed to reach a terminal state and no further deterioration is expected. Timber ply fall-off is accounted for in the design guidelines only when the 300°C isotherm reaches the bond line. The char is then assumed to fall off and expose the timber leading to double the charring rates. This assumption only accounts for ply fall-off after pyrolysis has occurred on the adjacent plies and relies on the bond line to remain perfectly intact up until the 300°C isotherm has reached the glue.

2.4 CLT Composite Action Mechanics

The design of CLT for ambient and fire conditions assumes that bond lines do not fail until the char layer (300°C isotherm) has reached the bond line. Since timber has no strength above 300°C, the implicit assumption is that the strength of the glue is adequate enough for failure to occur in the timber and not in the bond line. Failure of CLT should occur in the weakest portion, namely, the timber. Hence, any bond line failure of CLT is a failure of the product's overall design.

In order to properly understand the mechanics of CLT ply interaction and the role the glue plays in the composite action, an understanding of the interfacial shear ($\tau(x)$) and normal stresses ($\sigma(x)$) is necessary. Figure 4 shows the forces and stresses between two plies and the adhesive layer between them. An distributed applied load, *q*, is applied to a differential element, *dx*. Axial forces (*N(x)*), shear forces (*V(x)*) and moment forces (*M(x)*) all occur in both plies as a result of the applied load. Interfacial normal (*σ(x)*) and shear (*τ(x)*) forces develop as the axial, shear and moment forces are transferred from one ply to the next.

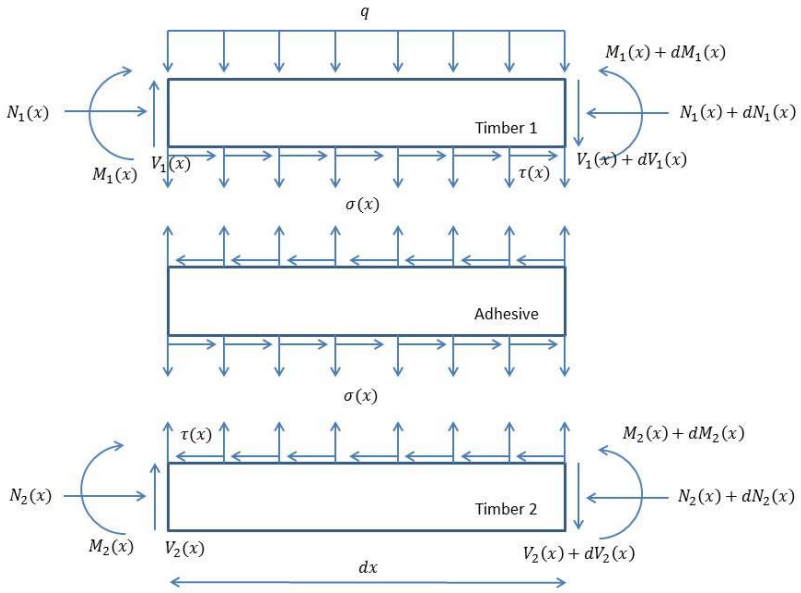

Figure 4: Interfacial and normal stresses (adapted from [34])

As shown in Figure 4, the adhesive needs to resist both shear and normal stresses (axial load carried by the adhesive layer is negligible due to low elastic modulus and relatively low thickness, thus ignored). Based on the assumptions from the charring models the glue should resist all stresses below 300°C. Current research shows that this assumption may not be appropriate.

Two previous studies have been conducted on the shear strength of popular adhesives used to bond CLT. Frangi et al. [35] performed shear tests on Glulam at temperatures ranging from 20 to 170°C. The bonded area was 1600 mm^2 (40 mm bond length). Resorcinol-formaldehyde (R-F), one-component polyurethane (1K-PUR) and epoxy were used. The blocks were heated in an oven to the desired temperature and loaded until failure. The study revealed that the shear strength varied significantly even among the same type of glue and that the shear strength reduced to 25-75% of the ambient strength. Table 1 shows the temperature at which cohesion failure dominated. The second study was conducted by Clauß et al. [36] on the thermal stability of adhesive under shearing loads at temperatures up to 220°C. The conclusions from this study were the same as Frangi et al. [35].

Table 1: Temperature of Cohesion Failure [35]

Adhesive	Failure Temperature (°C)
Kauresin 460 (R-F)	>170°C
Kauranat 970 (1K-PUR)	180-190°C
Balcotan 107 TR (1K-PUR)	50-60°C
Balcotan 60 190 (1K-PUR)	190-200°C
Purbond HB 110 (1K-PUR)	60-70°C
Purbond VN 1033 (1K-PUR)	150-160°C
Araldite AW 136 H (epoxy)	50-60°C

Based on these tests and the force diagram in Figure 4, the importance of the adhesive is clearly demonstrated. CLT failure is likely to be predominately in the adhesive above approximately 150°C. Furthermore, adhesive loses significant strength above 100°C. Hence, as the temperature increases, the adhesive will slip and deform and the overall CLT section will have greater deflection. Failure of the section by delamination will be gradual and not sudden. Failure of plies will occur before visual fall off [37, 38]. The temperatures and failure modes listed in Table 1 are all in the range of the thermal penetration found in Section 2.3.4. If the thermal compensation layer is not thick enough to eliminate the bond line from the strength calculation, then the residual cross-section method calculates the strength of the section as if the bond line is at ambient temperature. As demonstrated by the previous studies, this approach appears to be inappropriate.

Clauβ et al. [36] used 75x20x5mm pieces of timber with 200mm^2 of bonding (10mm bond length) between them to study the thermal stability of adhesive under shearing loads. The test series involved seven different types of adhesive ranging from one-component polyurethane to formaldehyde based resins. The specimens were heated between ambient and 220°C. The results of test were similar to the result by Frangi, et. al. [35]. The polyurethane results varied greatly between the manufactures and the specific chemical structure of the adhesive. One interesting finding of the study was that at approximately 70°C the shear strength measured from the test increased slightly until around 150°C. The authors hypothesized that this was due to moisture content decreasing—resulting in increased timber strength. Moraes et al. [39] attributed this behaviors to the increase in the glass transition temperature of lignin when oven dry. Experimental results showed this occurred around 140°C.

The problem with these previous studies in understanding the behavior of bond behavior is that bond length is a critical factor in determining the overall performance of a member. The bond length used in the studies differed. Clauβ et al.[36] used a 10 mm bond length while Frangi et al. [35] used a 40 mm bond length. In bonded joints with shorter bond lengths (i.e. not enough bond length to initiate inelastic deformations within the bonded interface), the bond length itself is a key parameter affecting the overall bond strength. Therefore, in test specimens with a shorter bond length, decoupling the effects of length and adhesive mechanical properties becomes difficult. The concept of effective bond length is detailed by Fernando et. al. [40]. According to Fernando et. al. who studied the CFRP and steel bonded joints, the ultimate load of a joint with a short bond length is proportional to the length of the bond multiplied by the maximum shear stress the adhesive can withstand (Eq. 12).

$$P_u = \tau_{max} b_p L \qquad if\ L \leq a_d \tag{12}$$

P_u = ultimate strength of the bonded joint

τ_{max} = maximum shear stress the adhesive can withstand

b_p = width of the bonded joint

L = length of bond

a_d = minimum length required to initiate inelastic deformations within the bonded interface before reaching the ultimate strength

For longer bond lengths, the ultimate load of a joint subjected to mode II (in-plane shear) loading is independent of the bond length and is given by:

$$P_u = b_p\sqrt{2G_f E_p t_p} \qquad if\ L \leq a_d \tag{12}$$

G_f = fracture energy in mode II

E_p = tensile elastic modulus of the adherend

t_p = thickness of the adherend

The complexity in calculating the ultimate strength of a bonded joint increases when the effective bond length is reached. The current study only highlights the necessity for understanding effective bond length in assessing the strength of bonded joint. The effective bond length must be reached before the performance of an adhesive bond at elevated temperature can effectively be studied. This study seeks to begin to analyze the problem and highlight a ranked order of importance in studying adhesive joints in fire conditions (Section 5.3).

Chapter 3: Conditions for Self-Extinction

Self-extinction is the phenomena that controls the performance of timber buildings during a fire event. Without the potential to self-extinguish flaming combustion after the complete burnout of the fuel in a compartment fire, timber structural members will continue to burn (and lose strength) until breaching of compartmentalization, the collapse of the member and potentially the building. As described in Section 1 and 2, the assumption that timber continues to burn is currently not captured in design philosophies. Encapsulation and other forms of protection are used as mechanisms for protection but all testing methodologies accept failure of the protection so long as the fire resistance requirements are met. While timber loses strength when subjected to a compartment fire, the ability for the timber to self-extinguish is the physical property that makes timber a viable building material to use. Furthermore, self-extinction is an assumed criterion that enables the approximation of fully developed fires by means of the fire resistance framework. This section describes self-extinction of CLT as well as the characteristics which enable and hinder self-extinction from occurring.

Section 3.1 describes self-extinction in context of fire safety and demonstrates the need for flaming combustion of timber to self-extinguish. Section 3.2 details previous work and the theory behind self-extinction in terms of an energy balance over the char and pyrolysis layers. Section 3.3 describes the methodology for studying self-extinction and the important parameters measured. Section 3.4 shows the results of self-extinction during the steady-state and transient regimes of burning when the external heat flux was completely removed. Section 3.5 shows the results of the critical mass loss rate and critical heat flux when the external heat flux was reduced to the self-extinction limit. Finally, Section 3.6 describes debonding of char and the CLT and the resulting effects on self-extinction and the mass loss rate of timber.

3.1 Self-Extinction in Fire Safety

The principle of self-extinction is a fundamental and inherent principle of fire safety engineering. A typical fire has four stages as shown in Figure 5. The fire starts with an ignition event and increases in size during the growth phase. At flashover, the room becomes fully involved with all the combustibles in the room igniting. Steady-state burning occurs after flashover and is defined by ventilation control. After a significant portion of the fuel has been consumed the fire transitions back to fuel control during the decay phase of the fire. The fire reaches extinction after the entire fuel load has been consumed. The key principle of fire safety engineering is to design fire safety measures to protect against this typical fire. While the magnitude and shape of the curve may be different, the basic principle is the same: a structure has to be able to withstand burnout of a fire.

If the amount of fuel can be calculated and the burning rate of the fuel is known, the time to burnout can be calculated. Researchers over the years have focused on measuring the burning rate depending on the ventilation conditions and the type of fuel. Current design methods classify the burning rate and the amount of fuel in a compartment depending on the occupancy type. Along with the ventilations conditions, the length of the fire and the maximum temperature of the fire can be calculated. The fire duration and the maximum temperature are used directly to quantify the thermal load on structural members. The required fire resistance of a structure is therefore based on the type of fuel and the length of the fire; the design framework is therefore derived from the assumption that a fire will behave in a similar manner that shown in Figure 5. At some point, the fire will reach burnout and thus the imposition of thermal load on the structure is assumed to cease.

Fire resistance was originally devised to equate real fires to a standard time-temperature curve in a fire. The area under the time-temperature curve of a real fire was determined to equal the same area under a standard fire. Thus the equivalent fire resistance time was formulated as a means of comparison between building products. Ingberg in 1928 [11] linked equivalent fire duration with the amount of fuel in a compartment and thus linked equivalent fire duration (fire resistance) to the burnout time of a compartment. However, as stated in the previous paragraph (and as acknowledged by Ingberg), the assumption that time to burnout is linked only to fuel load is wrong— as burning rates are a function of a host of other factors including ventilation, geometry, and type of fuel. Time to burnout has always been a complex function of fire resistance.

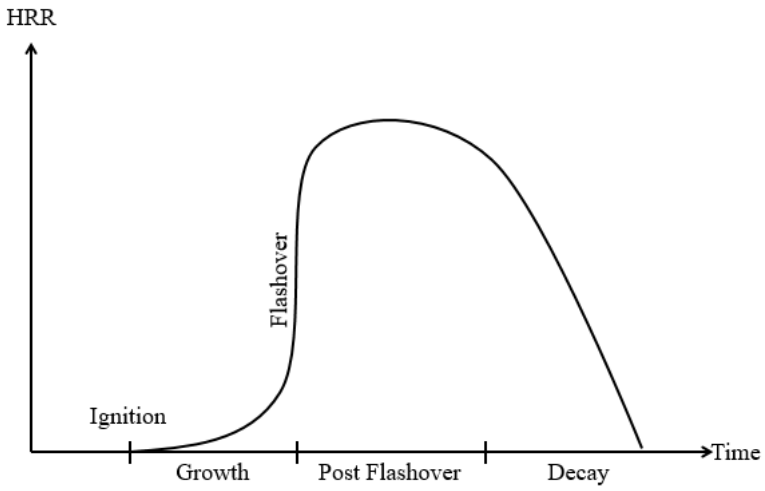

Figure 5: Heat release rate of a fire over time

Fire safety strategies can be made for exposed timber structures. Inherently, adding fuel to a compartment will increase only the duration as the maximum heat release rate in the compartment is

governed by the amount of ventilation. The fire curve will follow the same typical curve in Figure 5 and eventually reach burnout. The fundamental premise, though, is that the compartment fire eventually reaches burnout. Reaching burnout with exposed timber means that the timber has self-extinguished. If the timber continues to burn, then burnout will never be reached. Failure to achieve burn-out is against the fire safety strategy and design principles. In order to use timber correctly in design, self-extinction has to occur.

3.2 Theory and Previous Research

Self-extinction is an intrinsic quality of timber. Numerous studies have been conducted on the self-extinction characteristics of timber and have yielded similar conclusions on the properties that control this process. The most fundamental conclusion on the topic of self-extinction was observed by both Petrella [41] and Tewarson and Pion [42] when they showed that the heat flux from the flames of timber is smaller than the surface heat losses, $\dot{Q}''_F \leq \dot{Q}''_L$. In the study by Tewarson, the heat flux from the flames was approximately 23.9 kW/m^2 and the surface losses were approximately the same value. Therefore, in order for the wood to continue to burn, an external incident heat flux, $\dot{Q}''_E$, has to be applied to the surface. The study also showed that a linear relationship exists between the heat flux intensity provided by the flames and the mole fraction of oxygen the flames receive. The experimental procedure used was very similar to the one used for this study except that piloted ignition was used for Tewarson's tests. Tewarson tested a range of combustible materials that were exposed to an external heat flux and ignited. The amount of oxygen entering the system was measured and controlled for each test. The external heat flux was applied using two radiant heaters and the mass loss rate was measured using a load cell. The study tested a wide range of plastics, liquid, and solids. Ideal burning rates for each material and the heat flux from the flames was calculated using the energy balance of the burning material. Most materials had flame heat fluxes which would sustain burning. Wood based products, however, did not.

Babrauskas [43] compiled data from research tests on the ignition temperature of wood. The range in ignition temperature varied due to factors such as sample size, piloted vs. auto-ignition, and heat flux intensity. The range in minimum heat flux values necessary to achieve ignition were also summarized and explored. The lowest minimum heat flux was listed as 4.3 kW/m^2 while the highest minimum heat flux value for ignition was approximately 50 kW/m^2. The range of data though is widely scattered leading to uncertainty in the results and conclusions. Babrauskas [43] detailed unpublished work by himself and J. Hall on tests conducted on self-extinction of timber. In the work, a flame was applied to a wood sample between 1-5 minutes of flame impingement. After the allotted time, the flame was removed and in each test the flames were observed to self-extinguish.

Spearpoint, et al. [44] developed a model designed to predict the burning rate of wood. Charring, vaporization, flame and conduction were all included in the model and the model was validated for both charring and non-charring materials. In the study, wood samples were exposed to external heat fluxes ranging from 25-75 kW/m^2. Thermocouples were drilled into the sample to measure in-depth temperatures while the sample was burning. The study showed that the burning rate of wood was dependent upon species, grain direction, and moisture content among other variables. The model predicted the burning rate and the thermal profiles reasonably well, and the model was able to capture the changes in the burning rate due to the separation between short and long term burning. The study showed the model and the experimental data drifted from steady-state effects as the burning progressed far enough into the sample that the boundary conditions on the non-heated face of the sample effected the results. The study highlighted that the increases in the surface temperature play a critical role in the energy balance of the burning surface as both convection and radiation are dependent upon the surface temperature.

Reductions in the amount of energy the pyrolysis front receives all serve to reduce the burning rate and bring the sample close to self-extinction. Increases in the char layer create an increasing heat sink—reducing the amount of energy imposed on the pyrolysis front. The thermal properties in the char layer and the physical movement of the char layer away from the radiant energy source reduce the amount of absorbed energy [45]. Self-extinction occurs when the external heat flux decreases below a critical value for flaming combustion.

Drysdale [46] summarized the current research on self-extinction. Drysdale made the distinction between thermally thin and thermally thick samples of wood. Thermally thin pieces of wood will sustain flaming combustion after an external heat source has been removed whereas a thermally thick sample will self-extinguish. Drysdale highlights the importance of heat losses on the ability of a sample to reach self-extinction. Each of the studies listed that have studied self-extinction have completely removed the external incident heat flux.

3.2.1 Char Layer Energy Balance

The energy balance taken over the char layer and pyrolysis zone in Figure 6**:** is used to understand the physics behind self-extinction of timber. In this analysis several assumptions exist. The first assumption is that the applied external energy sources are uniform over the entire surface creating a one-dimensional heat transfer problem. The second assumption is that the material properties of the timber and char and spatially uniform. While the material properties may vary depending on the grain orientation of the timber, the thermal properties are assumed to remain constant.

Three control volumes exist in Figure 6**:** . The first control volume is the char layer (area shaded with diagonal lines). Energy is applied to the char layer from external heat sources ($\dot{q}"_{ext}$). These external heat sources could be radiant or convection energy from a hot gas layer or from fires remote from the timber. The external heat sources could also be from the flames produced by the burning timber itself. As the external surface increases in temperature, energy flux ($\dot{q}"_{loss}$) is lost from the control volume by convection and radiation. The char layer produces an energy flux ($\dot{q}"_{g}$) through oxidation of the char as the temperature of the layer increases—The storage of energy in the char is encompassed in the term ($\partial q"/\partial t$). The energy flux, ($\dot{q}"_{char}$), is transferred from the char layer into the second control volume (pyrolysis layer) by conduction.

Pyrolysis of timber occurs within a wide temperature range (Section 3.3.4) and as such the layer has a thickness. However, in order to simplify the problem, the pyrolysis layer while described as a control volume is idealized as an infinitesimally thin area. This is commonplace in literature and is typically represented as a single temperature or isotherm. Part of the energy flux transferred into the pyrolysis layer is used to decompose the timber into combustible gases and char. The remaining energy is transferred from the pyrolysis to the third control volume, the virgin wood. The virgin wood, acting as a semi-infinite solid with the back face at ambient temperature, then increases in temperature. As the pyrolysis layer nears the back face of the sample, the semi-infinite solid assumed becomes invalid. However, for the samples used in this study and the analysis conducted, the semi-infinite assumed remained valid.

For the energy balance of the char layer, the energy flux added and generated by the control volume has to equal the energy flux stored in the control and lost from the surface. A summation of all the terms leads to Eq. 13. The control volume reaches steady-state when a summation of all the terms in Eq. 13 equals zero.

$$\dot{q}"_{ext} + \dot{q}"_{g} - \dot{q}"_{loss} - \dot{q}"_{char} = \frac{\partial q"}{\partial t} \tag{13}$$

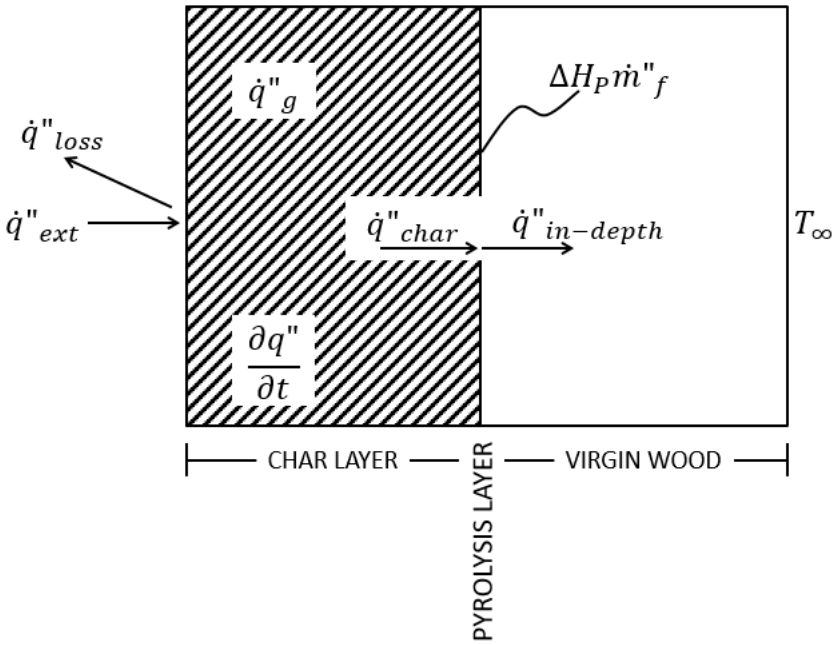

Figure 6: Energy balance of the various control volumes of burning timber

The energy balance of the pyrolysis layer is represented as the energy flux entering the layer equaling the amount of energy used for pyrolysis minus the energy flux transferred through conduction into the virgin timber. The energy transferred from the pyrolysis layer into the unburned timber ($\dot{q}''_{in-depth}$) is represented by the second term Eq. 14 where k is the thermal conductivity and dT/dx is the rate of energy transfer (Figure 7). The amount of energy flux used in pyrolysis is proportional to the heat of pyrolysis of wood (ΔH_P) and the mass loss rate ($\dot{m}''_f$).

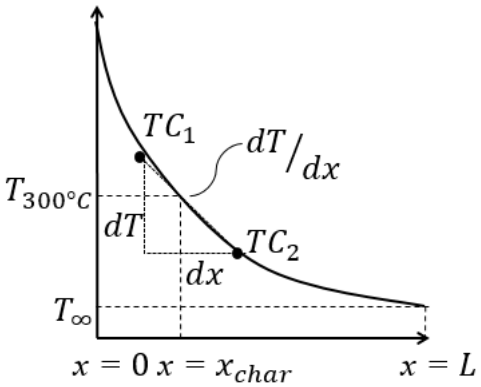

Figure 7: Thermal gradient calculation at the pyrolysis isotherm

$$\dot{q}''_{char} - \left(-k \left. \frac{dT}{dx} \right|_{x=x_{char}} \right) = \Delta H_P \dot{m}''_f \tag{14}$$

Combining Eq. 13 and 14 yields Eq. 15 which represents energy balance over both the char and the pyrolysis layer.

$$\dot{m}''_f = \frac{1}{\Delta H_P}\left[\dot{q}''_{ext} + \dot{q}''_g - \dot{q}''_{loss} - \left(-k\left.\frac{dT}{dx}\right|_{x=x_{char}}\right) - \frac{\partial q''}{\partial t}\right] \quad (15)$$

By analyzing Eq. 15 in terms of self-extinction, maximizing the burning rate and determining steady-state burning conditions becomes fundamental in determining worst-case scenarios. If self-extinction occurs when the burning rate is at a maximum or steady-state scenario, then all other heating scenarios will result in self-extinction. Minimizing $\dot{q}''_{in-depth}$ and $\dot{q}''_{loss}$ as well as the control volume trending toward steady-state, $\frac{\partial q''}{\partial t} \approx 0$, results in a maximum value of the burning rate.

Moreover, for flaming combustion, a critical value for the burning rate, $\dot{m}''_{f,critical}$, exists. If the burning rate of the sample is greater than this critical value then flaming combustion continues. If the burning rate decreases below this value, the self-extinction of flaming combustion occurs [46]. The self-extinction burning rate is similar to auto-ignition or the "fire-point" as auto-ignition requires the mass loss rate from the sample to be greater than the flow velocity removing the mass from the surface. For auto-ignition, the gaseous fuels have to absorb enough energy from external heat sources in order to reach ignition. This point of ignition is defined as the critical Damköhler number. The mass loss rate associated with auto-ignition versus extinction potentially differ depending on the source of applied energy. For auto-ignition, the source of energy is radiative or convective. In the case of extinction, the presence of the flame close to the surface adds a low level of heat flux [47]. The critical external applied heat flux between auto-ignition and extinction will always be less for extinction as the flame provides the difference between the two values. As soon as the mass loss rate drops below the critical rate for sustained burning, flaming combustion ceases.

The terms in Eq. 15 highlight several possible circumstances where the burning rate decreases. A complete removal or decrease in $\dot{q}''_{ext}$ could reduce the burning rate significantly. A reduction in the external applied energy flux could be from the sample heated surface regressing away from a fixed energy source, a reduction in the heat flux of a compartment fire due to the decay phase of a fire, or a complete extinction the heat flux due to extinguishment of a fire. Reduction in the burning rate could also occur by an increase in the amount of energy lost from the surface of the char, $\dot{q}''_{loss}$, through convection and radiation. Finally, maximizing the amount of energy transferred into the

unburned timber through conduction and maximizing the rate of energy stored in the char could result in a reduction in the burning rate sufficiently enough for self-extinction to occur.

Eq. 15 cannot be solved without an understanding of the formation of the char layer and the in-depth heat loss into the unburned timber. Therefore, the objective of this study was to conduct experiments to determine the conditions leading to a maximum value of the burning rate and steady-state conditions. For this study, the energy generated by oxidation of the char was neglected as the magnitude of the value compared with the other terms in Eq. 15 is significantly less. This is explained further in Section 3.3.4. For quantification of $\dot{q}"_{ext}$, the heat flux provide by the flames was neglected as measurement is extremely difficult. If self-extinction occurred with flames then this represents a worst-case scenario.

3.3 Methodology

Based on the theory of self-extinction presented in Section 3.2, several parameters needed to be measured in order to fully quantify self-extinction. First, self- extinction needed to be demonstrated to occur in both the steady-state and transient burning phases. In order to determine steady-state burning, both the mass loss rate, thermal gradient, and surface losses needed to be measured. Steady-state occurred when all three parameters reached steady-state. The first aspect of self-extinguishment was the complete removal of the heat flux in order to demonstrate the phenomena's occurrence under any circumstance. Then, in order to determine the critical mass loss rate and heat flux for extinction of flaming combustion, the external applied heat flux was reduced until extinction occurred. For every test, observational data was collected for instances when self-extinction did not occur or when flaming combustion was re-ignited.

A vertically oriented mass loss calorimeter (MLC) was used to expose CLT to various heat fluxes. The timber samples were positioned for heating perpendicular to the grain due to the grain orientation of the outside layers of the CLT. The vertical orientation of the incident heat flux ensured a well-defined boundary condition [48]. Before the testing series, a Schmidt-Boelter heat flux gauge and known mass were used to calibrate the cone heater and the scale of the MLC to ensure accuracy of the results. Prior to the start of the test, an aluminum sheet was used as a radiant shield to prevent the timber samples from preheating while the cone heater reached the desired temperature. The removal of the shield between the sample and the cone heater allowed for a definitive starting point for the test and ensured a constant incident heat flux boundary condition. The tests were conducted under normal atmospheric conditions and using auto-ignition. The properties for each timber sample can be seen in Table 2.

Table 2: Self-Extinction Experiment CLT Properties

Species	European Spruce (*Picea abies*)
Type	5-ply CLT
Bonding agent	Polyurethane
Thickness (mm)	145 (32-21.5-34-21.5-34)
Heating Area (mm)	120 x 120
Moisture (%)	13.1
Density (kg/m^2)	425

3.3.1 Heating Conditions

The heat fluxes used for each test and the combustion scenario can be seen in Table 3. The boundary conditions for the first series of experiments were kept constant to allow the study of steady-state heating and the burning behavior of CLT. The exposure time for each test was dependent upon the time to steady-state heating and constant mass loss rate. A typical test ran for between one and two hours. As the purpose of the experiments was to study one-dimensional burning and heat behavior, the overall dimensions of the heated surface area were chosen to maximize one-dimensional heating in the center of the timber sample when using a conical heater. All tests results yielded extremely reliable and repeatable results as the error between the tests was small.

Table 3: The Occurrence of Charring and the Type of Combustion for Each Heat Flux Boundary Condition

Heat Flux (kW/m^2)	Charring	Combustion	Number of Tests
6	N/A	N/A	1
30	Yes	Smoldering	2
40	Yes	Smoldering	1
45	Yes	Smoldering	1
47.5	Yes	Smoldering/Flaming	6
49	Yes	Flaming	2
50	Yes	Flaming	7
65	Yes	Flaming	8
80	Yes	Flaming	2
90	Yes	Flaming	3
100	Yes	Flaming	7

3.3.2 Instrumentation

To measure the temperature profiles within the CLT samples, twelve type K thermocouples (Ø1.5mm) were inserted into Ø2mm holes in the sample. The holes were drilled from the back (unheated) face of the sample in order to minimize the effect of conduction within the plane parallel to the heated surface as well as to minimize measurement errors from the heating of the thermocouple wiring. A minimum distance between thermocouples was calculated according to recommendations by Reszka [48]. The thermocouples were placed in a circle (Ø60mm) around a centrally located thermocouple. The spacing minimized the thermal effects of heat conducting through the metal thermocouple shaft and wiring and increasing the temperature of the nearby thermocouples. Centrally locating the thermocouples in the timber sample ensured one-dimensional heat transfer by eliminating the boundary condition effects of the unheated surfaces of the sample. For the first three layers of the CLT, the thermocouples were positioned every 5mm starting at 2mm from the heated surface. Several preliminary tests showed the temperatures in the final two layers of the samples did not increase above ambient for the duration of the test. These results confirmed the assumption of a constant ambient temperature as a boundary condition for the surface farthest from the heated surface.

A scale which was part of the MLC was used to record the mass of the sample for the duration of the test. Before each test, a Schmidt-Boelter heat flux gauge was used to measure the starting heat flux

as well as the heat flux at the distance the surface regressed to at the moment of self-extinction. The temperature profiles and mass of the sample were recorded with an Agilent Data Logger for the entirety of each test. A Nikon DSLR camera was used for time lapse photography for documentation of the tests as well post-processing to determine the charring rate.

3.3.3 Thermal Gradient Calculation

In order to calculate the amount of energy transferred through conduction into the unburned timber, the thermal gradient at the pyrolysis front of the char layer needed to be calculated. The amount of thermal energy conducted in-depth into the cross-section is shown in Eq. 4.

$$\dot{q}''_{in-depth} = -k \left.\frac{dT}{dx}\right|_{x=x_{char}} \tag{16}$$

where k is the thermal conductivity and dT/dx defines the rate at which energy is transferred from the control volume.

Since temperatures during the experiment were taken at discreet locations within the sample, the thermal gradient was approximated using the known distance between the thermocouples along with the difference in temperature (Figure 8). A trend-line equation was generated for distances and temperatures between two data points. A fifth-order polynomial was fitted to the data to obtain the temperature profile as this was the best fit to the overall shape of the data points. The first derivative of the fifth-order polynomial was calculated to find the slope, dT/dx, at any desired distance.

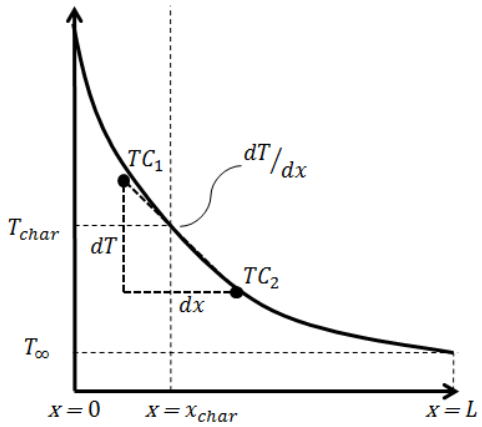

Figure 8: Thermal gradient calculation using a selected pyrolysis temperature

Since the thermal gradient at the location of the pyrolysis layer is the amount of energy transferred into the virgin timber, a specific temperature needed to be chosen in order to calculate the thermal gradient. However, selection of the value of the pyrolysis layer needed to be carefully done because the temperature of the pyrolysis layer is not a single value as the timber compounds decompose at different temperatures. In order to find the range in temperatures, a specific test was required.

3.3.4 Thermo-Gravimetric Analysis

A Thermo-Gravimetric Analysis (TGA) was completed for the various timber samples. The samples were heated from 30 to 900°C at a rate of 10°C per minute. Each timber species was tested in both air and in pure nitrogen. Testing the timber in air yielded the main oxidation range while testing in pure nitrogen showed the main pyrolysis range. Testing in pure nitrogen did not allow for any oxidation of the material; only decomposition occurs. The TGA tests were performed with gas flow at 20 mL/minute. A TGA graph of European spruce is shown in Figure 9. The main pyrolysis range occurred between 220°C and 400°C whereas the oxidation occurs primarily between 400°C and 550°C.

Since the pyrolysis region is idealized as an infinitesimally small layer at a specific isotherm, a specific temperature needs to be chosen for the analysis. According to the TGA analysis presented in Figure 9, a sharp increase in the mass loss rate occurs around 300°C. This value is commonly used in literature for modeling and other analysis on the pyrolysis of timber and thus was deemed appropriate for the current analysis. Therefore, for the calculation of the thermal gradient, dT/dx, the location of the 300°C isotherm was selected.

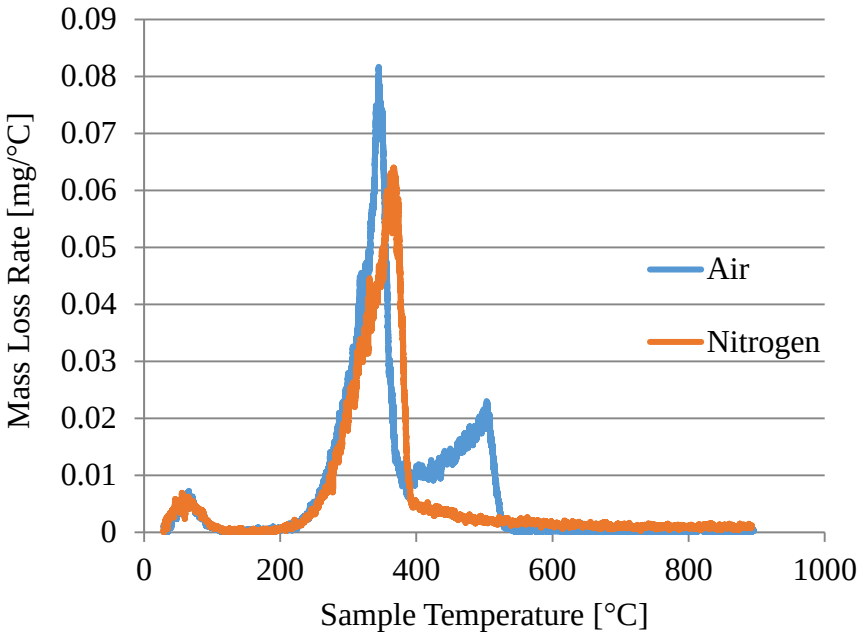

Figure 9: Thermo-gravimetric analysis of European spruce

Section 3.2.1 highlight that the energy generated by the oxidation of the char layer was neglected for this study. As shown in Figure 9, the relative difference in the amount of mass loss between the pyrolysis and oxidation region is minimal and hence validates the reasonableness of this assumption.

Both the surface temperature and the heat transfer coefficient needed to be measured and approximated respectively. Using both the surface temperature and the assumed radiation and convection heat losses, the total amount of energy lost from the surface of the char was calculated. The thermocouple located at 2mm was used to approximate the surface temperature at the start of the test. As the depth of the char layer and the temperature of the thermocouple at 2mm increased over the duration of the test, oxidation of the surface of the char took place and char layer regression occurred. The char layer was calculated to correspond with the end of oxidation at the upper limit of the TGA analysis in Figure 9 which is approximately 550°C. A 50°C increase in the end of the oxidation range was added to account for the change in sample size and any errors that would occur as a result. Once the upper limit to oxidation was reached, the surface temperature was assumed to remain at a constant 550°C for the duration of the test. Using a constant surface temperature results in steady-state energy losses from the surface. A typical total heat transfer coefficient of 45 W/m^2K was used and the energy flux lost from the surface was calculated as the difference between the surface and ambient temperature multiple by the total heat transfer coefficient. The location of the 550°C isotherm along with the 300°C isotherm was also used to calculate the thickness of the char layer. If the pyrolysis front progressed faster than the surface regression then the char layer increased

in thickness. If they progressed at the same rate then the char layer thickness had reached steady-state.

3.3.5 Other Analysis Considerations

The heat of pyrolysis, ΔH_p, along with the thermal conductivity, k, need to be approximated in order to make a full calculation of Eq. 15. Since Eq. 15 allows for the separation of the various energy terms only maximizing the terms within the brackets is necessary to maximize the burning rate. A value for the thermal conductivity of timber ($k = 0.13\ {}^{W}/_{mK}$) was selected from the literature provided by the manufacturer of the CLT samples [49]. The thermal conductivity value is necessary to estimate the in-depth heat losses into the unburned portion of the sample. The heat of pyrolysis term was assumed as constant in this study and thus was disregarded due to the fact that the mass loss rate is the only part in that term of the overall equation that changes throughout the combustion process. The mass loss rate would only need to be multiplied by the heat of pyrolysis if a magnitude comparison between the terms in the energy was to be completed. However, the focus of this study was on the relative movement of the values that change and thus the heat of pyrolysis was disregarded.

The analysis conducted assumes one-dimensional heat transfer with the location of the thermocouples in the experiment being placed to maximize the one-dimensional potential of the heat transfer. Minor lateral heat losses are possible due to any imbalance in the heating of the sample and progress of the pyrolysis front. A proper analysis of lateral heat losses would require an extremely high density of thermocouples through the sample. The thermocouples were placed in the middle of the sample and the sample was increased in size above the standard cone sample dimensions in order to minimize the lateral heat losses. Due to the increase in the size of the sample, the assumption to neglect the lateral heat losses was deemed appropriate.

3.4 Complete Removal of Heat Flux

The first step in developing a complete understanding of the self-extinction capacity of timber is to study the behavior after complete removal of the applied external heat flux. If timber does not self-extinguish after complete removal of the heat flux, then a study of intermediate heat fluxes is not necessary. If the timber does self-extinguish, then a series of tests where the applied heat flux is reduced during the test is necessary to find the heat flux at which self-extinction occurs.

The burning behavior of timber consists of two stages: transient burning and steady-state burning. Figure 10 is an example of the typical mass loss rate of timber over time. The two distinct zones of

burning are clearly evident in the curve. The first zone is a period of transient burning where the mass loss rate decreases over time. After ignition, a peak in the mass loss rate occurs. This peak is due to the absence of the char layer which insulates the unburned wood from the external heat flux. This period is marked by the presence of relatively tall flames (Figure 11, left). As the char layer increases in thickness, the mass loss rate decreases until steady-state burning. The height of the flames also decreases to relatively small flames which reach a constant height for the remainder of the test (Figure 11, right). A relatively constant mass loss rate is reached during steady-state burning and unless conditions of the burning timber sample are changed will continue to burn at this value.

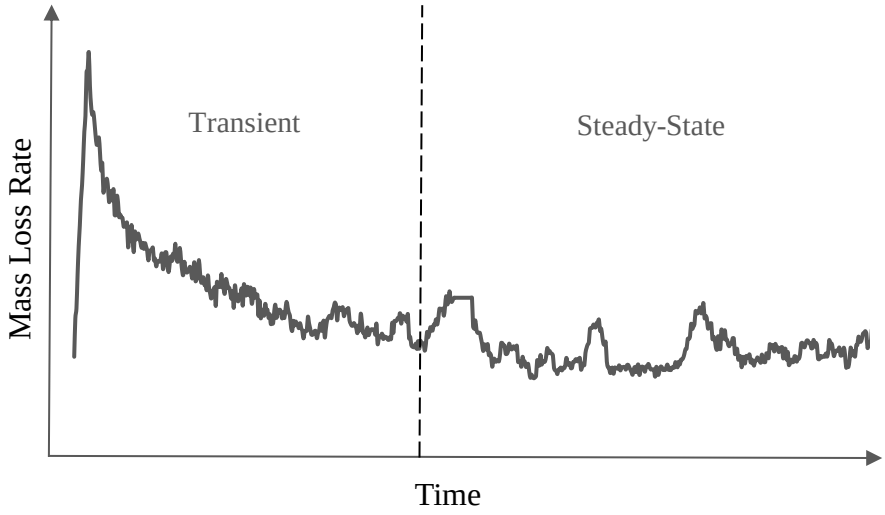

Figure 10: Example of the mass loss rate of timber over time.

Figure 11: Flame height during early stages of transient burning (left) and steady-state (right)

If self-extinction occurs during the steady-state portion of the burning duration, then self-extinction will occur at any time during steady-state. For example, if the steady-state mass loss rate of timber is

reached after 25 minutes of burning, then when self-extinction conditions are reached either at 26 minutes or 120 minutes, flaming combustion of the timber sample will self-extinguish.

The first section of tests focused on the complete removal of the heat flux during the steady-state portion of burning. If self-extinction was possible then the relatively low mass loss rate conditions was the best possible circumstances for the phenomenon to occur.

3.4.1 Steady-State Burning of Timber

In Section 3.2.1, the energy balance over the char layer was described. Steady-state energy balance is when $\frac{\partial q''}{\partial t} \approx 0$. To achieve this, each of the terms needed to remain constant over time. For this test series, the external heat flux was kept constant. As the energy generated in the char is small compared to the burning rate of the timber, the char energy generated term was neglected. Steady-state behavior of burning timber was therefore dependent on three terms: the energy lost from the surface, the thermal gradient at the pyrolysis layer, and the mass loss rate. The energy lost from the surface is dependent on the surface temperature. Each of these terms will eventually reach steady-state behavior but not necessarily at the same time. The following sections analyze each of the specific terms and show combined behavior compared to the external incident heat flux.

3.4.1.1 In-depth heat flux from the pyrolysis layer

The in-depth heat flux from the pyrolysis layer is proportional to thermal gradient and the thermal conductivity of the timber. For this analysis, the thermal conductivity was kept constant ($k = 0.13\ {}^{W}/_{mK}$) and therefore any changes in the energy were due to changes in the thermal gradient. The in-depth heat flux is the amount of the energy that is used to preheat the sample ahead of the pyrolysis front. If the amount of energy and the thermal profile remain the same then the charring rate will remain constant. The plot in Figure 12 is the in-depth heat flux over time for heat fluxes ranging from 30 to 100 kW/m^2.

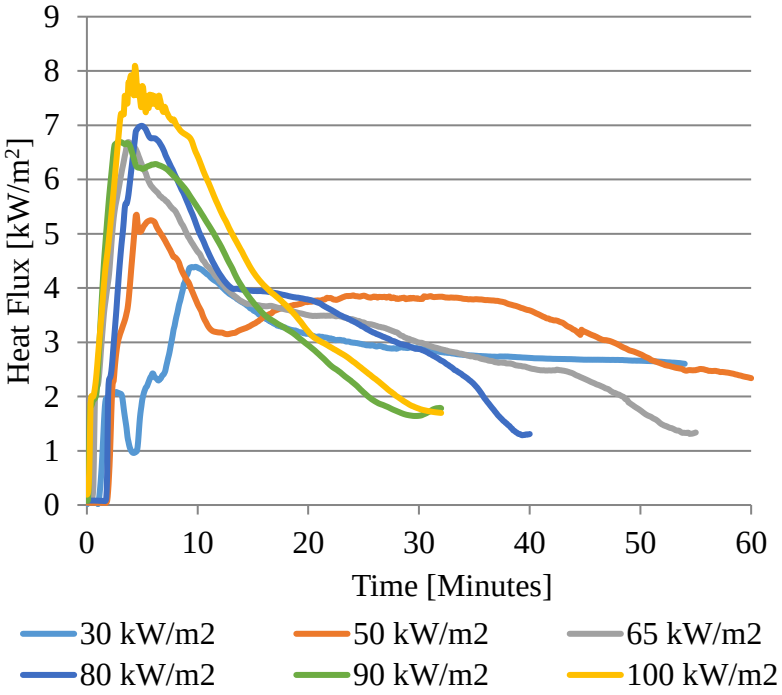

Figure 12: Transient and steady-state in-depth heat flux at the pyrolysis layer

The in-depth heat flux reaches a peak during the transient phase of the burning of the timber samples. The size of this peak increases with increasing heat flux intensity. After the peak has been reached, the in-depth heat flux decreases until a steady-state value is achieved. The lowest value in the graph was taken as the steady-state value according to theory as the heat flux values approximations via a curve fit of the thermocouple data are skewed due to the relatively low density of thermocouples deeper into the cross section. Based on the series of tests conducted for this study, the steady-state heat flux values appears to be a constant throughout the heat flux range. The magnitude of this value is approximately 1.5 kW/m^2. The value is, however, only an approximation due to the experimental set-up and the analysis techniques used to calculate the in-depth heat flux over time. As stated in Section 3.3.3, a polynomial fit of the temperature data was used to approximate a continuous thermal profile through the sample. The analysis technique works well until the pyrolysis front approaches the farthest thermocouples from the heat surface. As the thermocouples increase in temperature, the reduced density of thermocouples deeper into the cross-section does not allow for a complete thermal profile to be established. Thus, the analysis technique breaks down. Despite this, each in-depth energy profile over time has approximately the same minimum value. This implies that a lower bound exist in the in-depth energy throughout the range of heat fluxes tested.

3.4.1.2 Mass Loss Rate

The next term in the energy equation needed to be discussed is the mass loss rate. This term is fundamental in understanding the burning behavior because the mass loss rate is the rate at which the timber is being converted from solid into char and combustible gases. The mass loss rate can define whether flaming combustion is occurring and can be used to compare the burning behavior of timber while under a wide range of thermal loads. Figure 13 displays the mass loss rate over time for the timber samples with external incident heat flux ranging from 30 to 100 kW/m^2.

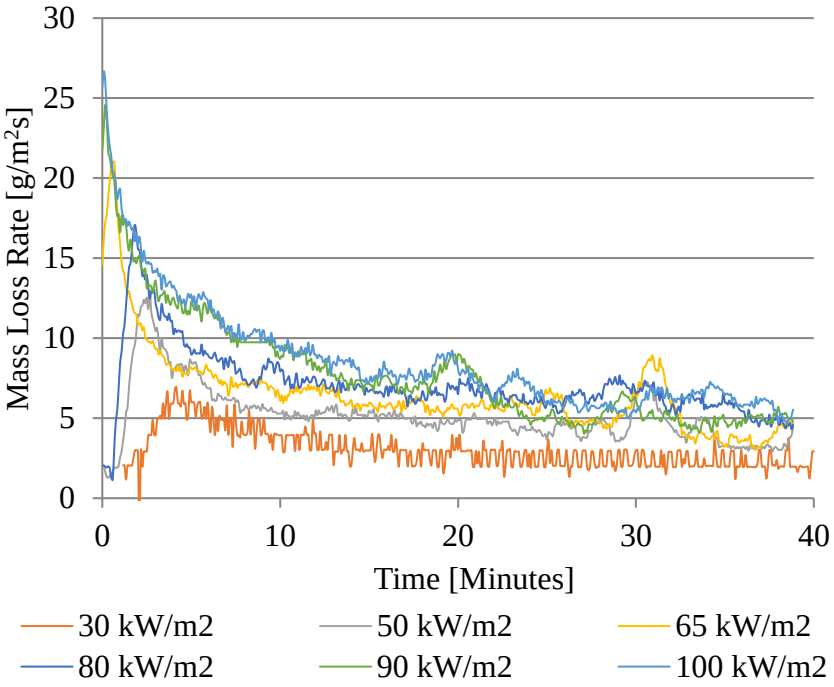

Figure 13: Transient and steady-state mass loss rate over time with increasing external applied heat flux

In Figure 13, time zero corresponds to the removal of the shield blocking the radiant heat from the cone heater to the sample. Once the heat shield was removed, the timber surface increased in temperature until ignition. Quickly after ignition the peak mass loss rate was reached followed by a decay phase which last between 10 and 15 minutes. Ignition times vary depending on the intensity of the applied heat flux. Faster ignition times correspond to higher heat fluxes.

Table **4** shows the ignition times and the type of charring that took place over the heat flux ranges. Flaming combustion occurred for every heat flux tested except for 30 kW/m^2. For this heat flux, the timber increased in temperature enough to reach the pyrolysis temperature which created a char layer;

however, the mass loss rate was not sufficient enough to initiate auto-ignition of flaming combustion. The values for the peak mass loss rate for each heat flux are in Table **4**. As the heat flux increases, the peak mass loss rate increases as well.

Table 4: Time to flaming ignition and average mass loss rate for increasing heat fluxes

Heat Flux (kW/m^2)	Charring	Time to Ignition (sec)	Average Mass Loss Rate (g/m^2s)	Peak Mass Loss Rate (g/m^2s)
30	Smoldering	N/A	2.4	5.9
50	Flaming	150	5.0	12.5
65	Flaming	60	5.8	17.1
80	Flaming	7	6.3	20.7
90	Flaming	5	6.3	24.6
100	Flaming	5	6.3	26.7

After the decay phase, steady-state mass loss rates were reached. The values of the average steady-state mass loss rates are shown in Table **4**. As the heat flux intensity increases, the average mass loss rates also increase. Above 80 kW/m^2 a constant value for the mass loss rate was observed. This suggests that heat flux intensities higher than 80 kW/m^2 will result in the same average steady-state mass loss rate.

3.4.1.3 Heat losses from heated surface

The final term in the energy equation that needs to be analyzed for a complete understanding of the burning behavior of timber is the amount of energy that is lost from the heated surface of the char layer. The total amount of energy is proportional to the surface temperature and the total heat transfer coefficient. The total heat transfer coefficient combines radiation and convection together so that a single coefficient can be multiplied to the difference between the surface temperature and the ambient temperature of the surroundings. The amount of energy lost from the surface over time is presented in Figure 14 as a heat flux.

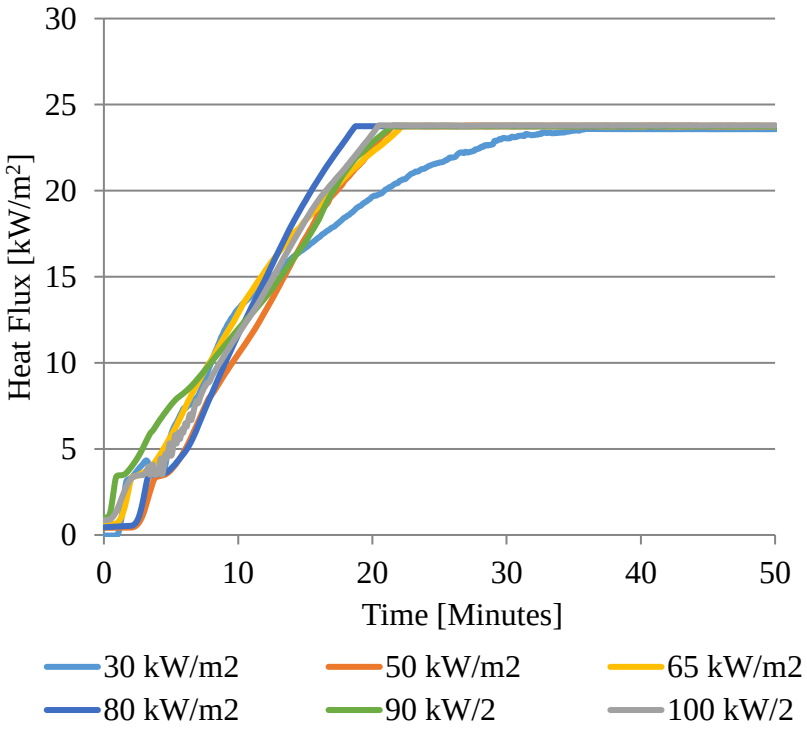

Figure 14: Transient and steady-state energy losses from the surface over time with increasing external applied heat flux

For the entire range of heat fluxes used in this study, the trend of the energy lost from the surface is nearly identical. The rate at which the energy increases between the samples is the same at 19.4 W/m^{2}s. Around 20 minutes after exposure to the thermal load, the surface temperature reaches a constant temperature and thus the losses from the surface reach a constant value around 23.4 kW/m^2. The surface temperature is assumed to then remain constant for the duration of the burning of the timber. Only when the heat flux is removed will the surface temperature of the char decrease in temperature.

The difference between the non-flaming and flaming combustion is apparent in Figure 14. Flaming combustion as shown in

Table **4** occurred at 50 kW/m^2 and higher. Auto-ignition of the timber did not occur at 30 kW/m^2 and therefore only charring (not flaming) of the sample occurred. The result is that the surface temperature took longer to increase in temperature and as a result the energy losses only reached the constant maximum value around 35 minutes as opposed to the 20 minutes of the rest of the samples where flaming combustion took place. This highlights the role of the heat flux from the flames in increasing the surface temperature of the samples.

3.4.1.4 Charring Rates

A factor which needs to be discussed is the charring rate. This pertains both to the heat transfer through the timber sample as well as the structural degradation of a timber member as outlined in Section 2.3. The charring rate is a principle that focusses on the progression of a particular isotherm throughout the timber during the burning process. This isotherm idealizes the pyrolysis layer from a wide thickness to a single differential element at a particular temperature. For the analysis in this study, the 300°C isotherm was chosen to be consistent with current literature on modeling of charring timber.

The charring rate, like the mass loss rate, has an initial peak at the beginning of the burning process as shown in Figure 15. The charring rate then decreases to a steady-state value for the duration of the exposure. The charring rate shown in Figure 15 is based solely on the location of the 300°C isotherm.

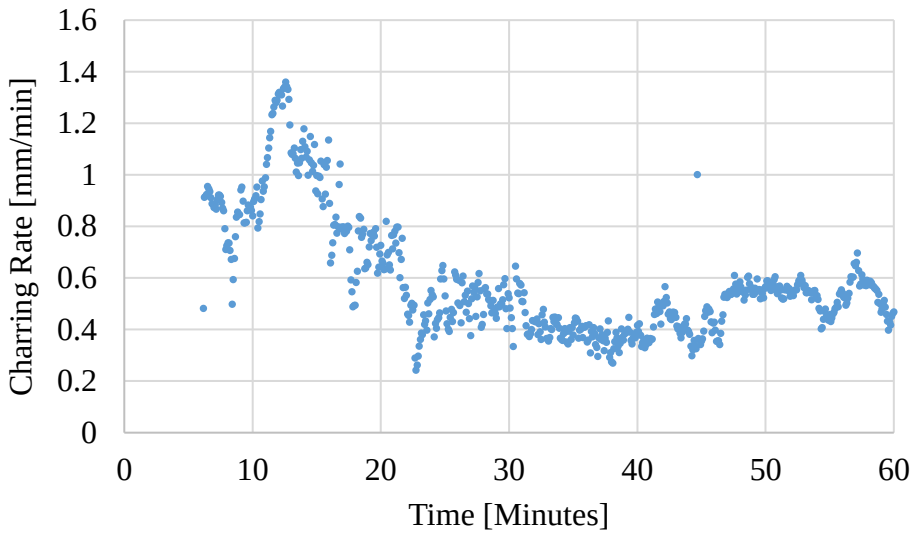

Figure 15: Charring rate of timber exposed to a 50 kW/m^2 heat flux

The charring rate can be calculated using two different methods: the isotherm method and the mass loss rate method. The mass loss rate method takes the mass loss rate measured from the scale and divides it by the density ($\rho = 425\ kg/m^3$) to calculate the charring rate. The two methods will always yield different results due to the presence of moisture in the timber and the fact that the char is decomposing as well. The mass loss rate method allows for the fact that pyrolysis occurs over a wide range of temperatures; however, the moisture and char mass loss is incorporated into the value as well. The 300°C isotherm method only accounts for the movement of the differential pyrolysis front at a specific temperature.

For this study, the average and peak charring rates are shown in Table 5. The values for the peak and average charring rates at a specific heat flux are similar but slightly different. The charring rates for the 300°C isotherm method tend to be lower for the entire range of heat fluxes tested.

Several trends are visible in the results. For the mass loss rate method, the peak charring rate increases with increasing heat flux; conversely, this appears to remain a constant value as with the isotherm method. The average charring rate is dependent of the method and reaches a constant value even as the applied heat increases in intensity. While the magnitude of the charring rate values between the two methods are slightly different, the overall trend remains the same. The average charring rate value over the entire range of flaming combustion heat fluxes for the isotherm method is approximately 0.56 mm/min. The most accurate way to determine the charring rate is with the isotherm method as the specific isotherm can be tracked through the cross section. The mass loss rate method includes sources of error such as moisture loss and migration.

Table 5: Average and peak charring rates at increasing heat fluxes

Heat Flux (kW/m^2)	Mass Loss Rate		300°C Isotherm	
	Average Charring Rate [mm/min]	Peak Charring Rate [mm/min]	Average Charring Rate [mm/min]	Peak Charring Rate [mm/min]
30	0.34	0.83	0.3	0.9
50	0.71	1.76	0.5	1.3
65	0.82	2.41	0.6	1.2
80	0.89	2.92	0.7	1.2
90	0.89	3.47	0.5	1.5
100	0.89	3.77	0.5	1.6

3.4.1.5 Steady-State Burning of Timber

In order to assess the complete steady-state burning regime of timber, an analysis which compares the three variables listed in Section 3.4.1 was completed. Each of the variables has the potential of reaching steady-state burning at different times during the burning process. This section highlights both flaming combustion and smoldering combustion of the timber samples.

The graph in Figure 16 displays the individual variable results for a timber sample exposed to a heat flux of 30 kW/^{2}. The 30 kW/m^2 did not ignite and therefore only smoldering combustion occurred. The mass loss rate reached steady-state around 20 minutes after initial exposure to the thermal load. The in-depth energy as well as the energy losses from the heated surface reach steady-state around 30 minutes. Therefore, the burning behavior of the entire block reached complete steady-state at 30 minutes. Without any disruption of the sample and with the external heat flux kept constant the burning timber would continue to burn at these variable values.

A graph of individual variables for a typical flaming combustion test are shown in Figure 17. This graph specifically shows the results for a timber sample exposed to a 90 kW/m^2 heat flux. Similar trends to the 30 kW/m^2 test are seen. The duration to steady-state, however, is slightly shorter. The energy lost from the heated surface and the in-depth energy conduction reach steady-state around 20 minutes. The mass loss rate also reaches steady-state around 20 minutes. One of the most notable difference between the 30 kW/m^2 and the 90 kW/m^2 is the magnitude of the mass loss rate. Due to the presence of flaming combustion, the average mass loss rate for the 90 kW/m^2 thermal load is approximately double the average mass loss rate of the 30 kW/m^2 exposure.

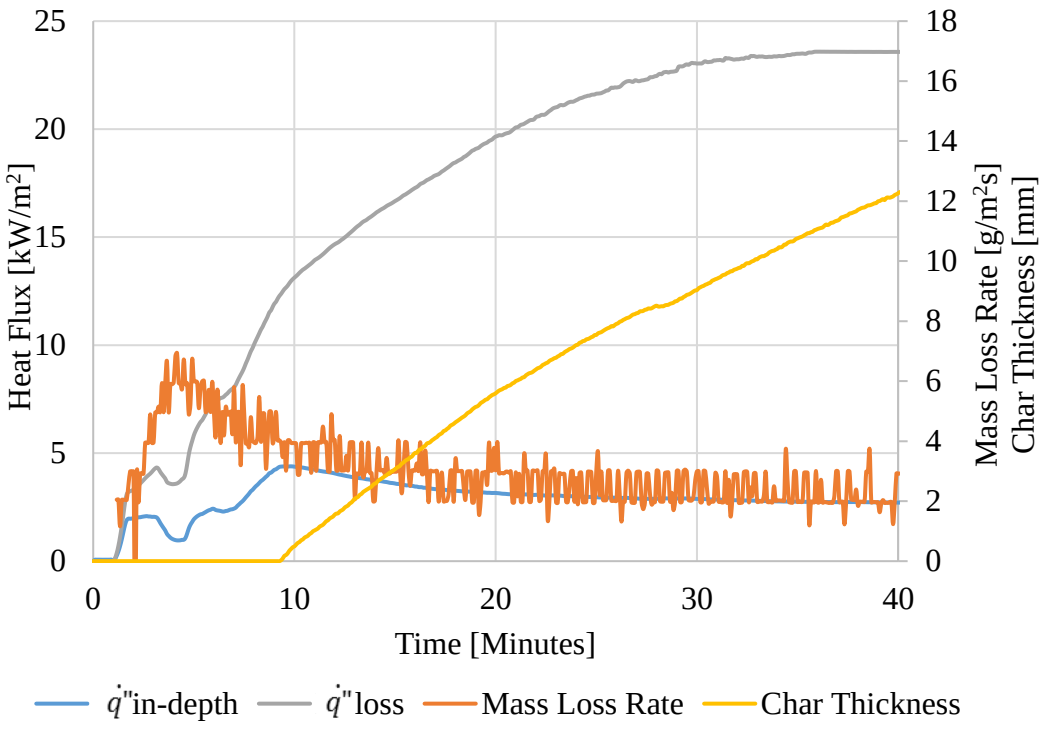

Figure 16: Mass loss rate, surface energy losses, char thickness, and in-depth energy transfer from the pyrolysis layer for 30 kW/m^2

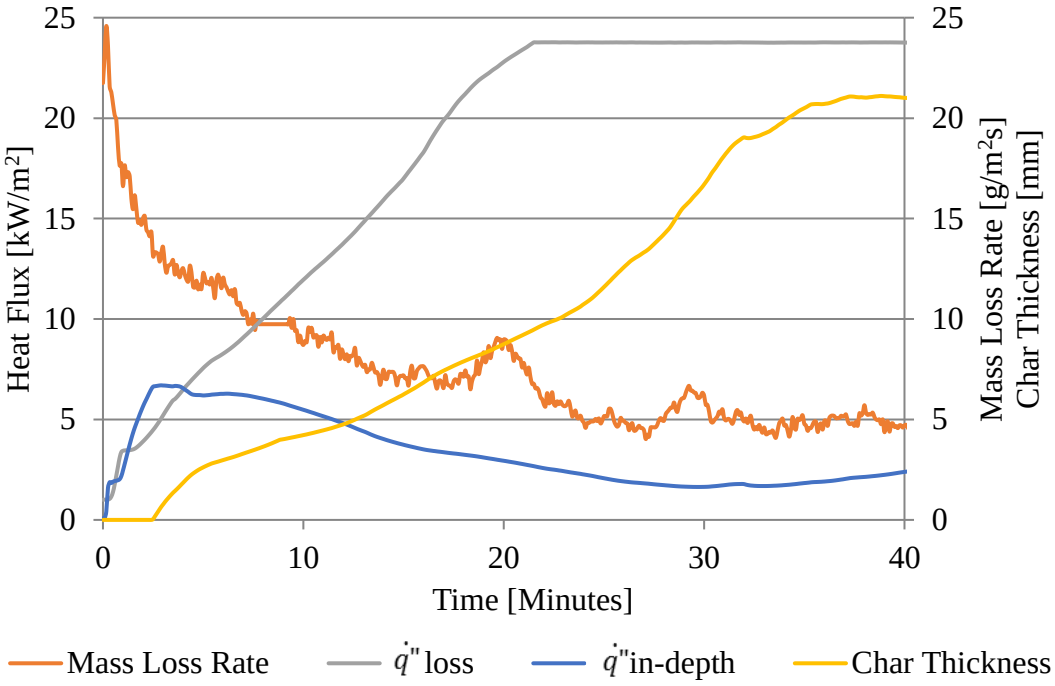

Figure 17: Mass loss rate, surface energy losses, char thickness, and in-depth energy transfer from the pyrolysis layer for 90 kW/m^2

In comparing the char thickness with the energy transferred from the pyrolysis layer, a trend among all the tests conducted becomes apparent. The peak in the in-depth energy corresponds to the start of the char layer increasing in thickness. Without the char layer present, the transfer for energy from the surface into the unburned timber is solely through conduction through the timber. However, as the char layer is formed, the insulating properties of the char act as a barrier which regulates the amount of energy that enters the pyrolysis layer and then into the unburned timber. The trend seen in Figure 16 and Figure 17 was seen in every test conducted in this study.

3.4.1.6 Self-extinction Results

In order to assess the self-extinction threshold of the timber samples, the thermal loading conditions needed to be changed. The first variation in the process was complete removal of the heat flux. The radiant energy was completely blocked by usage of a thermal shield placed between the sample and the cone heater. The external heat flux to the sample was reduced to zero. Complete removal of the heat flux was done for every value of heat flux tested.

Figure 18-Figure 20 are plots of the individual variables of the energy equation for external heat fluxes of 50, 80 and 90 kW/m^2 respectively. The black vertical lines towards the latter stages of the

graph indicate the time when the external heat flux was eliminated. Almost immediately after the removal of the external heat flux, self-extinction of flaming combustion occurred. The mass loss rate reduced to either smoldering combustion or complete extinction of combustion altogether. The flames from the combustion of the timber could not provide a heat flux of sufficient magnitude to continue the pyrolysis of the timber.

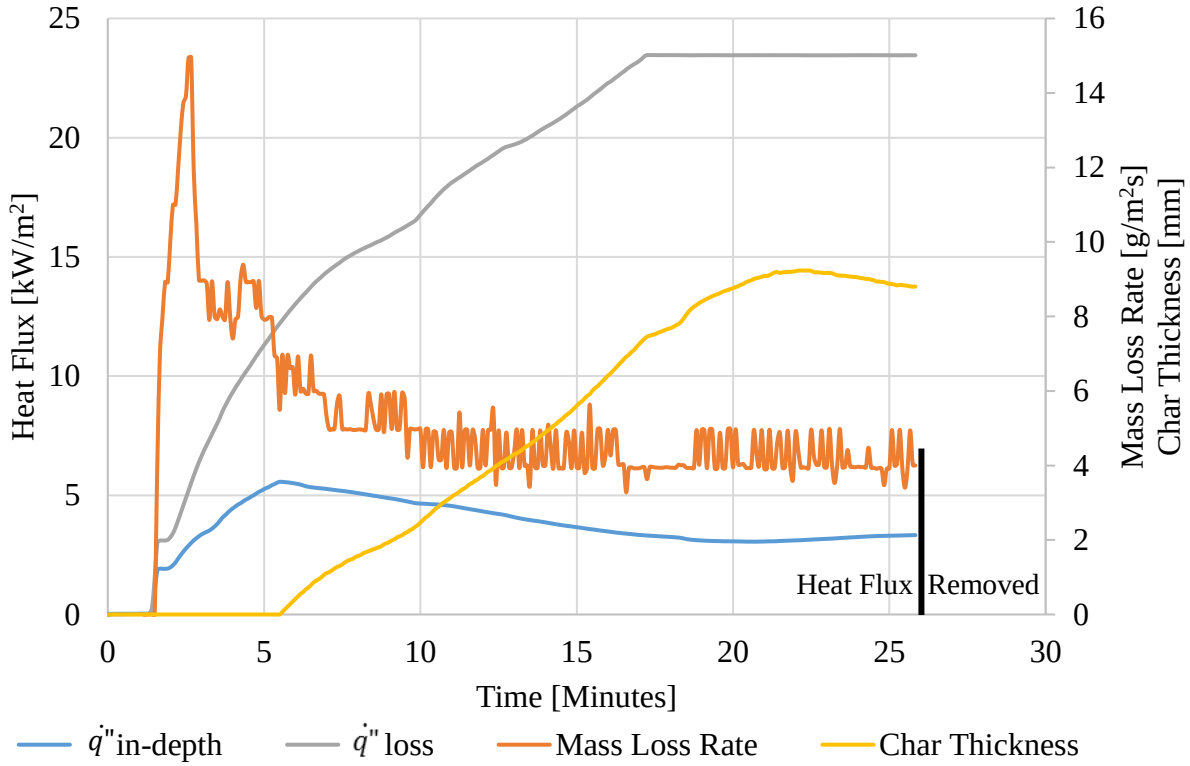

Figure 18: Mass loss rate, surface energy losses, char thickness, and in-depth energy transfer from the pyrolysis layer for 50 kW/m² before removal of heat flux

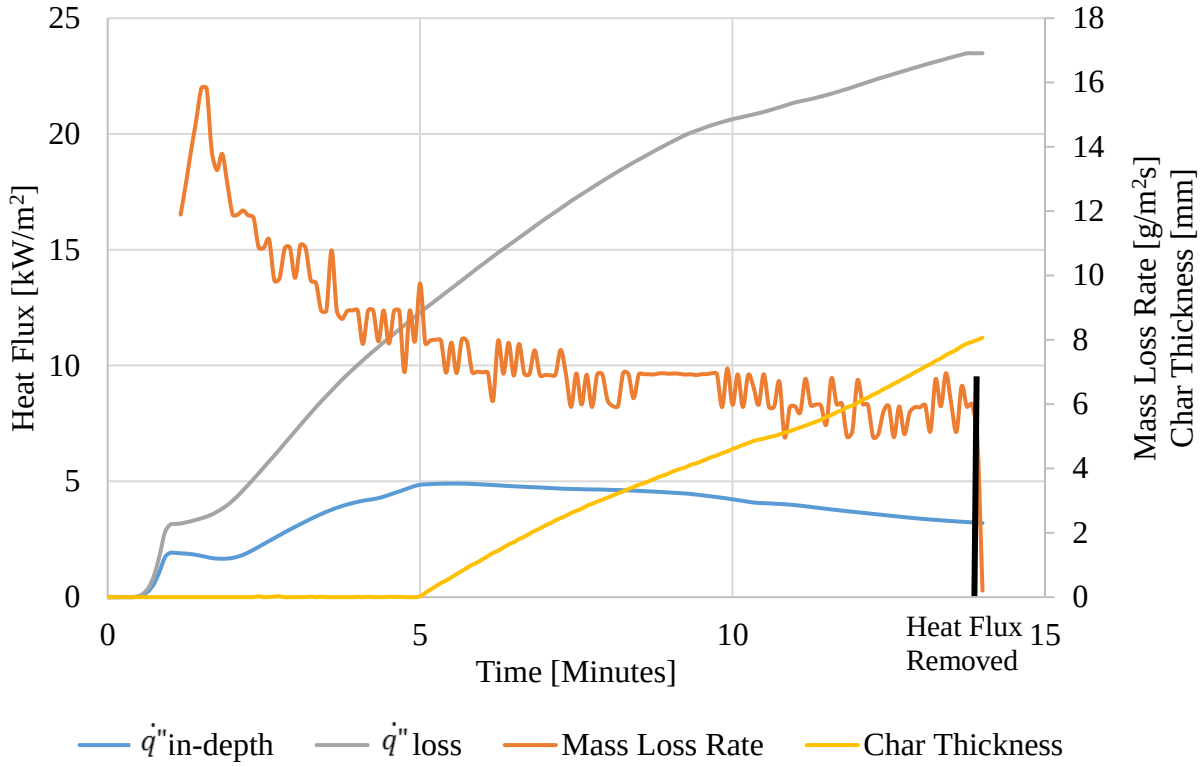

Figure 19: Mass loss rate, surface energy losses, char thickness, and in-depth energy transfer from the pyrolysis layer for 80 kW/m^2 before removal of heat flux

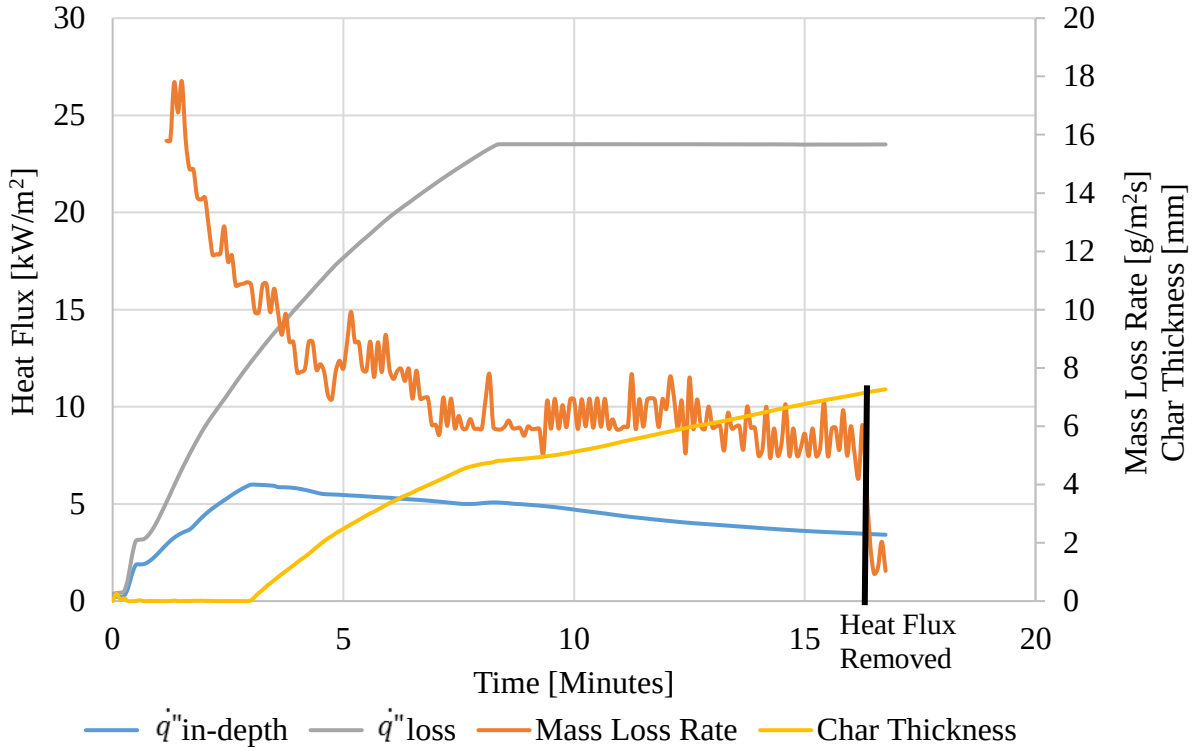

Figure 20: Mass loss rate, surface energy losses, char thickness, and in-depth energy transfer from the pyrolysis layer for 90 kW/m^2 before removal of heat flux

Self-extinction after the complete removal of the external heat flux occurred in every test while the sample was under steady-state conditions. Since self-extinction occurred during the steady-state portion of the burning process, then self-extinction will occur independent of the length of the time in steady-state burning. Whether steady-state burning lasts for 5 minutes or 50 minutes, self-extinction will occur according to the results presented in this section. The results in this section covered the steady-state portion of the combustion of timber.

The next section concludes the analysis of completely removing the heat flux by analyzing the effects of removing the heat flux during the transient portion of the combustion process.

3.4.2 Transient Burning of Timber

In order for self-extinction of timber to occur during the entire combustion process, self-extinction has to occur during the transient portion as in the case of steady-state burning. The transient portion of the combustion process actually represents a worst-case scenario as the thermal gradient and thus the amount of energy transferred from the surface into the unburned timber is at higher values than at steady-state. As shown in Figure 12, Figure 16 and Figure 17, the peak in-depth energy transferred

through conduction occurs at the beginning of the heating when the char layer is just beginning to form. After the char layer begins to increase in temperature, the in-depth energy values decrease to steady-state. The peak in-depth energy values can be seen in Table **4**. If self-extinction is achieved at the peak of the in-depth energy consumption then self-extinction will occur at any point during the transient heating stage.

The amount of energy that is transferred from the external heat flux to preheat the unburned timber is shown in Figure 21. The plot shows the ratio of the energy conducted into unburned timber to the external incident heat flux. As the external heat flux increases in magnitude, the percentage of the amount of the energy that is transferred into the unburned timber reduces. In the case for flaming combustion, the worst-case scenario is represented by the 50 kW/m^2 external applied heat flux. For the 50 kW/m^2 heat flux, approximately 10% of the energy applied to the system is used to preheat the timber in front of the pyrolysis zone. If self-extinction occurs during the transient stages of the 50 kW/m^2, since this represents the worst-case scenario for preheating, then self-extinction will occur for higher heat fluxes if the external heat flux is completely removed.

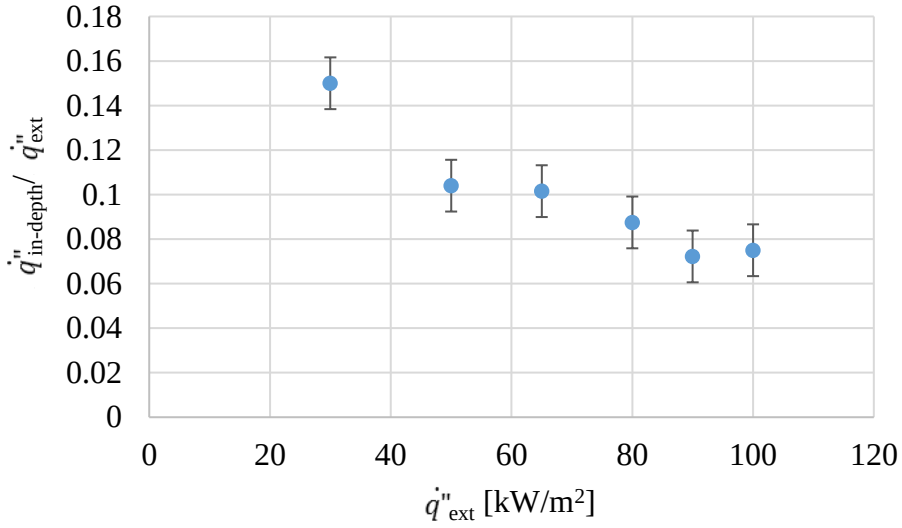

Figure 21: Ratio of peak in-depth energy losses through conduction and the external heat flux.

In order to assess the self-extinction capacity during the transient portion of the heating, the heat flux was removed at various times during the transient stage. The heat flux used for this aspect of the study was 65 kW/m^2 and the timber block was allowed to burn for 0.5, 1, 2, 3, 6, and 9 minutes after exposure to the thermal load.

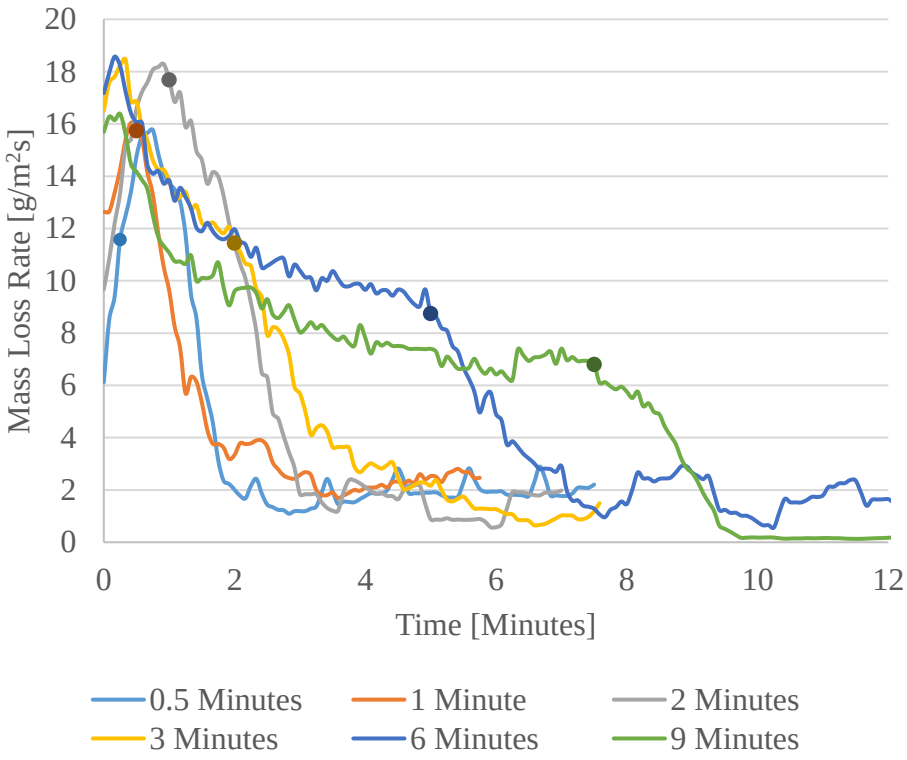

Figure 22: Mass loss rate of timber exposed to 65 kW/m^2. Complete heat flux removal indicated by solid dots.

Figure 22 shows the results from the 65 kW/m^2 heat flux test with decreasing exposure times. Until the heat flux is removed the results from each separate test are consistent. After the removal of the heat flux, the mass loss rate drops to zero or nearly zero in every scenario tested. Since self-extinction occurred at approximately the worst-case scenario heat flux and for the peak mass loss rate and in-depth energy values, self-extinction will occur for every flaming combustion scenario during the transient portion of the burning process. Therefore, for the complete removal of an external heat flux during any stage of the combustion of timber, self-extinction of flaming combustion will occur.

3.5 Reduction of Heat Flux Results

The previous section has demonstrated that self-extinction occurs during both the transient and steady-state phases of burning timber; the next step in understanding self-extinction is to characterize the critical heat flux and mass loss rate for extinction of flaming combustion. To achieve this, an experimental methodology was implemented in exactly the same manner as in detailed in Section 3.3 and 3.4; however, instead of reducing the external heat flux to zero by blocking the radiant heat from the cone heater, the external heat flux on the heated surface was reduced. In several experiments the heat flux was reduced by turning the cone heater down and in others the experiment was left to burn until the surface regression of the char layer moved the heated surface away from the cone heater

enough to reduce the heat flux to self-extinction levels. For tests where the external applied heat flux was a combination of the reduced heat flux from the cone heater and the surface regression, a heat flux meter was used to measure the heat flux at the distance the char layer had receded to at the time of self-extinction.

Figure 23 shows the mass loss rate from a timber sample with an initial thermal load of 50 kW/m^2. The mass loss rate was allowed to reach steady-state after which the heat flux was reduced. The heat flux was reduced to approximately 33 kW/m^2 at 10 minutes after exposure to the heat flux. The mass loss rate immediately started to decrease and self-extinction occured several seconds after the heat flux was reduced. The point of self-extinction is marked by the solid vertical black line in Figure 23. Due to the reduced yet sustained thermal load the mass loss rate plateaus to a rate below the critical value for extinction and continues to smolder.

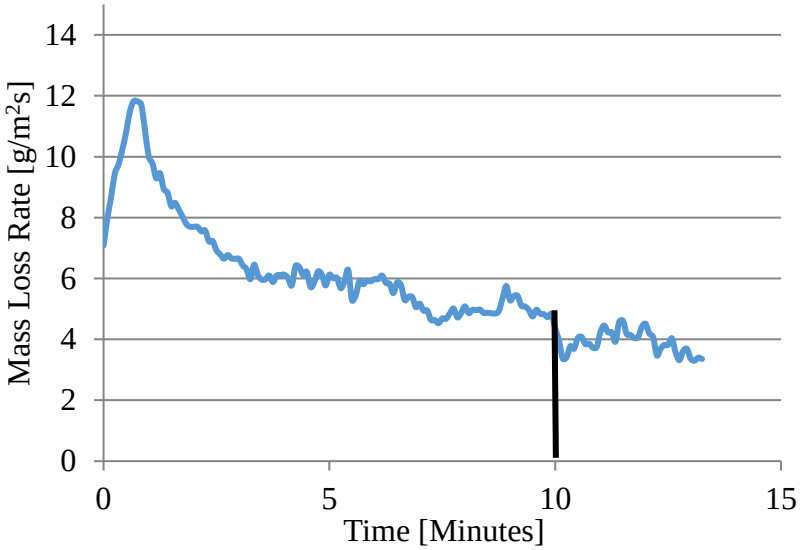

Figure 23: Mass loss rate curve of a 50 kW/m^2 heat flux exposure. External heat flux was reduced at 10 minutes

Figure 24 shows the mass loss rate curve in the case where heat flux was initially set to 100 kW/m^2. The mass loss rate was allowed to reach steady state and was held constant for approximately 28 minutes. The heat flux of the cone was then reduced to 50 kW/m^2. A decrease in the mass loss rate can be seen between 28 and 32 minutes. At approximately 31 minutes, self-extinction of flaming combustion occurs. The char had regressed approximately 25mm and the thus the heat flux was measured from 50mm away from the cone. The corresponding external heat flux at self-extinction was 41.8 kW/m^2.

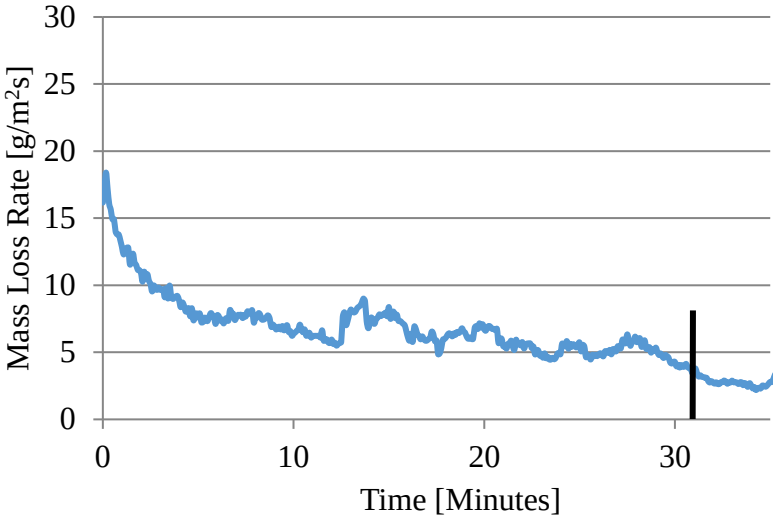

Figure 24: Mass loss rate curve of a 100 kW/m^2 heat flux exposure. External heat flux was reduced at 28 minutes to 50 kW/m^2.

In each test after self-extinction had occurred, the mass loss rate reduced to smoldering combustion values similar to the 30 kW/m^2 heat flux test shown in Figure 16. In the 30 kW/m^2 test, flaming combustion never occurred and the charring was solely due to smoldering combustion of the timber.

If the results from each of the tests are combined, then a trend in the critical mass loss rate and the associated external heat flux can be seen. Figure 25 shows the mass loss rate at self-extinction plotted against the external heat flux at self-extinction. The critical mass loss rate for self-extinction is 3.93 ± 0.45 g/m^{2}s. The external heat flux at self-extinction is 43.6 ± 4.7 kW/m^2. This point on the graph separates two distinct zones: flaming combustion and self-extinction. Self-extinction in this region is self-extinction of flaming combustion. As shown in Figure 23 and Figure 24, smoldering will continue as long as an external heat flux is present at a sufficient level to sustain smoldering combustion. The critical mass loss rate for self-extinction is consistent with the results from previous studies [50-52]. Based on the time to ignition, the critical heat flux for auto-ignition was determined to be 47.5 kW/m^2. The slight difference in magnitude between the auto-ignition and extinction heat flux could be due to a number of different processes but in particular to the significant period where flames were present to degrade the surface; none of these phenomena can be easily quantified using the current experimental methodology.

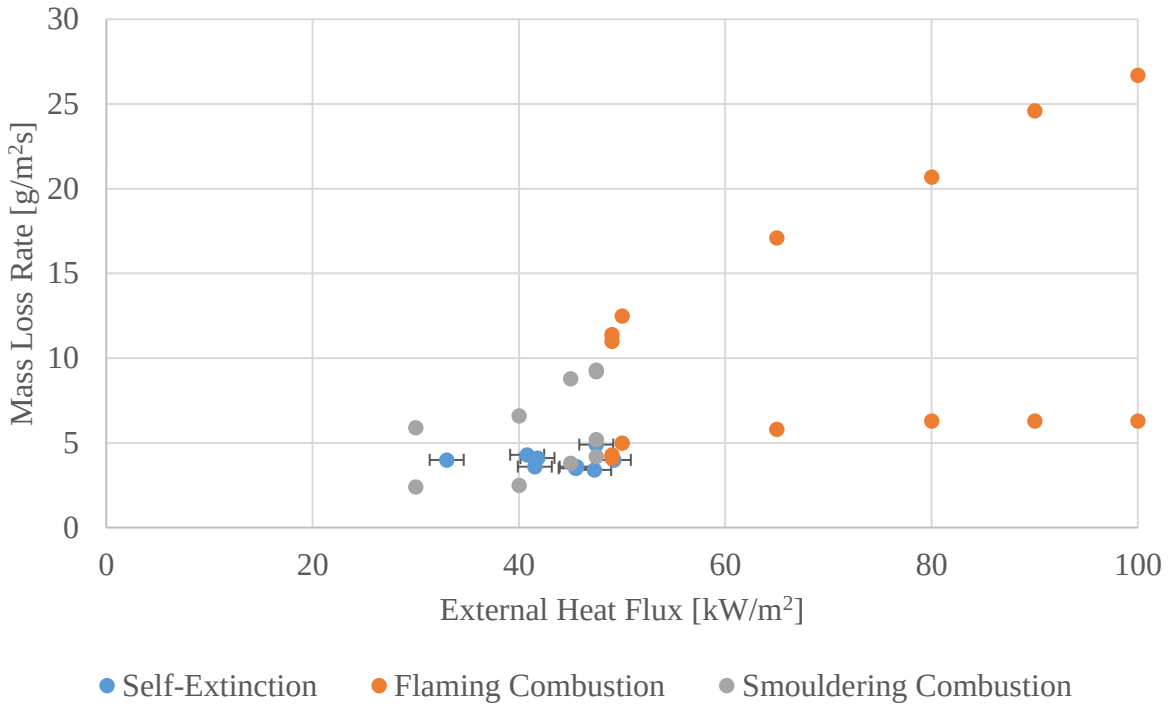

Figure 25: Mass loss rate and external heat flux at self-extinction

3.6 Debonding and Other Re-Ignition Scenarios

Sections 3.4 and 3.5 have comprehensively identified the characteristics for self-extinction of CLT. However, a major caveat must be placed upon the validity of this data; the results are valid only while the samples remain in one piece and without major fissures. Through the tests, variations in the ability of the samples to self-extinguish were observed. The instances where self-extinction either failed or re-ignition occurred can be clearly seen in the mass loss rate curves and by comparing these curves to the results presented in Section 3.5.

The first type of debonding was instances where small gaps in the adhesive bond line opened allowing spaces for combustible gases to collect increasing in fuel concentration until the flammability limit was reached. Once the flammability was reached re-ignition or partial re-ignition occurred. Small localized flames and puffing action of the flames was visible. This scenario was particularly evident in two tests at 55 kW/m^2 heat flux exposure. The first test is presented in Figure 26. After the mass loss rate reached steady-state, self-extinction occurred at approximately 53 minutes (solid black vertical line). After smoldering for 11 minutes, re-ignition occurred on the top surface of the timber block after a slight gap opened up on the top of the sample. Flaming combustion continued for around six minutes before self-extinction occurred again. In Figure 26, the period of re-ignition is indicated by the orange block. Figure 27 clearly shows the gap in the bond line forming (left figure) and then flaming combustion occurring around the gap on the top surface (right figure). When re-ignition of

flaming combustion occurs, the mass loss rate value increases above the critical mass loss value for self-extinction presented in Figure 25.

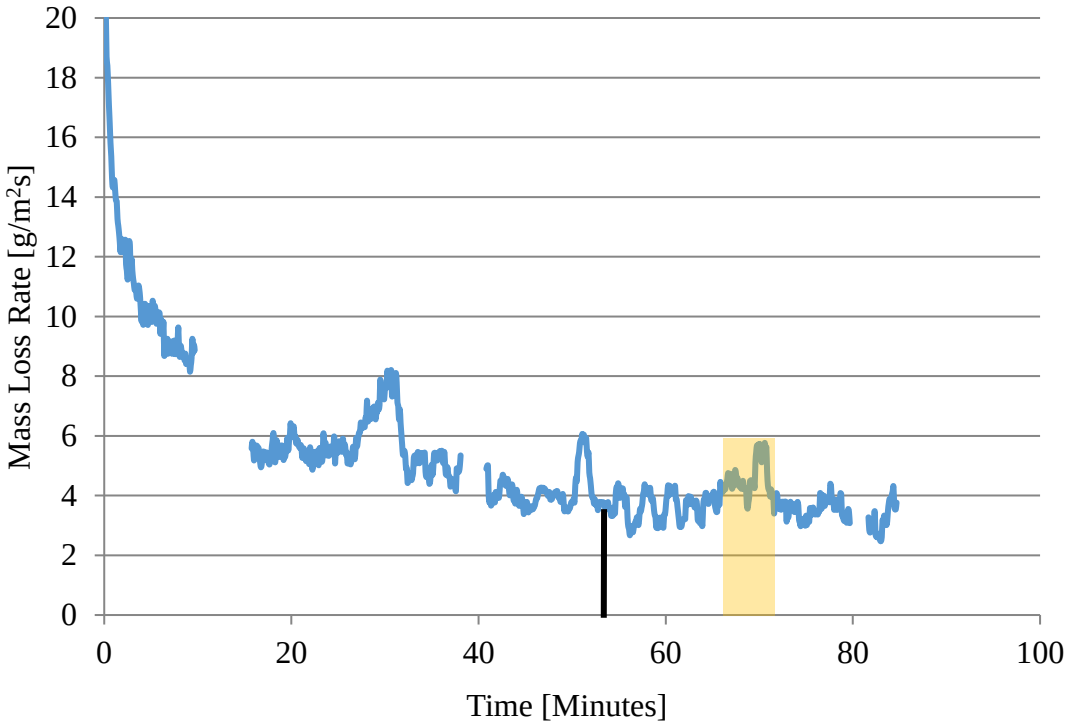

Figure 26: Mass loss rate over time for a sample exposed to 55 kW/m^2 heat flux. Gaps in the data are due to errors in the data logging.

Figure 27: Bond line separation and re-ignition near the top surface of a sample exposed to 55 kW/m^2 heat flux.

The flames were relatively small and only lasted for a small period of time. Nevertheless, the mass loss rate and increased the burning duration. In the second test at 55 kW/m^2, the gap in the bond line was not as apparent but as shown in Figure 28 small flames were still on the top surface. The small flames are positioned directly over a bond line indicating that a gap had formed where combustible gases could collect and increase the local fuel to air ratio. These flames only lasted several seconds

because as soon as the combustible gases ignited, the fuel was consumed and self-extinction occurred again.

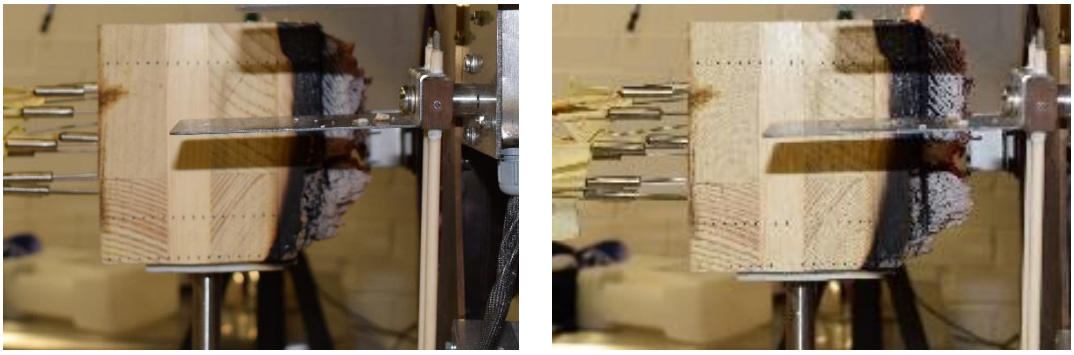

Figure 28: Re-ignition near the top surface of a sample exposed to 55 kW/m^2 heat flux.

Another instance of debonding that prevented self-extinction was the case where re-ignition occurred along the entire height of the bond. The type of re-ignition shown in Figure 29 produced flames much larger than those in Figure 28 because of the amount of timber and glue that was exposed to oxygen and heat due to the debonding. The larger flames caused peaks in the mass loss graph as shown in the shaded boxes of Figure 31. When the entire bond line was compromised and a large separation opened, greater increases in flame height and mass loss occurred as shown in Figure 30. The large flames and the large increase in the mass loss rate did not last for extended periods; however, a combination of all these variables could lead to instances where self-extinction would never occur.

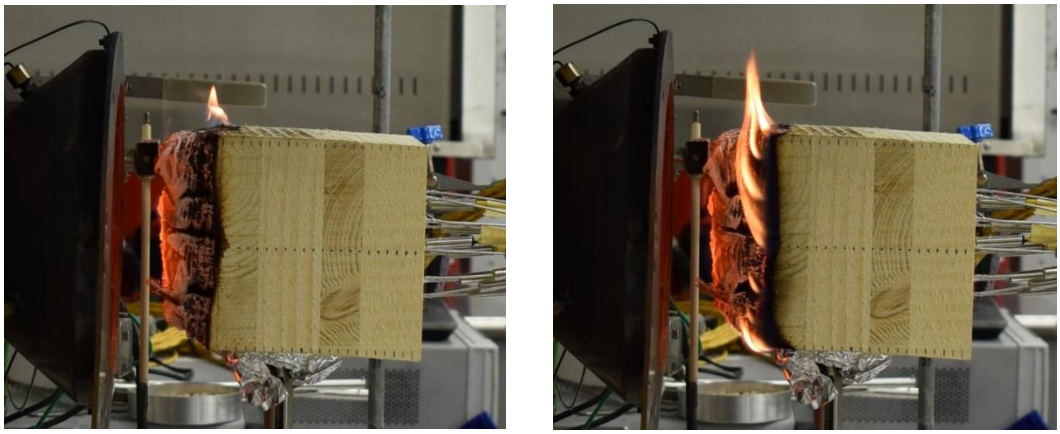

Figure 29: Re-ignition along the height of the bond line of a sample exposed to 65 kW/m^2 heat flux.

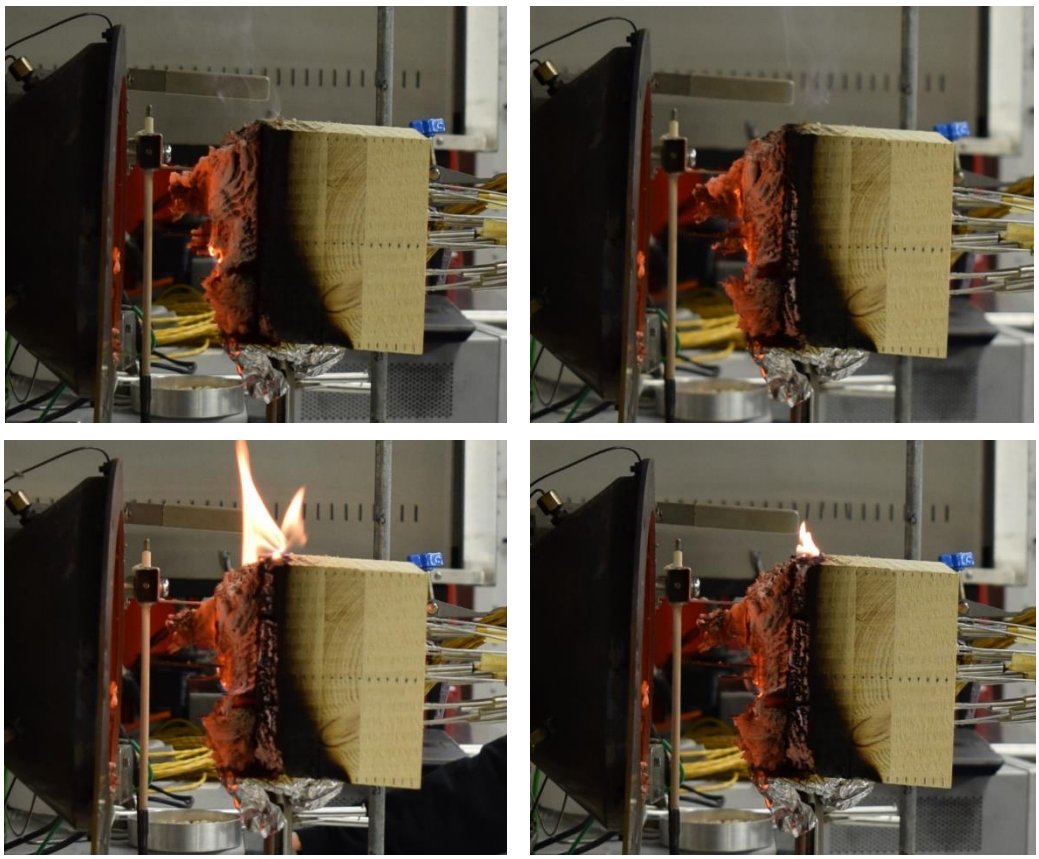

Figure 30: Re-ignition near the top surface of a sample exposed to 65 kW/m^2 heat flux. Progression from top left (clockwise).

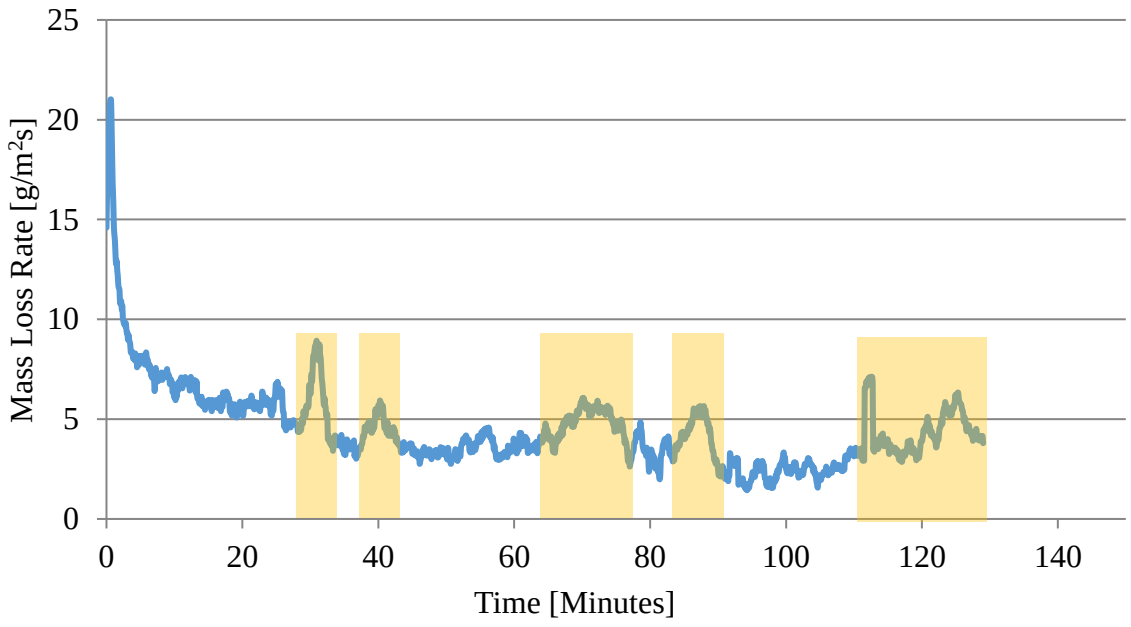

Figure 31: Mass loss rate of CLT sample exposed to a 65 kW/m^2 heat flux. Instances of increases in flame height and re-ignition are boxed.

Larger pieces of char fall-off produced more sustained burning. Figure 32 highlights the progression from full intact char to char fall-off; this progression also induced a corresponding large increases in mass loss rate (Figure 33). In this test, thermocouples prevented a significant portion of the char from debonding; hence, the mass loss rate was not representative of a non-instrumented sample. The lower right pictures in Figure 32 show this clearly. The lower part of the char remained while the thermocouples positioned in the middle of the sample kept the top char layer in position between the heat flux and the unburned timber. Figure 32 again shows the position of the flames on the upper surface of sample. The flames were oriented directly over a bond line. In this case the bond line was the first bond line away from the cone heater. Larger amounts of char yielded smaller flames when re-ignition occurred; however, smaller amounts of char left in place allowed a greater amount of heat flux to reach the pyrolysis front.

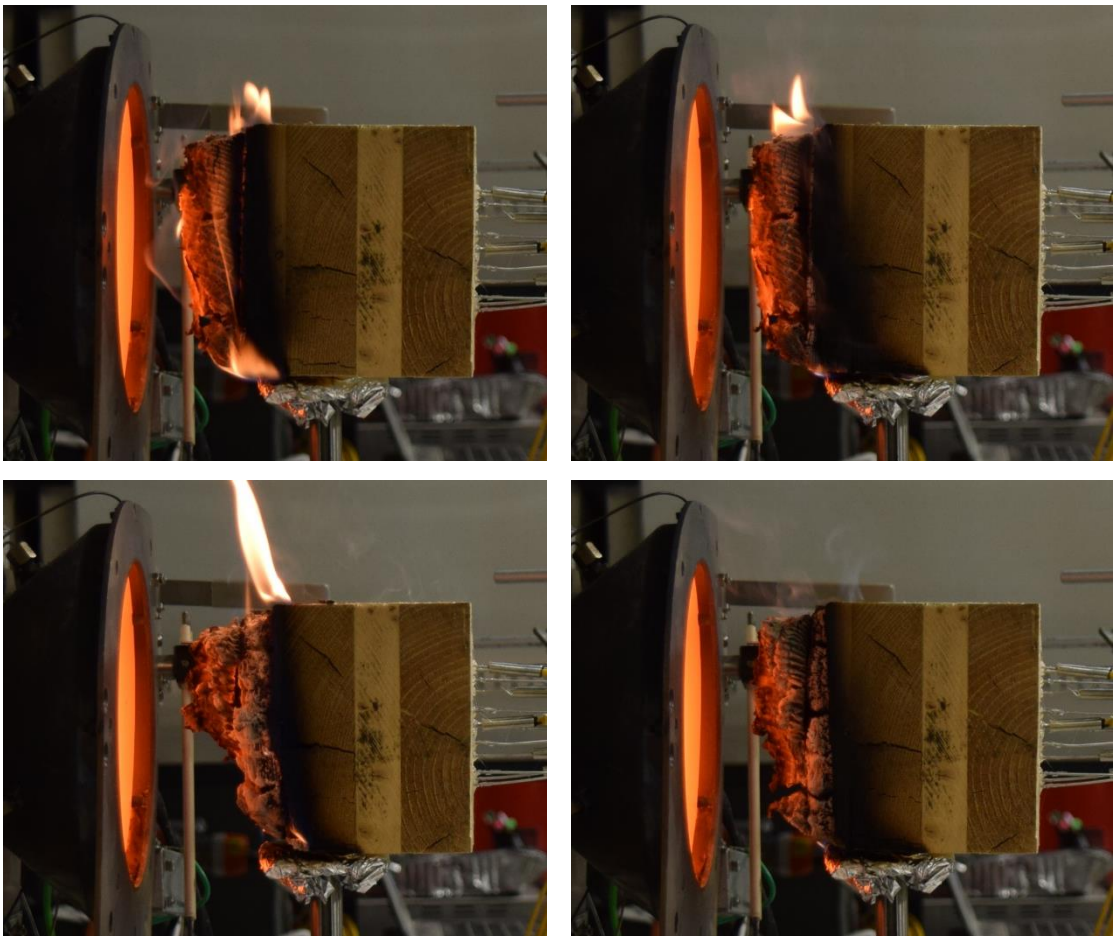

Figure 32: Re-ignition near the top surface of a sample exposed to 80 kW/m^2 heat flux after char debonding fall-off. Starting top left and proceeding clockwise.

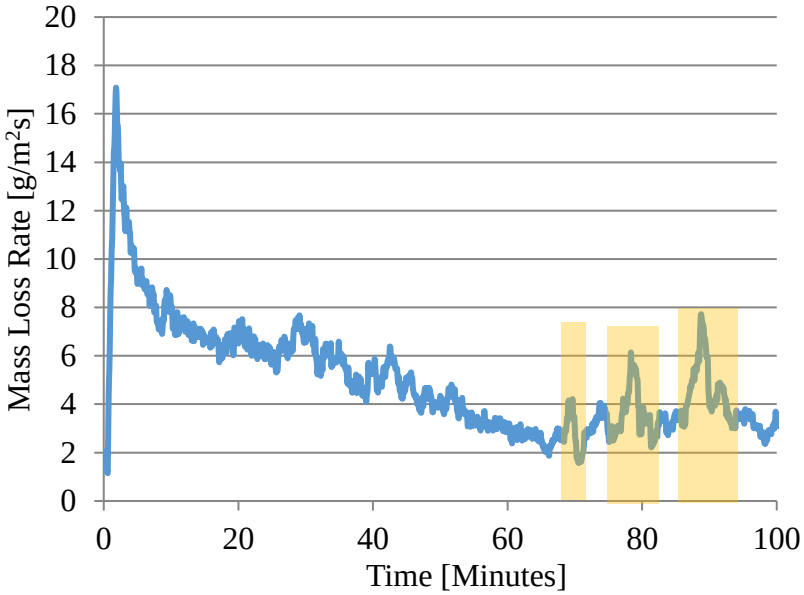

Figure 33: Mass loss rate of CLT sample exposed to an 80 kW/m^2 heat flux. Instances of increases in flame height and re-ignition are boxed.

Other forms of non-steady state flaming occurred in a number of samples where self-extinction would not have been possible due to the high heat fluxes used. Figure 34 shows the increase in flame height after a crack formed in the char layer—ignition of flames was along the bond line edge. A crack in the char began to form which allowed an area with excess oxygen to form and allowed pyrolysis gases to increase. The location close to the unburned timber led to an increase in the mass loss rate and increased the flame height at that location. The non-uniform cracking that forms in the char layer allowed locations for the heat flux to penetrate deeper into the char layer, closer to the pyrolysis zone. While not seen in this study due to the selection of the sample types, gaps in the engineered timber such as space between two boards in a CLT slab have the potential to provide a "weak point" that after self-extinction occurs) may lead to increased charring and re-ignition.

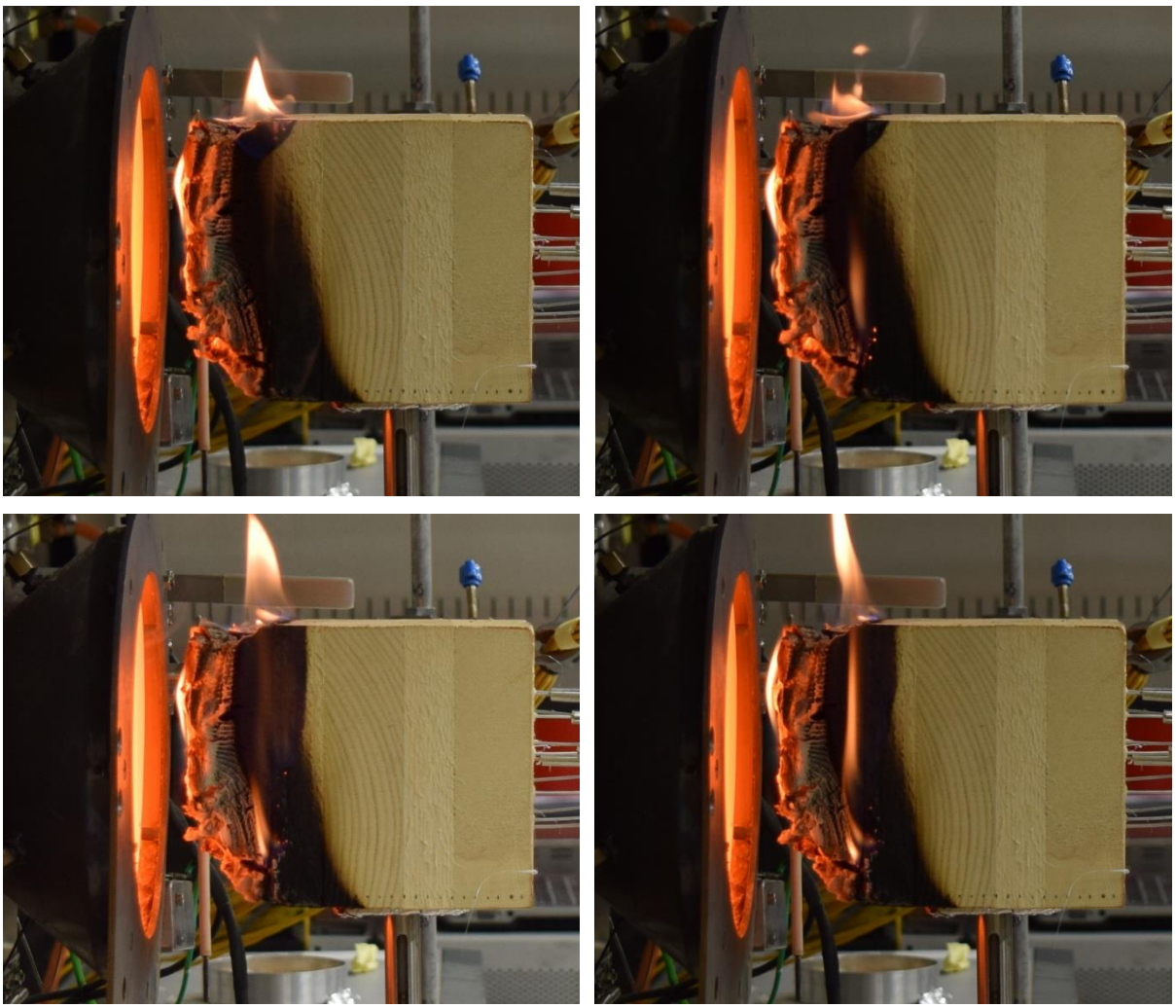

Figure 34: Ignition near the top surface of a sample exposed to 90 kW/m^2 heat flux. Starting top left and proceeding clockwise.

The final type of debonding failure was a complete debonding of the char layer (Figure 35). In this case, the thermocouples held the char layer in place. However, the top right picture clearly shows the entire bond line separated from the rest of the section. Slowly over the next several minutes, pieces of the char fell off from the thermocouples until most of the char layer had fallen off and large flames returned as in the case of the beginning of the test.

These scenarios represent the cases where self-extinction either did not occur and re-ignition or a return to higher mass loss rates occurred as a result of the loss of the char layer.

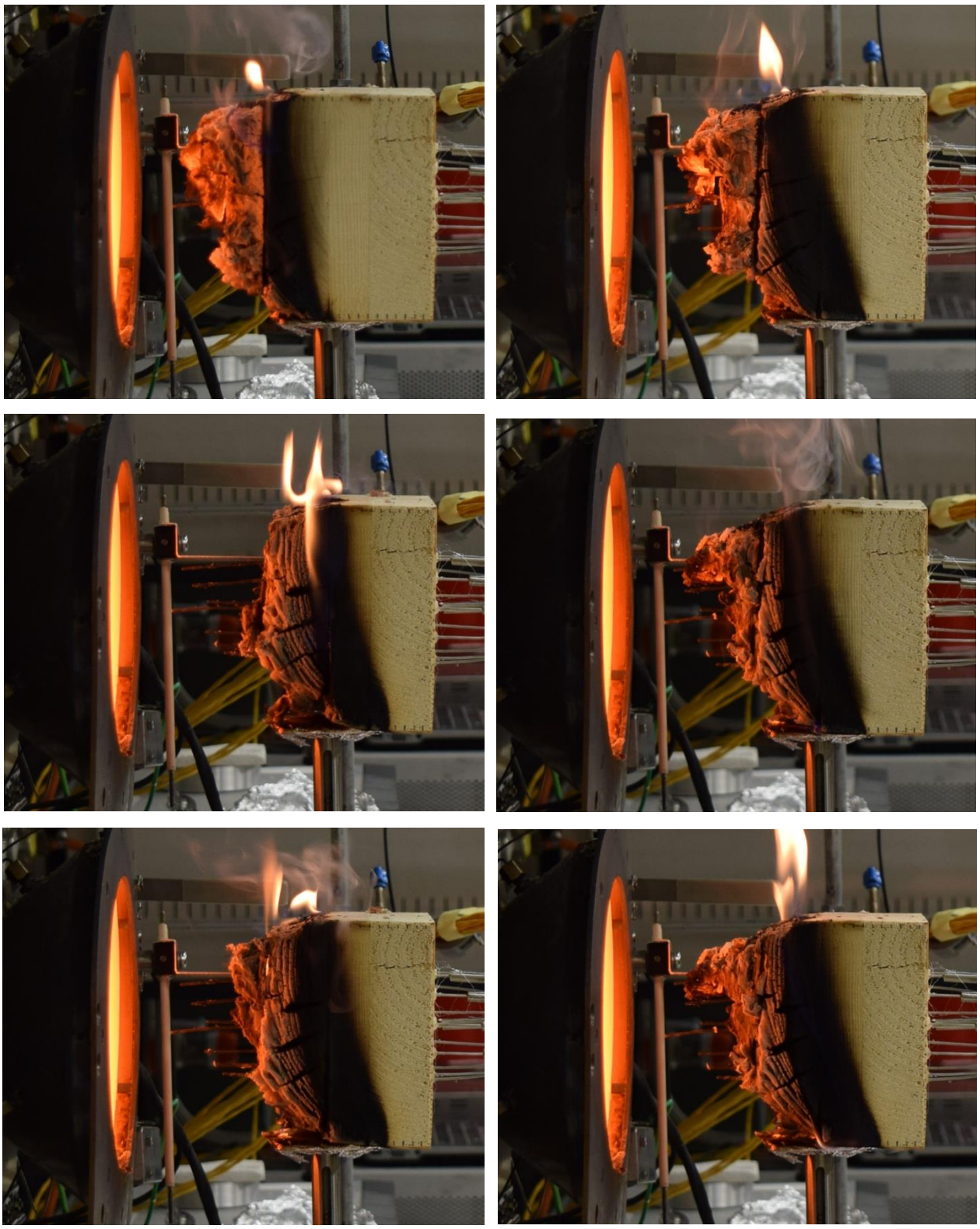

Figure 35: Ignition near the top surface of a sample exposed to 100 kW/m^2 heat flux. Starting top left and proceeding clockwise.

3.7 Summary and Conclusions

Self-extinction occurred in every test where the external heat flux was completely removed. This applied for both transient and steady-state burning conditions for the samples.

The in-depth conduction was found to reach a peak heat flux slightly before char began to form. As the char increased in thickness the net amount of energy transferred from the heated surface to the unburned timber decreased. A steady-state value for in-depth heating is therefore implied.

The peak mass loss rate increased with increasing external heat flux while the steady-state average mass loss rate reached a constant value with increasing external heat flux. This leads to the conclusion that higher heat fluxes than those tested would result in similar average mass loss rates.

A critical heat flux and mass loss rate criteria was found for self-extinction of flaming combustion. The critical mass loss rate for extinction was 3.93 ± 0.45 g/m^{2}s; the external heat flux at self-extinction was 43.6 ± 4.7 kW/m^2. These values are slightly less than the critical heat flux for auto-ignition (47.5 kW/m^2).

Consequently, if the mass loss rate or critical heat flux drops below these values, and CLT maintains cohesion during the combustion process (i.e. gaps do not open, or debonding does not occur) – self-extinction of flaming combustion will occur.

While this chapter highlights the fire exposure and the consequences of debonding on self-extinction, the next section of this study focuses on the structural aspect of debonding and the relationship between the heat transfer and thermal loads to the propensity for a timber adhesive bond to debond resulting in structural failure.

Chapter 4: Cross Laminated Timber Failure Modes Changes

In order to correctly understand the complete behavior of CLT in fire conditions a proper understanding must be formulated of not only the characteristics of timber combustion but also CLT failure modes over the entire heating duration. Flaming combustion of timber and the reduction of the strength of the section by charring is only part of the complex mechanisms that dominate CLT behavior and ultimate strength.

Structural performance of CLT relies on the composite action between two adjacent timber plies. This composite action is dependent on the performance of the adhesive which binds the timber plies together. The standard mechanical theory outlined in Section 2 for design of CLT in both ambient and fire conditions is that the adhesive remains completely intact for the entire duration of the fire. However, if the strength of the adhesive to resist normal and shearing stresses decreases in increasing temperatures then the standard theory is called into question and quantification of the strength reduction due to the deterioration of the adhesive strength is necessary. A series of tests were designed in order to study the effects of increasing adhesive temperature on the overall performance of CLT.

4.1 Previous Research into Debonding

Very few studies directly studying debonding in engineered timber have been conducted as the need has never been previously identified. These studies range from purely modeling research to large-scale furnace tests. Debonding has only been noticed in furnace tests and various definitions for debonding occurrence have been made. The problem with the definitions formulated was that they were based on temperature data and complete separation of the panels [27, 37, 53]. While this definition is adequate for ply separation in a fire sense, this definition does not incorporate actual structural deterioration and thus cannot be used to predict or begin to investigate structural behavior.

Frangi, et al. [24] studied horizontal and vertical CLT behavior under standard ISO-fire conditions. Small-scale tests were conducted on horizontal samples of 54mm 3-ply CLT and were placed in a 1.0 x 0.8m furnace. The glue used to bond the CLT was a polyurethane based adhesive. Debonding of the char layer was visible after 28 minutes of exposure. The temperature of the bond line at failure of the temperature was assumed to be 300°C. This assumption was based the temperature achieved in an ANSYS FE model around the time of debonding. Comparisons from the small-scale test were made to large tests conducted on vertical and horizontal wall and slab tests. The samples ranged between 3.0 and 4.85 meters in length and height. Each sample was subjected to the standard ISO fire curve as in the small-scale tests. Debonding of CLT char was less pronounced in the vertical tests than the horizontal oriented samples [24, 54]. The adhesive used in the large-scale tests was polyurethane based but not the sample brand as in the small-scale. Each of the studies previously

conducted on the performance of CLT have been conducted within the standard furnace framework. The many assumptions made implicit in the test standard (previously mentioned in Section 1) mean that, drawing conclusions about performance based on furnace testing is questionable.

Debonding has been studied heavily in disciplines other than timber and fire. Several of the major works in debonding have been on the performance of fiber reinforced plastics bonded to reinforced concrete. In particular, the bond length has been shown to play a critical role in the overall strength of a bonded section and whether debonding or material failure occurs [40]. The interfacial stresses which transfer the loads between the two materials have been shown to be the drivers for debonding. The magnitudes of these stresses and their role in crack propagation is clearly documented [34, 55].

4.2 Testing Regime

Understanding the changes in thermal profiles for a range of scenarios allows specific knowledge of the temperature change variations in adhesive bond lines depending on the ply thickness of the engineered timber. Knowing the temperature of the bond allows the quantification of the reduction in modulus of elasticity and other properties of the adhesive. While the specific adhesive properties were not studied in this thesis, the effects of the changing material properties were studied by subsequent testing regimes. To investigate these phenomena more closely, CLT samples were exposed to a range of heat fluxes while measuring the in-depth thermal profiles and comparing the temperatures at the bond line locations.

The next series of tests was designed to isolate a specific bond line and study the behavior changes at increasing temperatures. Using the temperatures achieved in the first series of tests, a range of steady-state bond line temperatures were chosen. A heated glued joint was subject to a shearing force and the results were collated to study the changing behavior and failure modes.

Finally, CLT beams were loaded in a three point bending test while under heated and ambient conditions. This allowed a comparison of the results from the small-scale joint tests with large-scale behavior in the CLT beams. The entire results of the test series highlight the deviation between standard design methods and realistic CLT behavior in fire conditions.

4.3 Thermal Penetration Depth

In order to study the effects of temperature on bonded timber joints, a series of experiments were conducted to measure the depth of thermal penetration within a timber sample over time and under a wide range of thermal exposure intensities. The experiments conducted were similar the self-

extinguishment tests described in Chapter 3—except that the tests were allowed to run for approximately two hours. A cone heater was oriented in a vertical position and timber samples were heated perpendicular to the grain. A radiant shield was placed between the cone heater and the sample to allow the cone heater to reach the target heat flux for the test without preheating the timber sample. Each test was conducted under normal atmospheric conditions and using auto-ignition. The sample properties for the test series can be seen in Table 2 (Section 3.3).

The heating intensity range selected for each test was chosen to cover a wide variety of heat fluxes seen in typical compartment fire scenarios. Each test was run until steady-state thermal profiles were formed and lasted between one to two hours. The exact heating regimes, the form of combustion, and whether charring occurred are documented in Table 3 (Section 3.3.1) An extra external heat flux level was added to the experimental methodology in order to assess the thermal profiles of a timber block where no charring occurred. The highest heat flux possible without charring was selected which was found to be 6 kW/m^2.

Twelve type-K thermocouples (Ø1.5mm) were place into Ø2mm holes in the sample. The orientation and spacing were similar to Section 3.3.2. The thermocouples were positioned starting 2mm from the heated surface and then with 5mm spacing after the first thermocouple. The samples were allowed to increase in temperature and combustion for approximately an hour before extinguishment. This allowed sufficient time for steady-state burning and heating to be achieve as described in Section 3.

4.3.1 Results

An analysis of all the thermal profiles yield several key aspects of the heating of timber blocks. Figure 36 highlights the first principle. The figure is a graph of the temperature histories of various depths within a CLT block exposed to a 6 kW/m^2 heat flux. The graph shows that the temperatures will eventually trend towards steady-state values. This confirms the results of the constant steady-state thermal gradient. If the thermal gradient reaches a constant value then the temperature profiles should trend towards constant steady-state. This principle is easier to see in a non-charring test as in the case of the 6 kW/m^2 heat flux exposure; however, the same trend can be seen in the 30 kW/m^2 exposure. Steady-state constant temperatures occurred in the flaming combustion tests; however, due to the high charring rate, the thermocouples quickly were subjected to direct flame impingement and convective cooling and thus major fluctuations occurred which reduced the temperature.

In Figure 36, exposure to the external heat flux occurred at around 10 minutes. The heat flux quickly increased the surface temperature (represented by the 2 mm thermocouple). The thermocouples at

other depths followed the same trend as the energy is transferred deeper into the cross-section. A plateau between 90-100°C indicates the moisture gasification point. As the amount of energy decreases deeper into the cross-section, more time is required to gasify all the moisture at a particular depth. The increase in the amount of time a particular temperature curve plateaus is clearly seen in Figure 38.

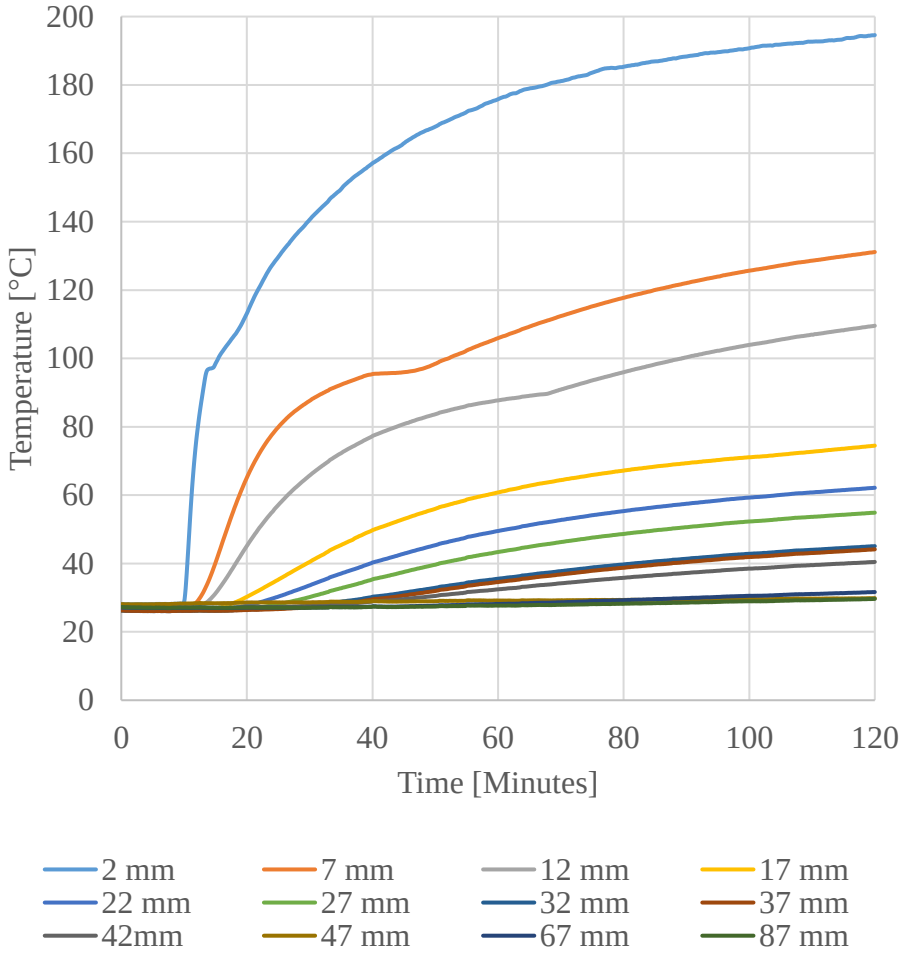

Figure 36: Temperature-time histories of various depths within a CLT block exposed to a 6 kW/m^2 heat flux

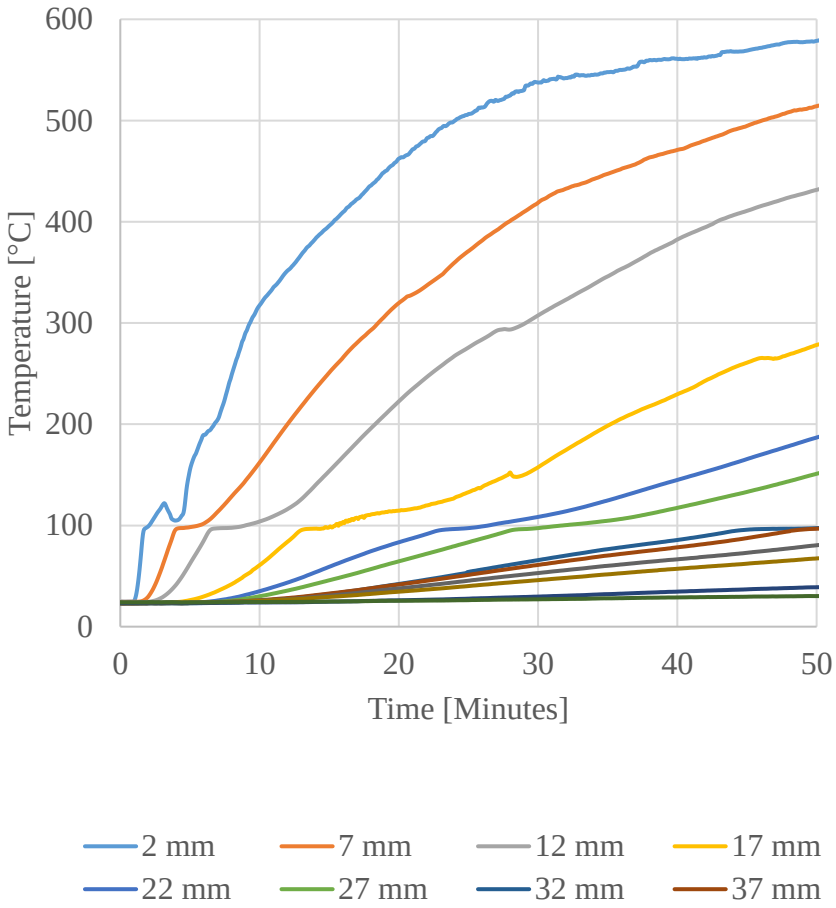

Figure 37: Temperature-time histories of various depths within a CLT block exposed to a 30 kW/m^2 heat flux

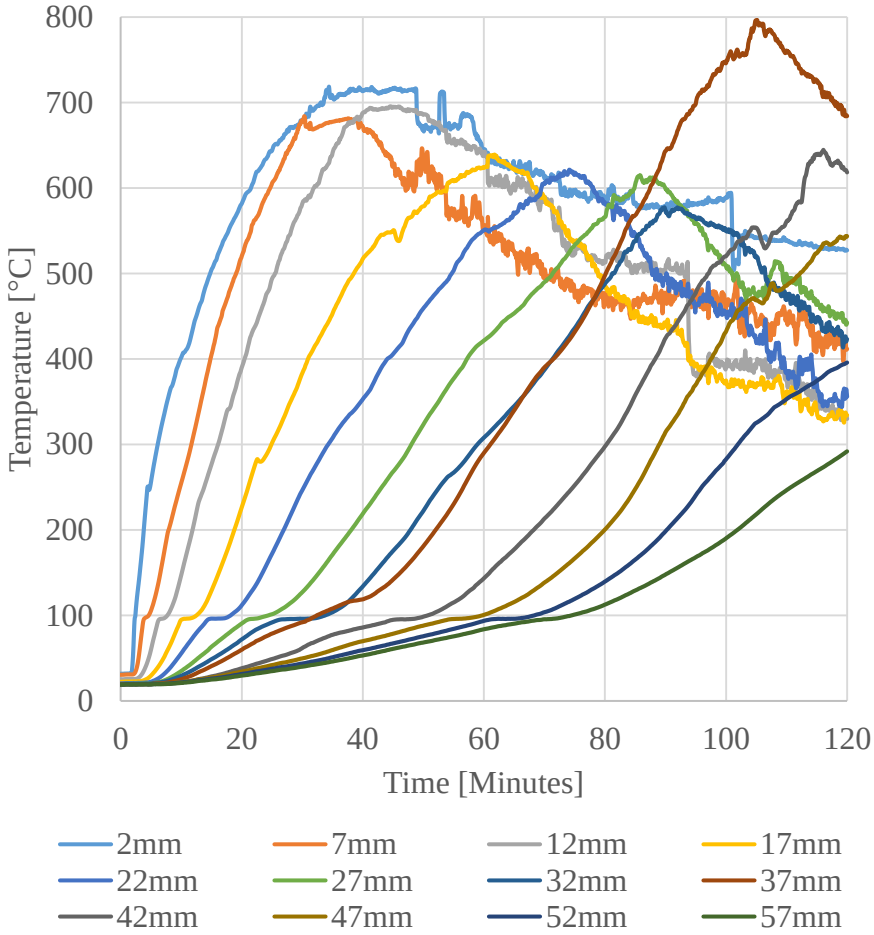

Figure 38: Temperature-time histories of various depths within a CLT block exposed to a 50 kW/m^2 heat flux

In the context of adhesive layer temperature, the thermal penetration depth is the most relevant parameter to quantify. The thermal penetration depth dictates the rise in the adhesive temperature and thus the decrease in the strength properties of the bond between two timber plies. The thermal profile for the 6 kW/m^2 test can be seen in Figure 39. During the first 30 minutes of the test, the thermal profile changes but after 30 minutes, the shape of the profile remains the same with the magnitude of the values changing slightly. Increases in temperature can be seen from the heated surface through approximately 40 mm. Depending on the sensitivity of the adhesive to temperature, slight changes at this depth could affect the overall bond performance.

The increase in the temperature of the bond line occurs at temperatures below the pyrolysis temperature. Plotting the results of the thermal exposures in which charring occurred show the consistency in the thermal profile. Figure 40 shows the thermal profiles from a 50 kW/m^2 exposure from ambient to about 400°C. From the 10 minute mark, the thermal profiles are consistent in shape and magnitude.

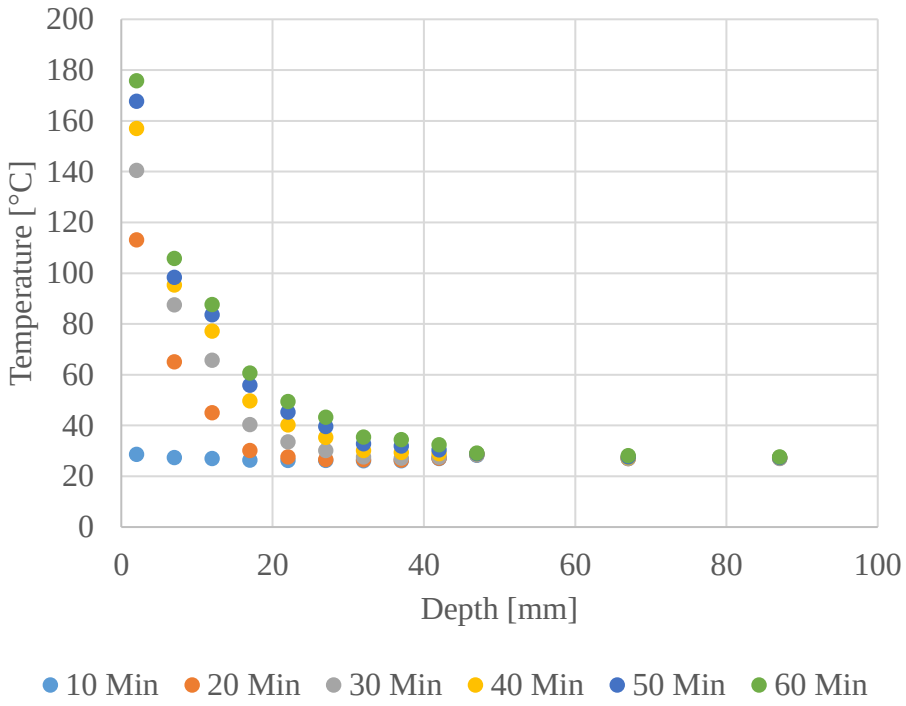

Figure 39: Temperature profiles through depth into the cross-section for a 6 kW/m^2 exposure.

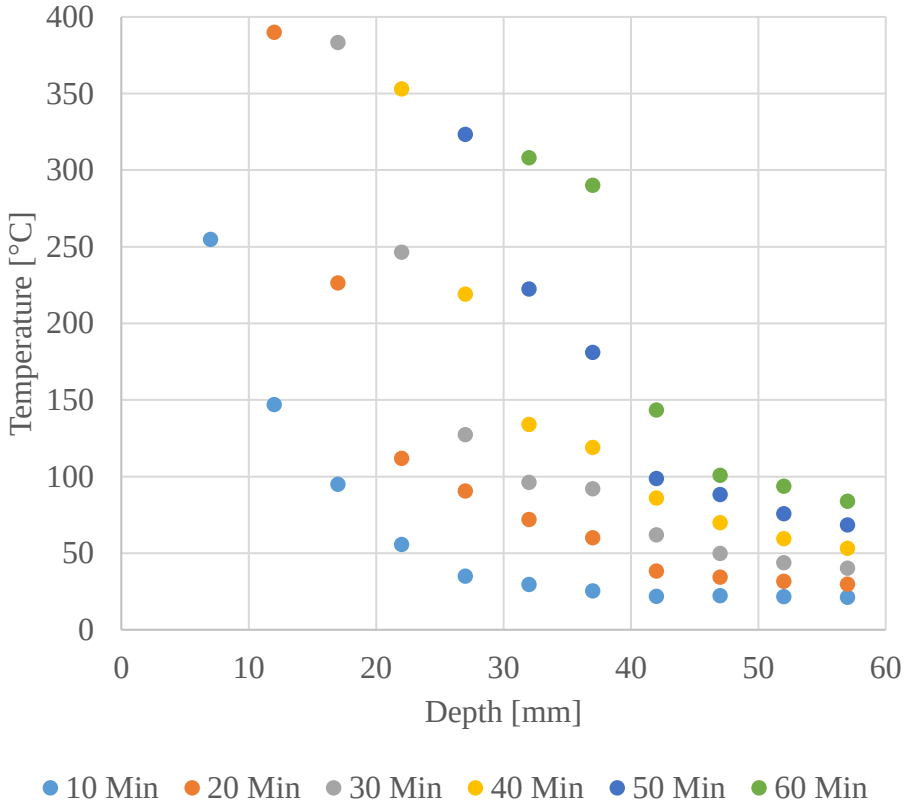

Figure 40: Temperature profiles through depth into the cross-section for a 50 kW/m^2 exposure.

For the charring cases (30 kW/m^2 and higher), the thermal profile reaches a steady-state shape due to the presence of the char layer (Figure 41). The shape and magnitude of the thermal profiles are the same at steady-state giving a constant thermal thickness ahead of the pyrolysis front. However, the regression rate (charring rate) determines the progression of that front through the sample. For the non-charring cases such as the 6 kW/m^2, a different steady-state shape and magnitude exists as the char layer is not present.

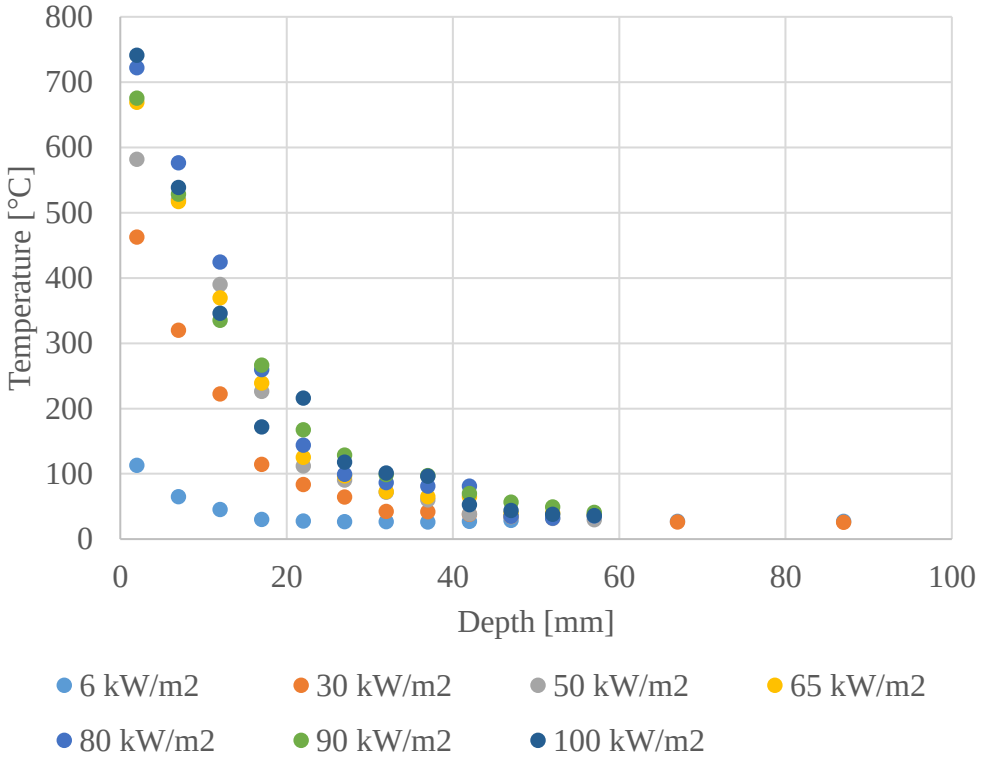

Figure 41: Temperature profiles through depth into the cross-section for every heat flux tested at 20 minutes after exposure.

The actual thermal penetration depth is dependent upon the temperature at which the bond line fails. However, the failure temperature is highly dependent on factors including but not limited to the glue strength, interfacial shear and normal stresses developed due to the applied load, and bond length. Each of these dictate the ultimate strength of a bonded joint and temperature plays the primary role in deteriorating each of the factors. The temperature of the surrounding timber also plays a critical role in determining whether the strength of the joint is dictated by the following factors:

- the strength of the timber at elevated temperature,
- the bond strength at temperature, or
- a combination of both the adhesive strength and the surrounding timber.

The theory described in Section 2.3 does not account for the increase in the adhesive as the thermal compensating layers are generally between 7-15mm.

4.4 Single-Lap Shear Tests

Once the isolating typical temperatures that affect a bond line ahead of a pyrolysis front were identified, a test series of single-lap shear tests was conducted to study glue bonded joints at temperature. Each sample was instrumented to measure and analyze the displacement and interfacial stresses developed in the bond line over the course of the heating and testing regime. The methodology used for the single-lap shear tests remained constant for each of the samples.

4.4.1 Methodology

The methodology for the study of the single bond timber joint was an elevated temperature single-lap shear test. The samples were placed within an environmental chamber and heated to a steady-state temperature before a tensile force was applied to the joint until failure. The timber species for the single-lap shear test samples was Radiata Pine (*Pinus radiata*). The samples were manufactured under standard conditions for bonded joints by the Queensland Department of Agriculture and Fisheries. The one-component polyurethane adhesive was applied to the samples and then a constant pressure (1 MPa) was applied to the joint for approximately 2 hours for sufficient bonding. The structural adhesive was chosen to be consistent with typical adhesives used in the manufacturing of CLT.

The dimensions of the samples are shown in Figure 42. A bond length of 600mm was chosen as this was the maximum length that the environmental chamber could accommodate. The width of the sample was chosen based on available timber sizes from local suppliers. An extra bonded length of 350mm was added onto the end of the sample in order to provide an area for the 1 MN MTS Universal Testing Machine to grip the sample. The grip thickness was chosen so the resultant of the applied force was applied as close to the center of the adhesive bond as possible to minimize bending effects prior to the application of the tensile force.

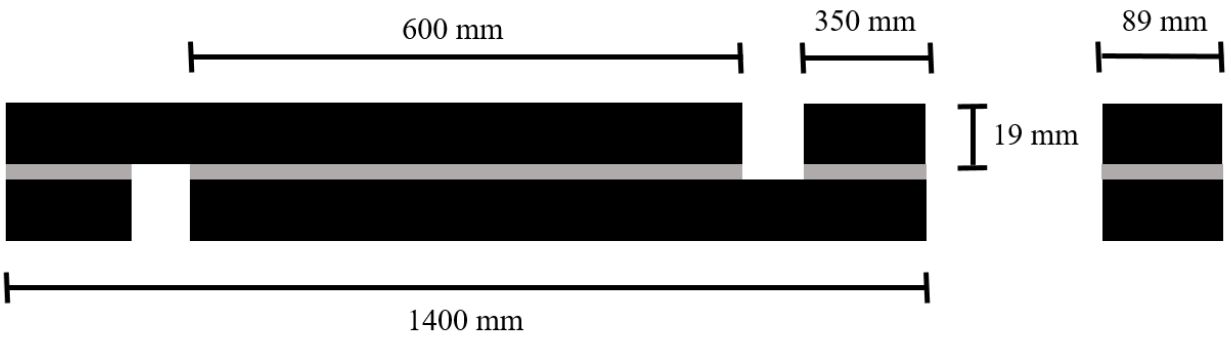

Figure 42: Single-lap shear sample dimensions. Length view (left). Width view (right).

To capture the strains developing in the adhesive bond, the samples were instrumented with strain gauges and prepared for use with Digital Image Correlation (DIC). Strain gauges recorded the strains at specific points where the gauges were applied to the samples. For these tests, strain gauges were placed on the samples in the location of the sample with no bond (Figure 43). The location was selected in order to calculate the elastic modulus of the timber through the loading. The elastic modulus could then be used to calculate the stresses within the bond line.

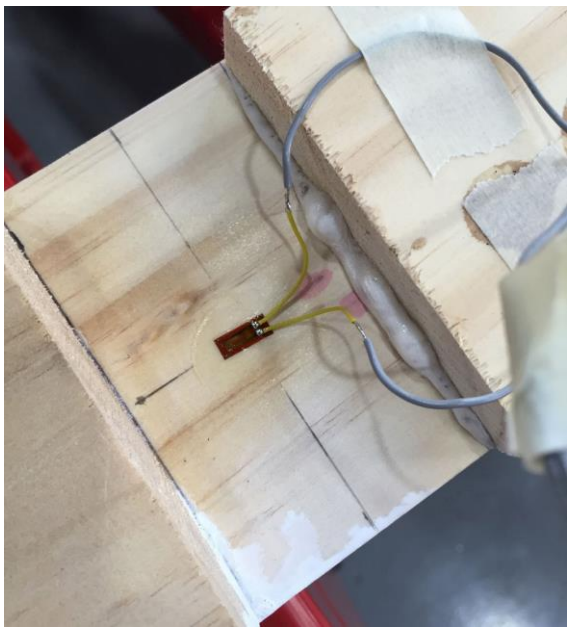

Figure 43: Strain gauge placement for calculation of the elastic modulus of the timber.

The DIC results were utilized for calculating the strains on the bonded joint. The samples were all prepared with speckle patterns for DIC measurements. The middle 600mm area of the bond was painted white and a random pattern of 1 mm circles were painted over the entire area (Figure 44). The speckle pattern was the optimum size and distribution for the dimensions of the imaged area. A

dual camera system was used to measure 3D displacements of the sample over the entire duration of the test. Calibration of the system was performed after every test series.

Figure 44: Speckle pattern distribution over the single-lap bonded joint.

Based on the temperatures seen in the thermal profiles in Section 4.3, the TGA results for the pyrolysis of timber (Figure 9), and the strength reduction in timber (Figure 3), the samples were tested at the ambient (approximately 20°C), 80°C, 110°C, and 150°C. This temperature range ensured that the relevant temperature range was studied without charring of the timber occurring.

The time duration of heating of the samples to ensure that the target temperatures were achieved needed to be calculated to ensure consistency between the results, to minimize the thermal gradient between the bond and the surface of the timber, and to determine the homogeneity of the bond line temperature. Preliminary tests were conducted to measure the temperature of the bond line over time compared to the gas temperature in the environmental chamber. Test samples with thermocouples inserted at the center of the joint (Figure 45) were placed within the chamber. The temperature profiles of the samples were then recorded and the time to steady-state corresponding to the target temperatures were noted. The target temperatures (with associated heating times) and the gas temperature in the environmental chamber are provided in

Table 6.

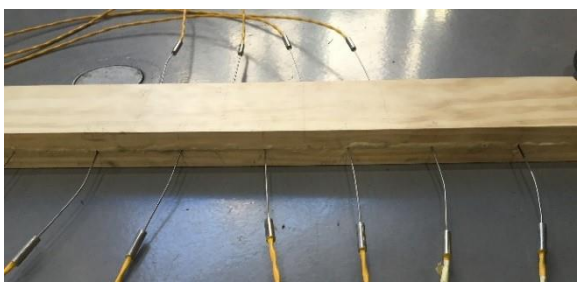

Figure 45: Thermocouples placed in temperature test samples.

Table 6: Target temperatures, heating times and gas temperatures for single-lap shear tests

Target Temperature (°C)	Heating Time (hours)	Gas Temperature (°C)
80	1.0	100
110	1.5	150
150	1.5	195

For each test the procedure was as follows:

- The sample was initially gripped with the top grip of the testing machine.
- The sample was heated to target temperature.
- After time to target temperature had been reached the door of the environmental chamber was opened to allow the DIC images to be capture.
- Only after the sample had reached the target temperature was the bottom grip activated—this procedure ensured that strains would not develop within the timber due to restrained thermal expansion.
- After the top grip had been secured, a tensile force was applied using a displacement controlled rate of 0.6-1.5mm/min depending on the test.
- The tests were run until failure of the timber joint.
- Each test was stopped when the joint was broken into two pieces and were no longer connected (although the failure mode between each test was different).

The length of each test and the relatively low thermal inertia of the timber allowed the bond line to remain at approximately the target temperature for the duration of the loading period. The experimental set-up is illustrated in Figure 46.

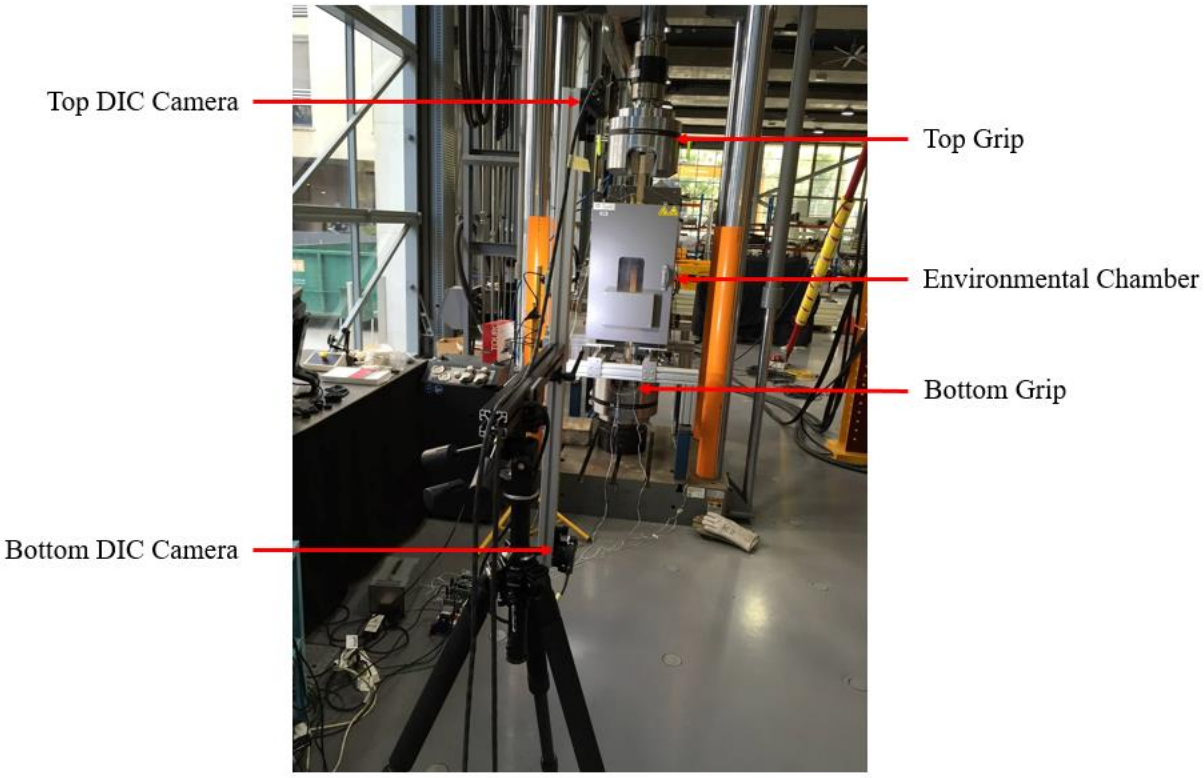

Figure 46: Elevated temperature single-lap shear tensile test experimental set-up

4.4.2 Results

A total of 15 bonded timber joints were tested as shown in Table 7. Of these tests, several of them were eliminated due to failures of the test and the type of failure that occurred. In the ambient temperature test, debonding occurred in Test 2 which was found to be due to manufacturing defects. Test 4 and 6 of the 80°C tests and Test 1 of the 110°C tests were discounted due to failure of the timber gripped by the testing machine. The rest of the samples failed at the joint as a result of timber failure, debonding, or a combination of both.

Table 7: Single Lap Shear Tests at Temperature with Failure Load, Failure Type, and Displacement

Number	Bond Temperature (°C)	Failure Type	Failure Load (kN)	Overall Displacement (mm)
1	Ambient	Timber	44.22	3.36
2	Ambient	Timber/Debonding	41.57	3.56
3	Ambient	Timber	33.07	1.87
4	Ambient	Timber	18.4	1.2
1	80	Timber/Debonding	39.4	33
2	80	Timber	25.13	2.48
3	80	Debonding	36.12	7.35
4	80	Timber (Grips)	32.43	9.18
5	80	Timber/Debonding	30.57	5.61
6	80	Timber (Grips)	34.75	5.39
1	110	Timber/Debonding (Grips)	26.88	4.32
2	110	Timber	29.43	2.46
3	110	Timber/Debonding	24.26	1.54
1	150	Debonding	25.95	1.82
2	150	Debonding	32.73	2.94

The overall load displacement results for the tests selected for analysis are shown in Figure 47. Two of the 80°C samples showed lower initial stiffness compared to the rest. Variations during the beginning loading period should be very minor if at all. This may have resulted due to slippages at the grips. The remainder of the test showed good consistency. Ultimately the tests were kept in the analysis as they demonstrated the difference in failure mode with the remaining 80°C test.

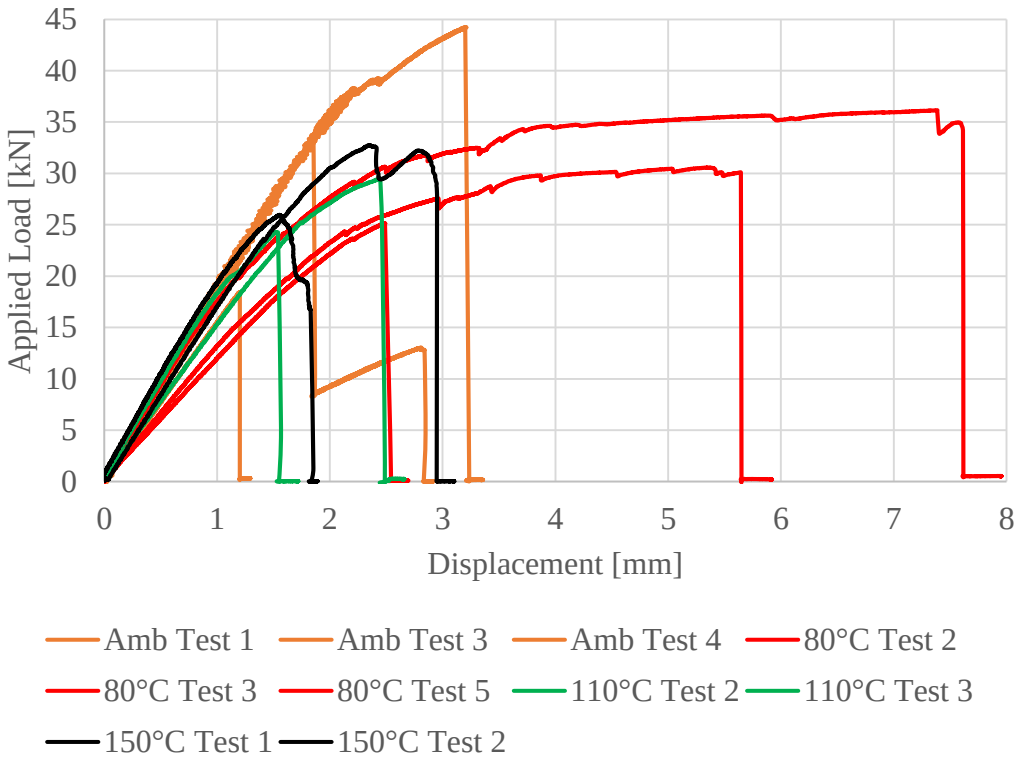

Figure 47: Load vs. displacement for each test selected for analysis

The ambient temperature tests generally reached higher ultimate loads at the lowest level of overall deflection. The resulting failure for each of the tests was entirely timber failure as shown in Figure 48. Timber failure was expected as the adhesive bond should have been the strongest part of the joint. Failure should occur within the timber with no slip in the bond. The failure was sudden and not gradual.

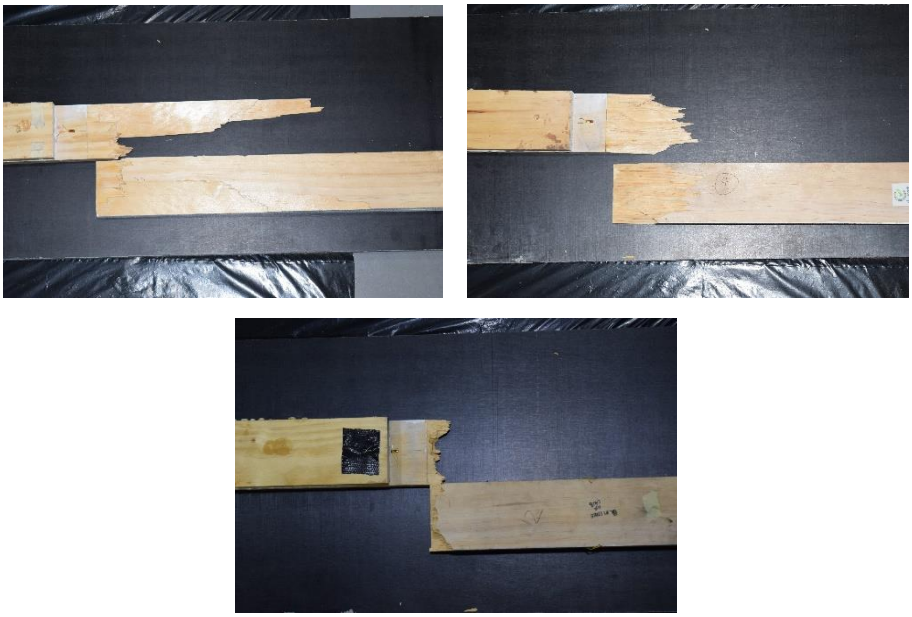

Figure 48: Ambient temperature test failures. Test 1 (top left). Test 3 (top right). Test 4 (bottom)

As the temperature was increased to 80°C the failure mode changed and a plateau in the load displacement curve appeared. The plateau in the load displacement curve is indicative of gradual debonding propagation along the bond. During the debonding propagation, the load does not increase further, but the displacement increases resulting in a plateau in the load displacement curve [56]. The bonded region begins to shorten as the debonding progresses through the adhesive layer. Eventually either the entire bond will fail or timber failure will occur due to a weaker portion of timber. The plateau observed in the load displacement curves of the 80°C specimens is evidence that in these specimens effect bond length is reached. As the elastic modulus of the adhesive reduces, the effective bond length increases. This means that concluding that the ambient temperature specimens have a bond length longer than the effect bond length is reasonable. However, the ultimate load of the ambient temperature tests is not a representative of the ultimate bond strength, due to early failure within timber.

In the 110°C tests, debonding initiation at the plated ends was visible during the tests. However, shortly thereafter, complete failure occurred without debonding propagation. Failure then was due to combined timber failure and debonding, while in the second specimen failure was predominantly due to timber failure. Absence of a clear plateau in the load displacement curve can be due to the following reasons:

- The effective bond length being larger than the bond length of the specimen due to significant degradation of the adhesive elastic modulus, or
- The low tensile strength of the timber (lower than bond strength).

The failure of Test 2 in the 80°C specimens is purely due to timber failure and resulted in a similar load capacity to Test 1 and 3 in the 110°C tests which debonded partially (Figure 49). This demonstrates the difficulty in assessing the effective bond length from the test results as the timber exhibited high variability between the tests.

Figure 49: 80°C and 110°C temperature test failures. 80°C Test 2, 80°C Test 3, 80°C Test 5, 110°C Test 2, 110°C Test 3 (clockwise from top left)

At even higher temperatures (150°C), failure was due to debonding (Figure 50). The bond length was concluded to be lower than the effect bond length because the plateau stage did not occur in the test and adhesive failure occurred. Therefore, a longer bond length was necessary in order to fully utilize the bond joint and reach the ultimate load of the bond joint. Consequently, the ultimate load of these

specimens cannot be taken as a true representation of the bond strength, but a combined effect of the adhesive mechanical property degradation and bond length.

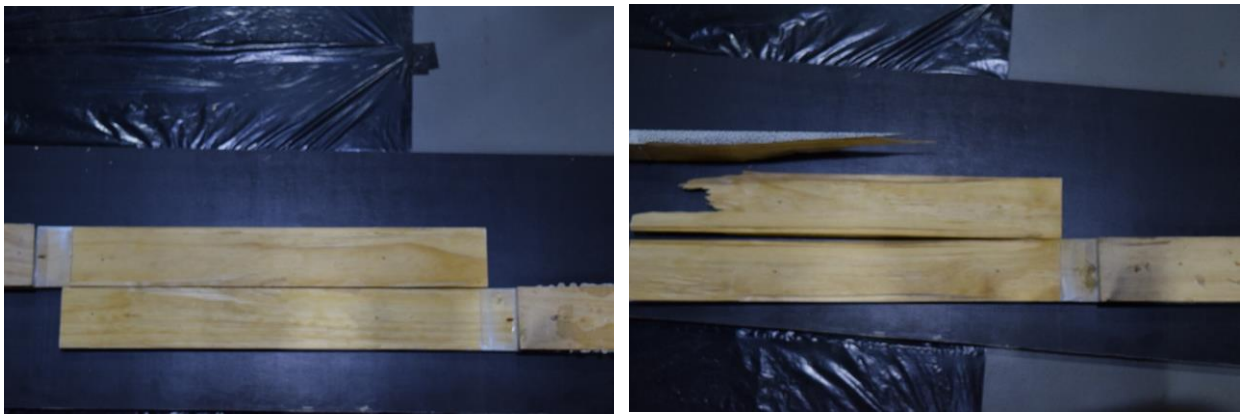

Figure 50: 150°C temperature test failures. Test 1 (left). Test 2 (right)

Based on the type of stress within the bonded interface, each test can be divided into two categories: normal and shear. These forces are described in more detail in Section 2.4. Each of these forces can be divided again to show the influence of both load and temperature on the resulting strains and bond slip of the joint.

The first type of force analyzed was the shearing forces which resulted in axial strains.

4.4.2.1 Axial Strains

From the DIC measurements, the overall displacements of the two timber boards comprising the joint were measured over the length of the joint. The displacements were taken as close to the adhesive bond as possible. To calculate the slip, the displacements of the two boards were subtracted from each other with the resulting being the overall bond slip of the joint.

The first derivative of the slip data was taken over the entire bond length, and the relative axial strains in the timber plies were calculated. The gradient in the axial strains represents interfacial shear stress (i.e. a higher gradient means higher interfacial shear stress while constant axial strain or zero axial strain means zero interfacial shear stress [56]. These axial strains from different tests at different load levels are compared in Figure 51-Figure 53. At 25 kN load level, the strain values of 110°C specimens were found to be higher than ambient tests, while lower than the 150°C tests. This is unsurprising as the elastic modulus of adhesive degrades with the increasing temperature.

The strains for the same load would be expected to increase with decreasing elastic modulus (i.e. increasing temperature). As the higher gradient of the axial strains curve represents higher shear

stresses, most of the bond length in the 150°C specimen was under non-zero shear stress Figure 54. At the same load level, the 110°C and the ambient test specimens only had part of the bond length under non-zero shear stress. As the load increased to 30 kN, significant parts of the bond length in 110°C tests can be seen under non-zero shear stress. Smaller gradients of the axial strain curves in ambient temperature tests (Figure 55) also meant much lower interfacial shear stresses in those specimens compared to higher temperature test specimens.

Comparing the ultimate axial strain values at the bonded interface, closer to failure of each specimen, ambient test specimens showed approximately 0.008, while the 110°C and 150°C tests showed 0.002. This shows clearly that with the increase in the temperature the maximum strain capacity of the adhesive also increases.

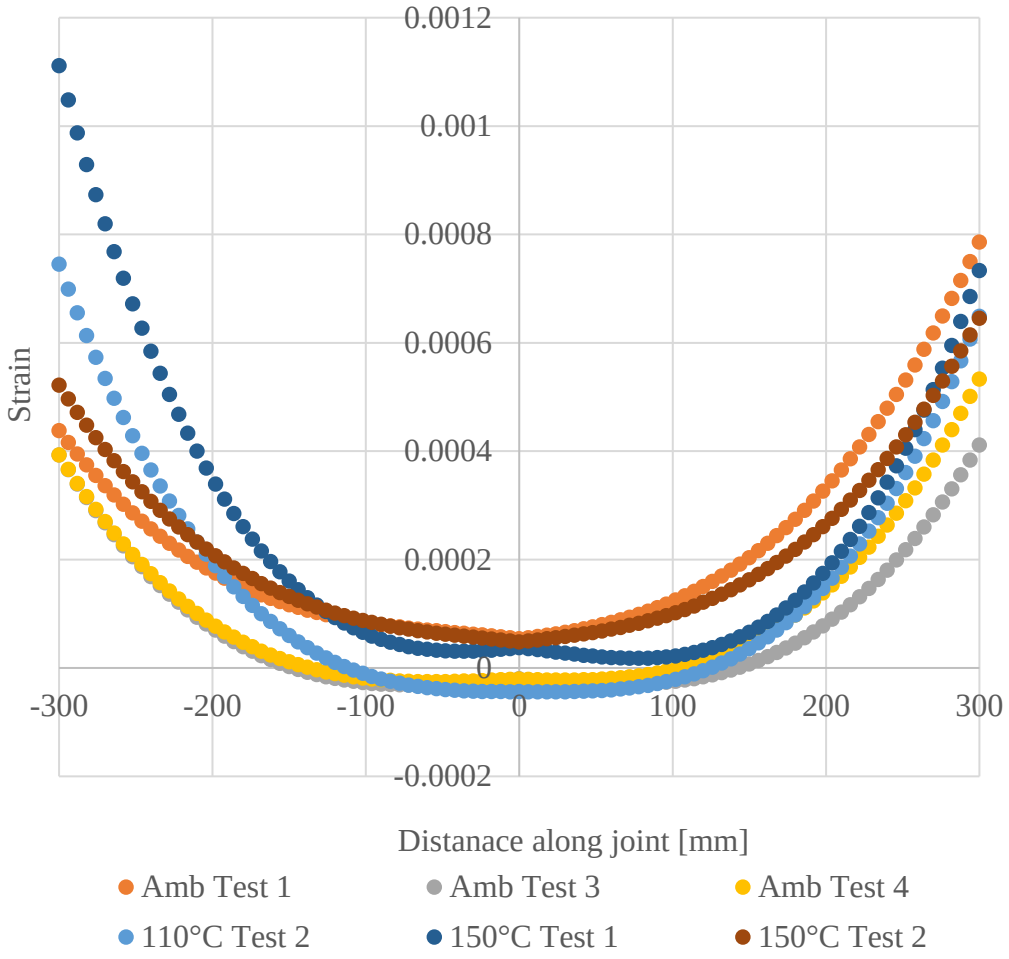

Figure 51: Strains due to shear forces at an applied load of 25 kN

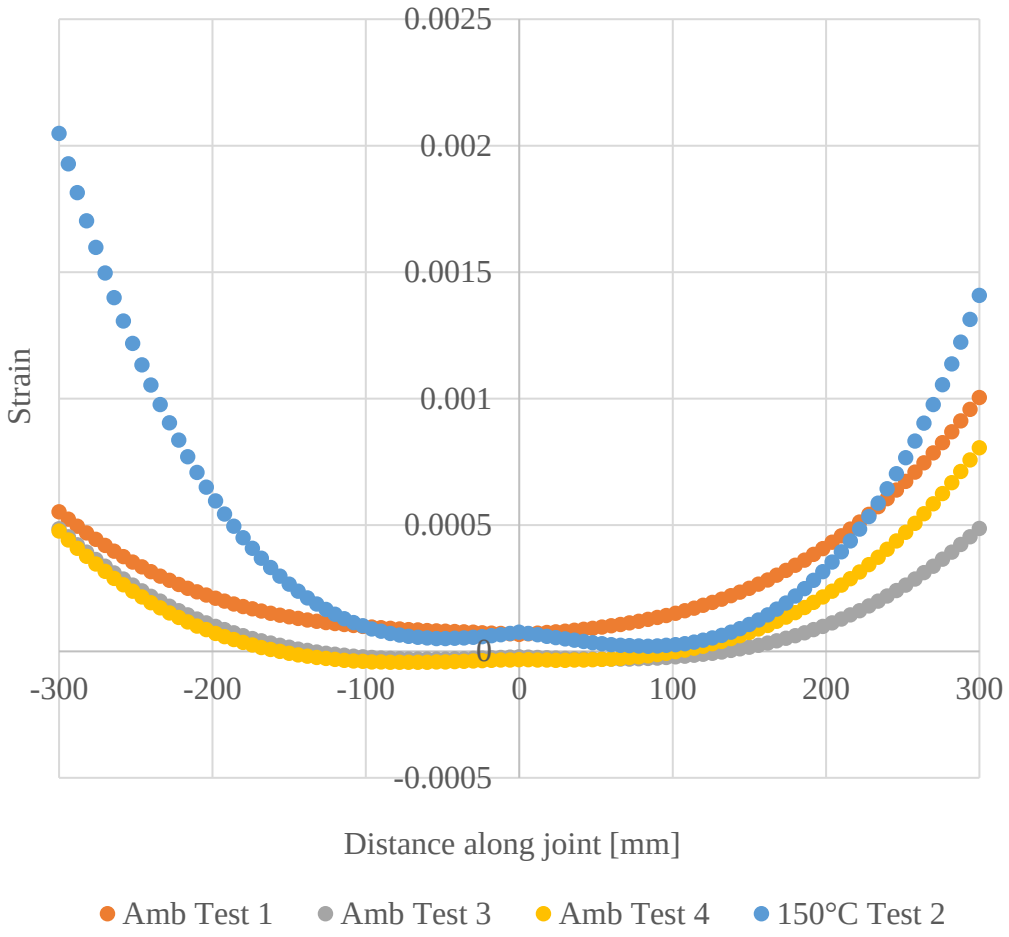

Figure 52: Strains due to shear forces at an applied load of 30 kN

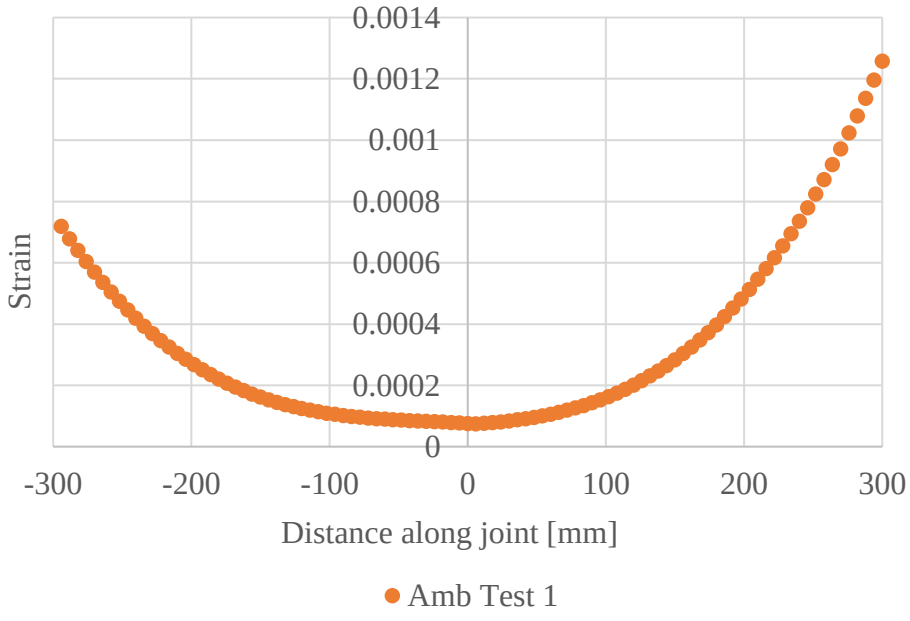

Figure 53: Strains due to shear forces at an applied load of 35 kN

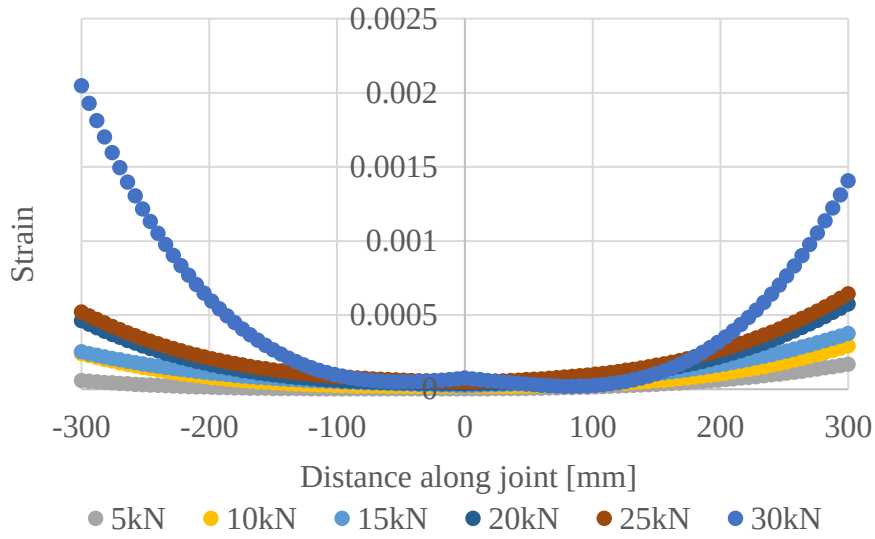

Figure 54: Strains due to shear forces 150°C Test 2

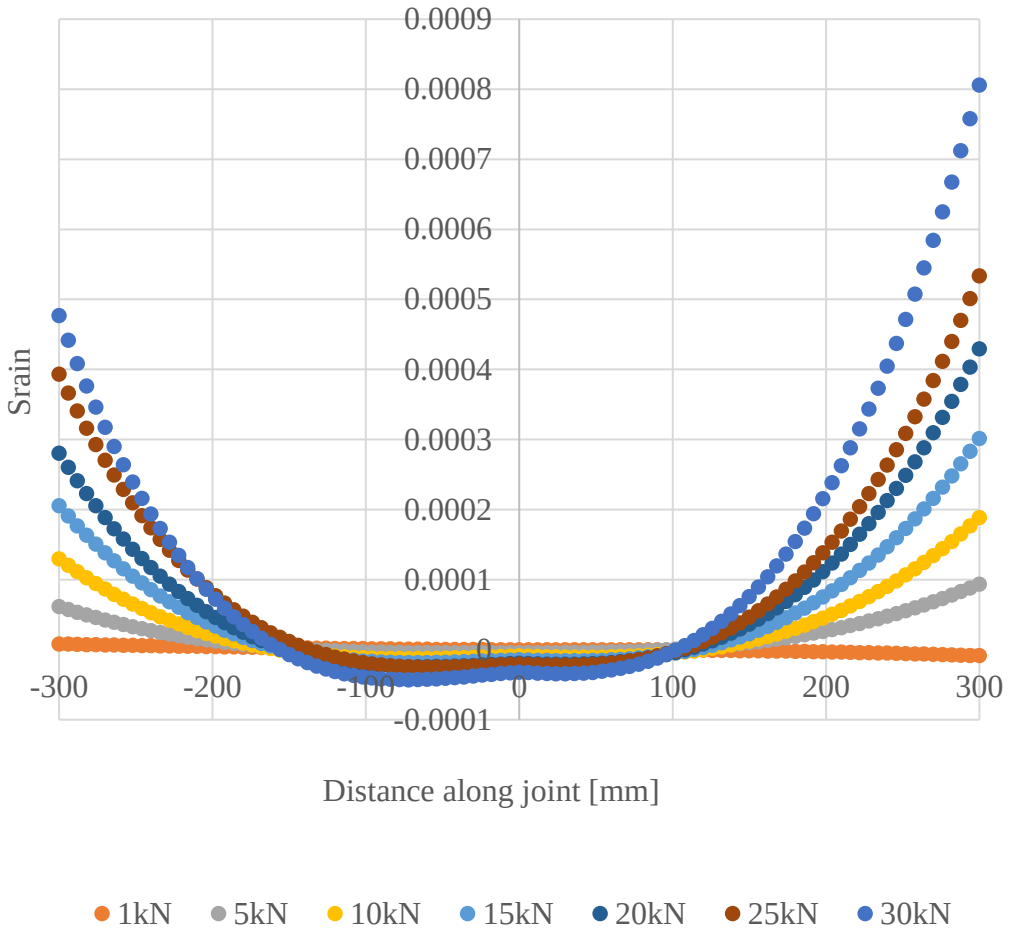

Figure 55: Strains due to shear forces of Ambient Test 3

4.4.2.2 Separation Due to Normal Forces

The bonded interface is also subjected to normal stresses. Unlike the bond shear stresses which are typically distributed over a certain length along the bonded joint, bond normal stresses are concentrated over a small length closer to the plate ends [56]. In these regions, debonding is due to combined normal and shear forces. Often in adhesive joints, fracture energy in mode I (opening), is much smaller than the fracture energy of mode II (in-plane shear). Therefore, understanding the normal forces is also very important to understanding the debonding of the specimens.

An analysis of the normal strains that are exhibited in the adhesive bond due to the applied load and the temperature changes demonstrate the significance that normal forces play in peeling apart the timber bond. At the load just before failure (Figure 54), the shearing strains reached a magnitude of around 2000 microstrain. The normal strains exhibited by the normal forces are equal in magnitude and in some cases an order of magnitude greater than shearing strains.

At the very beginning of the loading (Figure 56), the normal strains are approximately zero. As the load increases and the peeling forces begin to stress the ends of the joints, the strains begin to increase as the glue begins to yield. The higher temperature conditions exhibit greater strains at a given load than the samples at ambient conditions (Figure 57). A potential cause for the increased strains is the adhesive losing strength as a result of the increase in temperature of the bond line.

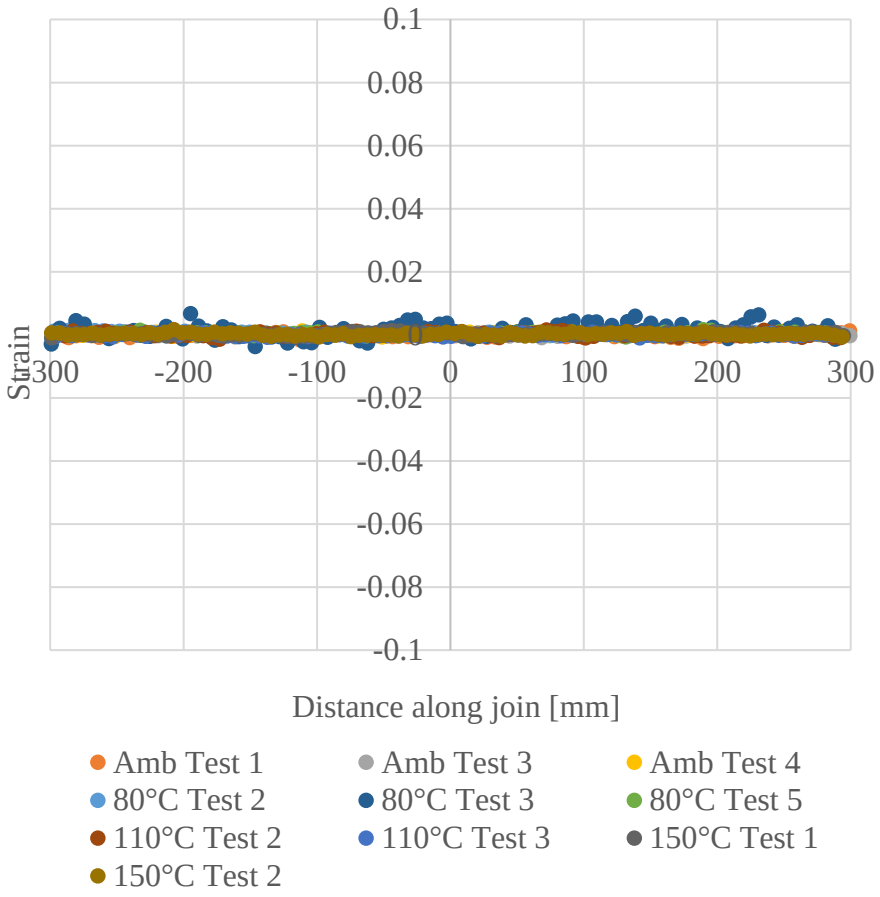

Figure 56: Strains due to normal forces at 5 kN of applied load

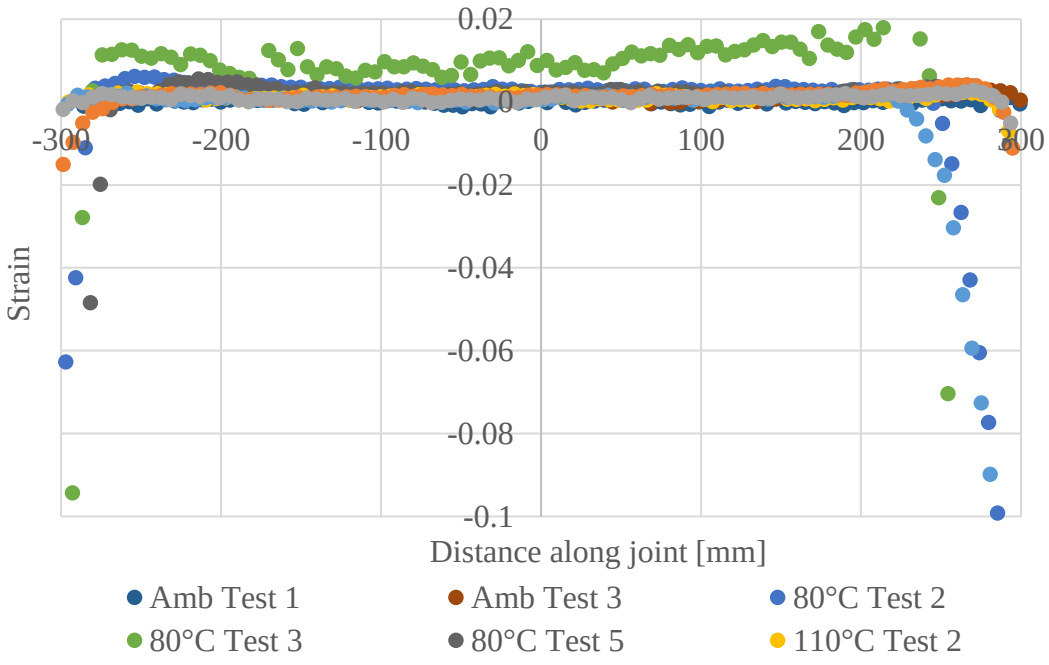

Figure 57: Strains due to normal forces at 25 kN of applied load

Figure 58 shows the normal strains for an elevated temperature test that had partial debonding on one end of the joint. The strains remained small until about 20kN when the strain begin to increase. At an applied load of 25kN, significant strains occurred in the joint. The increase in strains along with the ply separation data showed that potential debonding on that end had occurred for a length of approximately 50-75 mm. Failure occurred in the timber before the load reached 30 kN. The failure of the 110°C Test 3 can be seen in Figure 49.

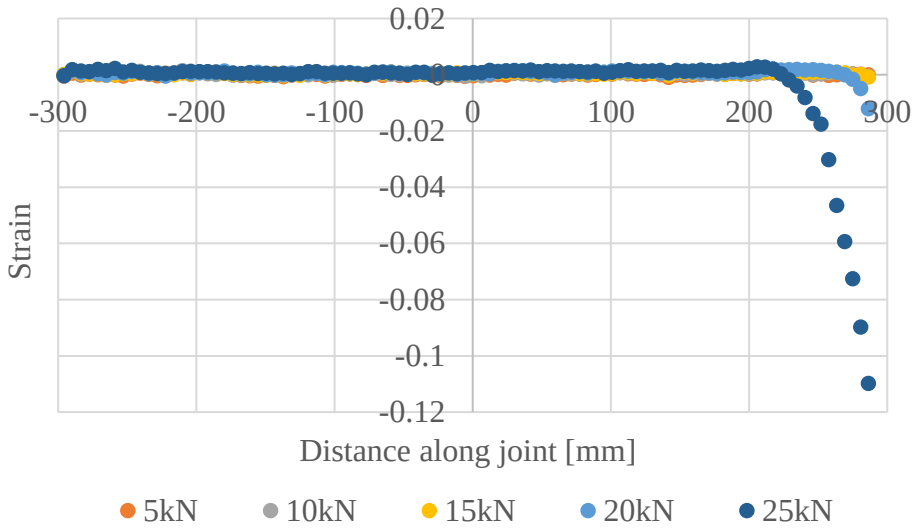

Figure 58: Strains due to normal forces at for 110°C Test 3.

The large magnitude of the normal strains compared to the shearing strains highlights the importance of a complete understanding of the all the forces in a bonded joint and the behavior of the adhesive to withstand the forces applied. While the shearing strains are present throughout the entire length of the bonded joint, the normal strains are generally only high around areas of discontinuity. Discontinuities can be anything from changes in the elastic modulus of the two materials to separations between the boards. Any discontinuity will have high normal forces and lead to high strains.

The interfacial fracture energy of a bonded joint failure due to cohesive failure within adhesive is a function of adhesive mechanical properties, especially the strain energy [56]. While the strength of the adhesive may decrease the strain energy, increases in strain capacity may increase the strain energy. Therefore, total energy (interfacial fracture energy) should be investigated in terms of both strength and strain capacity, but not solely on the strength. While the tests presented above can verify the effect of bond length and the increase in strain capacity, due to variations in the tests, which is believed to be due mainly to variations in timber properties, quantification of the effects of bond length and adhesive strain energy on bond strength is not possible. This is reserved for future

investigations. Nevertheless, the experiments in this study clearly show that when the temperature is high enough, failure of the timber-timber bonded joints is governed by debonding.

4.5 CLT Beams

To complete the study of elevated temperature effects on CLT, a study was completed to observe if the results from the single-lap shear tests were present in larger CLT beams. This study would give an indication of the overall performance of CLT under elevated temperatures. The purpose of this study was to focus on the adhesive bond of CLT at elevated temperatures and the performance of the entire section.

4.5.1 Methodology

The beams were comprised of 5-layer CLT from the same stock as the samples tested for the self-extinction and heated layer tests in Sections 3 and 4.2, respectively. Ensuring that the samples were identical in species and properties enabled consistency between the results for the entire study. The CLT was cut into 1.5 meter long beams and subjected to a three-point bend test (Figure 59-Figure 60) at both ambient (control test) and elevated temperatures. The samples were loaded using displacement control at a rate of 3 mm/min.

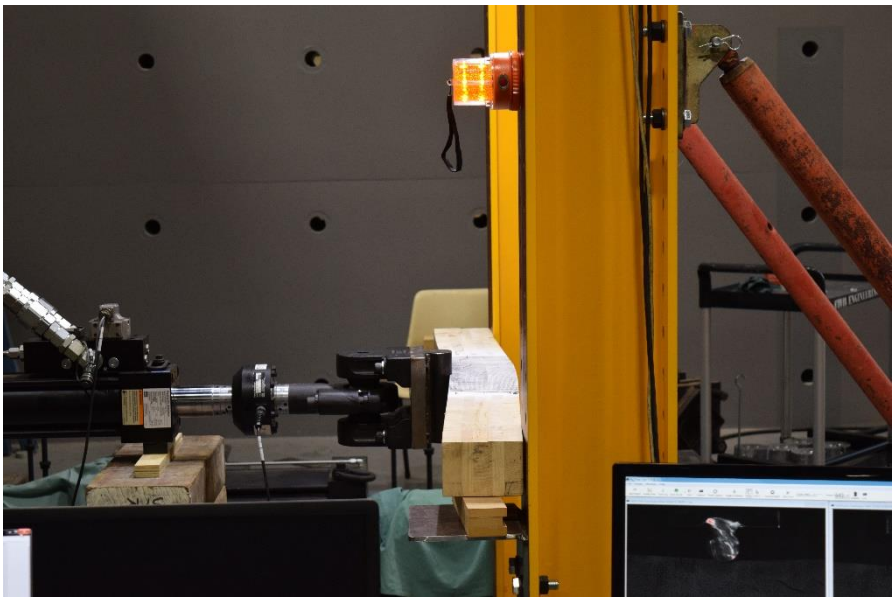

Figure 59: Side view of CLT beam three-point bending test with horizontal actuator.

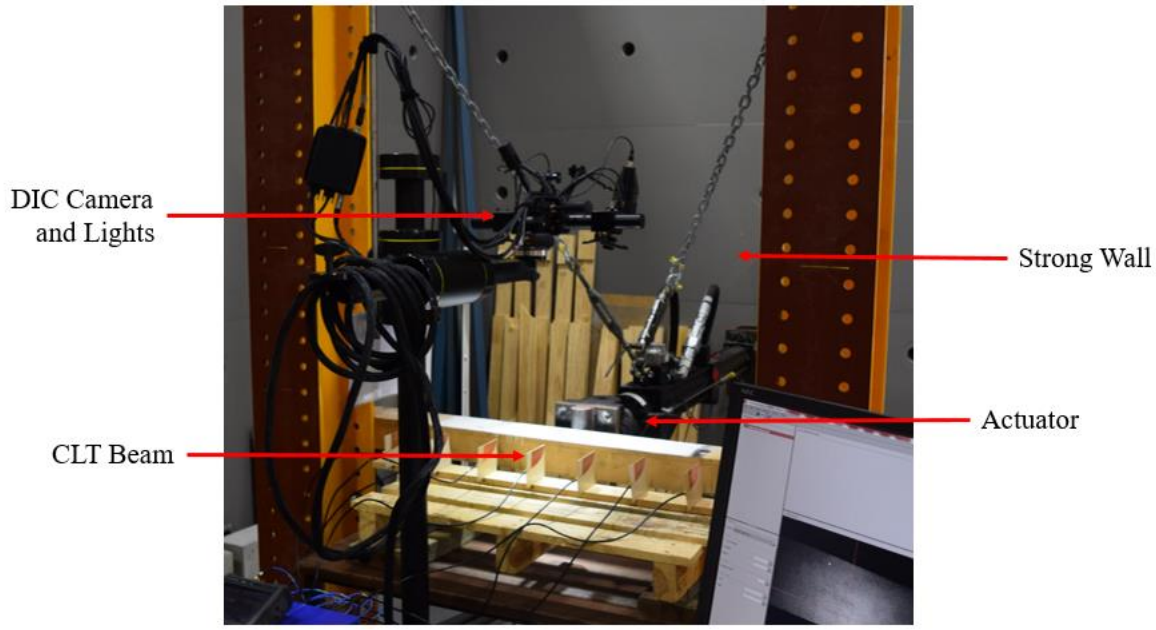

Figure 60: Components of the CLT beam three-point bending test.

In order to focus solely on the adhesive bond strength degradation and the overall effects on the performance of the CLT beam, a non-charring heat flux (6 kW/m^2) was used to heat the beam for 2 hours (Figure 61). Since char would not be formed at the low heat flux, the only strength reduction of the cross-section would be from the strength losses due to the increases in temperature of the timber and the corresponding adhesive layer. While the length between the supports of the structural was 1253mm long, the entire 1500mm of the specimen was heated to ensure the entire bond line would be approximately at the same temperature and to eliminate any colder temperature boundary conditions within the sample which would prevent any failure modes from being observed. The beams were heated away from the actuator and then moved into position and loaded within 1-2 minutes after removal from the heat flux. The testing period was short enough that the sample would have only cooled slightly during the duration of the test.

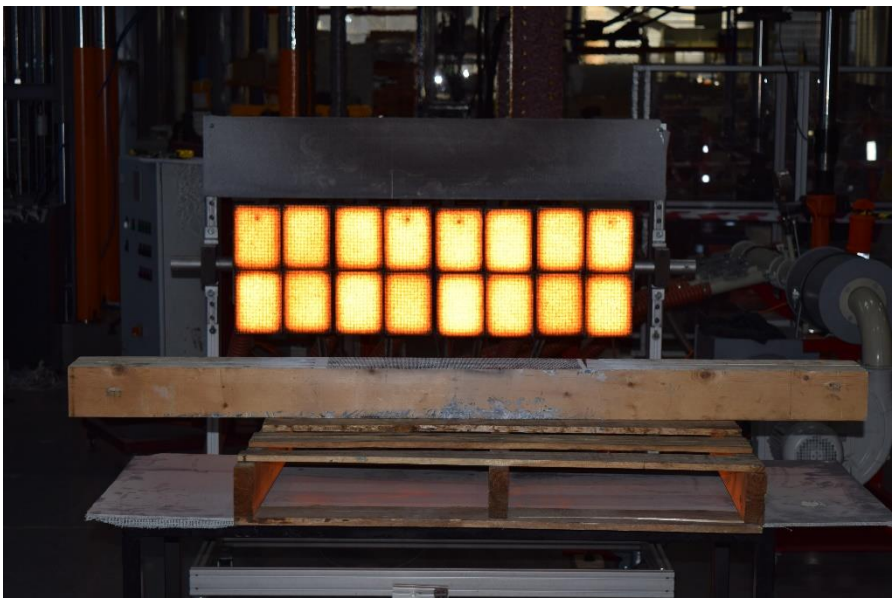

Figure 61: CLT beam heated to 6 kW/m^2 from gas-powered radiant burners.

The sample width was chosen as 100 mm so that any failure in the either the timber or the bond would show on either side of the sample in order to be captured by the instrumentation. Force and displacement data was captured by the actuator (150 kN MTS), DIC cameras were used to capture images in order to document failure mode propagation and for strains and deformation analysis post-test.

4.5.2 Results

A comparison between the three ambient and the three elevated temperature tests showed no discernable difference between the tests. Figure 62 shows the load versus displacement curves of each of the tests. Each test showed that the samples distributed the load after the failure as each test reached a peak load before failure and then maintained a reduced yet relatively high load while continuing to displace. The peak loads before the initial failure occurred between 20 and 35 kN with the lowest being at ambient temperature. Part of the reasoning behind the inhomogeneity in the results was determined from an analysis of the failure modes of the CLT beams as follows.

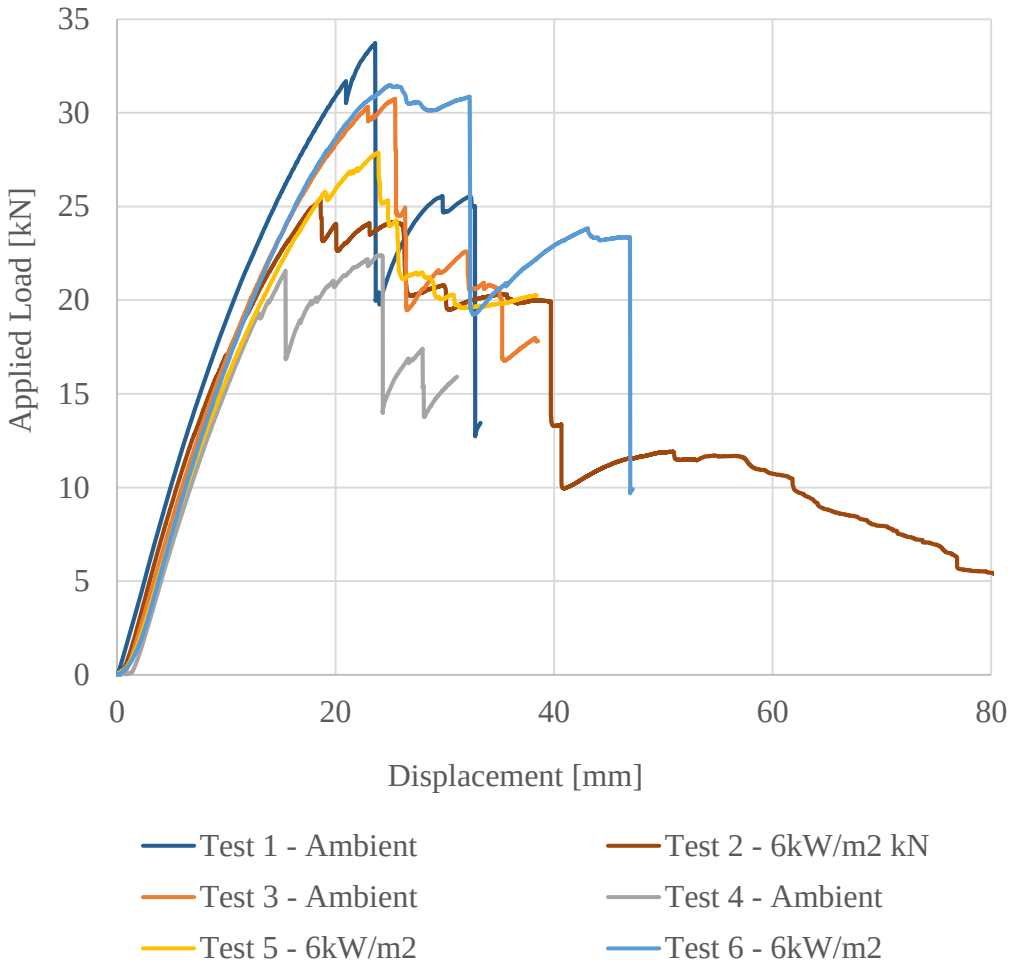

Figure 62: Load vs. displacement curves for both ambient and elevated temperature tests.

4.5.2.1 Failure modes

The most common failure mode between the tests was rolling shear which occurred in the second and fourth lamella as shown in Figure 63. Since the rolling shear modulus is orders of magnitude lower in the second and fourth plies (load applied perpendicular to the grain) as opposed to the first, third, and fifth plies (load applied parallel to the grain), rolling shear failure occurred in the second and fourth plies. The rolling shear failure was the first failure to occur in every test. This highlights the overall strength reliance on the ability of the CLT to resist rolling shear. The occurrence of rolling shear served to homogenize the results (bending and elevated temperature effects were negated).

The other failure mode which was present in every test was debonding of the adhesive bond. Figure 63 also shows the debonding. Debonding should not have occurred at ambient temperatures but an explanation to this could be that the rolling shear which occurred as a result of the narrow width of the CLT beam (100mm) created local discontinuities which created a local bond length less than the

local effective bond length and could not support the loads that were being applied. Insufficient length could allow the failure to propagate through the weakened bond.

Figure 63: Rolling shear and debonding in the second and fourth plies of a CLT beam in Test 3 at ambient temperature

4.5.2.2 Debonding Failure Mode Mechanism and Propagation

While the tests ultimately were not conclusive in determining the difference between elevated and ambient temperature CLT beams, the importance of understanding all the stress in adhesive bonds is clearly demonstrated.

As described in Section 2.4, a bonded joint relies solely on the adhesive to maintain composite action between two plies. As a result, interfacial shear and normal stresses develop in CLT adhesive layers when subjected to flexural bending. These interfacial stresses reach their maximum values at areas of discontinuity such as gaps in the adhesive, gaps between two materials, and cracks forming in the adjacent materials. If the adhesive losses enough strength such that the material around the bond becomes stronger than the adhesive itself, then the failure, if it occurs, will propagate through the bond line. The failure will always find the weakest path and in the case of an adhesive bond could potentially be the entire joint. While the interfacial shear forces are relatively high throughout the entire joint, interfacial normal forces are highest around the discontinuities and almost zero throughout. This drastic increase in forces makes the end conditions of the bond length extremely important. Once a crack starts to propagate with the normal forces peeling the bond apart, the bond length becomes shorter and thus becomes even less able to withstand the applied forces.

The rolling shear failure which occurred first created local areas of discontinuity which can be seen in Figure 63. From these failure points, the debonding failure propagated down the bond line to the supports as the adhesive bond was the weakest portion of the member.

Figure 64 shows the initiation and propagation of debonding through the adhesive bond in the CLT test. A weak point in the timber developed a crack which increased the normal forces around the bond. The failure then followed the weakest portion of the bond which was the adhesive bond itself. The failure continued to grow in length until complete failure of the joint.

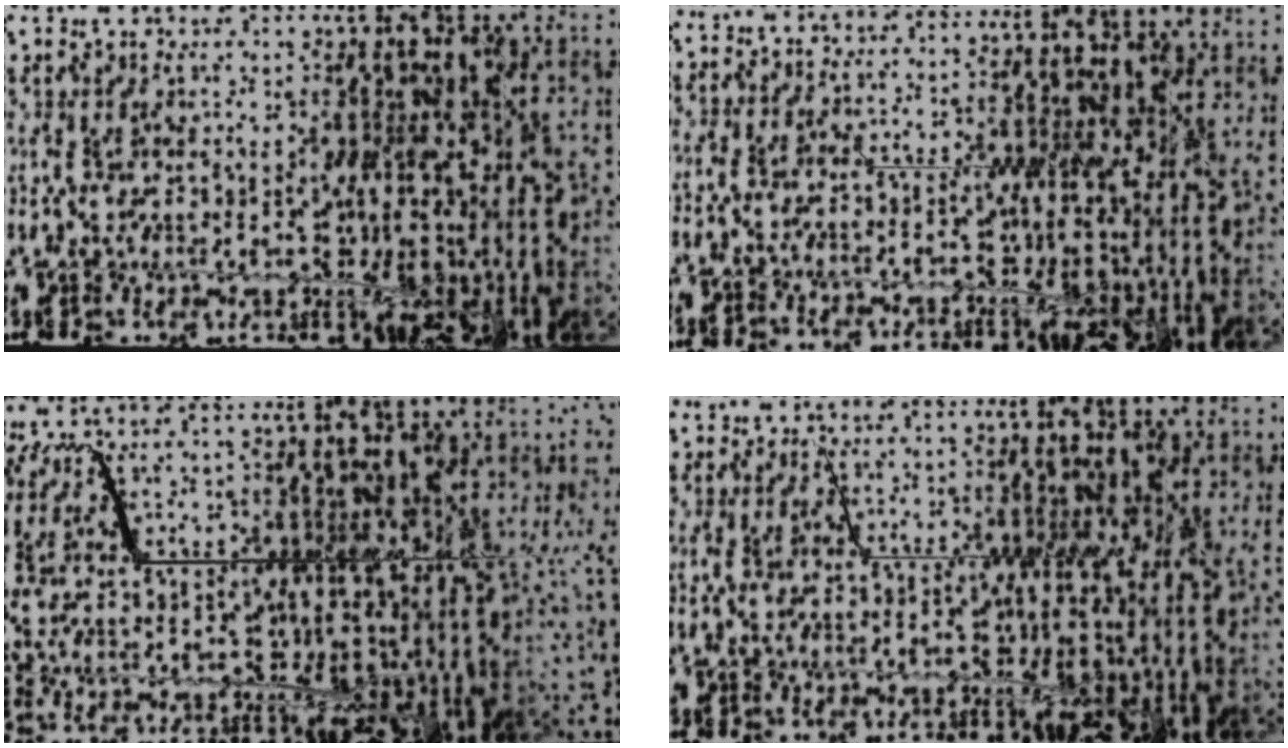

Figure 64: Debonding propagation through the adhesive bond (clockwise from top left)

4.6 Summary and Conclusions

The thermal profiles for a range of heat fluxes were measured in order to quantify the thermal penetration for CLT under known thermal boundary conditions. The CLT used was identical to the CLT used for the self-extinction tests and for the subsequent CLT beam tests. The thermal profiles for heat fluxes for which combustion occurred were similar. The only difference was the rate at which the energy proceeded through the sample due to charring.

Single-lap shear tests were performed (while using the range of temperatures the adhesive bond lines would experience during relevant fire conditions) in order to measure the interfacial strains and to observe any changing failure modes. At 80°C, debonding with a long plateau in the load displacement

graph occurred. The long plateau is an indication that the bond length (300 mm – half of total bonded length) was larger than the effective bond length of the timber joint. At 150°C, debonding occurred without the plateau. This means that the effective bond length of the timber joint at 150°C is longer than 300 mm. At 110°C, the joint failed without a plateau but in the timber not in the bond. The reasoning for this is the presence of a weaker area of timber.

Axial strains were calculated from the DIC measurements. Higher strain values were calculated at higher temperatures and higher loading levels. A comparison between the axial and peeling strains was conducted and the strains due to peeling were found to be an order of magnitude greater than the axial strains. This highlights the importance of understanding not only mode II (in-plane shear) but also mode I (opening) fracture mechanics for adhesive bonds. With the mode I fracture energy being significantly lower than mode II, the importance is only further emphasized. The interfacial fracture energy should be a combination of both strength and strain capacity.

To try and identify the changing failure modes in CLT, three-point bending tests were performed at both ambient and thermal loading conditions. Debonding failure was seen in each of the tests due to the onset of rolling shear. The myriad of cracks in the second and fourth plies along with the inherent local areas of discontinuity in the CLT adhesive bond increased the peeling forces in the adhesive layer. Crack propagation at areas of local discontinuity was clearly visible.

Chapter 5: Summary and Conclusions

The design of buildings and the applicability of existing fire resistance requirements are fundamentally linked to withstanding the thermal load until complete burnout of the fire. Designing for timber construction is not different. In order for timber, a combustible material where ignition is unavoidable, to be used in construction as an exposed feature or as exposed structural members, self-extinction of timber must occur after burnout of the compartment furnishings. If self-extinction does not occur, a time to burn-out does not exist and eventual structural failure is inevitable and therefore the concept of fire resistance becomes irrelevant. This thesis has studied the phenomena controlling self-extinction of flaming combustion, whether it can be achieved, and the key criteria that are relevant for structural behavior.

Two regimes exist for burning timber: steady-state and transient. Steady-state burning is governed by a constant mass loss rate while the transient is characterized by a relatively high initial peak in mass loss. Self-extinction of flaming combustion was found to occur during both regimes when the external heat flux is completely removed as well as when the heat flux was reduced to level where the mass loss rate fell below a critical value. Consequently, the tests demonstrated that (on removal or reduction of heat flux) self-extinction of CLT (European spruce) will occur irrespective of the previous duration of burning. Higher heat fluxes reach a constant steady-state value in mass loss rate. When the heat flux was reduced, self-extinction occurred when the mass loss rate dropped below 3.93 ± 0.45 g/m^{2}s. The critical mass loss rate corresponded to an external heat flux of 43.6 ± 4.7 kW/m^2 (Figure 65).

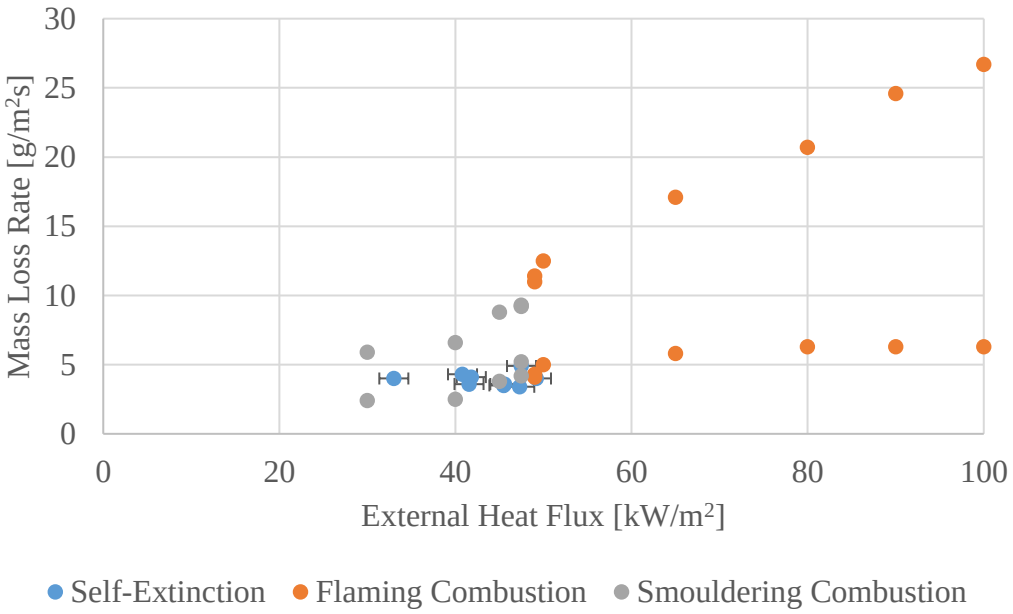

Figure 65: Mass loss rate and external heat flux at self-extinction

Self-extinction occurred at these values only if the CLT remained intact. If debonding or other gaps formed in the bond line, re-ignition of the timber occurred. Whenever the mass loss rate fell below the critical mass loss rate for extinction, flaming combustion self-extinguished. When re-ignition occurred, the mass loss rate rose above the critical mass loss rate. Several variations of behavior were found that induced re-ignition. For example, small flames could occur in pockets where combustible gases could collect until the lower flammability limit was reached. In some cases, larger flames occurred when significant portions of the char and CLT debonded. Self-extinction was concluded to be reliant on the CLT remaining intact.

Another fundamental requirement for the design of timber buildings is ensuring the structural members behave as expected in both ambient and elevated temperature conditions. The adhesive layer is the critical component to ensuring composite action in an engineered timber product occurs consistently. Under fire conditions, elevated temperatures progress ahead of the charring front. Consequently, the adhesive will reduce in strength prior to the onset of charring as increases in temperature reduce the elastic modulus of the adhesive. The thermal profile of unburned timber was found to reach a steady-state shape and remains constant above 50 kW/m^2. However, the thermal profile and penetration depth are not sole indicators of whether debonding will occur. Debonding is a combination of the temperature of the adhesive, the strength reduction of the timber relative to the strength reduction in the adhesive and the forces applied to the bond.

The effective bond length, which is an indicator that the entire strength of the bond is utilized, was assessed from ambient to 150°C. The effective bond length was less than 300mm for both ambient and 80°C. However, at 150°C, the effective bond length increased to above 300mm.

Two failure modes were analyzed: mode I (opening) and mode II (in-plane shear). Strains due to mode I were orders of magnitude greater than mode II. This, coupled with the fact that the fracture energy is significantly less for mode I, highlights the importance of understanding both types of forces along with changes in the strain capacity.

Normal strains are known to be highest around areas of local discontinuity and are the drivers of debonding. Crack propagation by normal forces unzipping the bond were visible in CLT beam tests at both ambient and elevated temperatures. The relatively thin width of the beam allowed rolling shear to govern the failure mode. The secondary failure mode after the rolling shear fractures occurred was debonding of the adhesive layer due to insufficient bond length to withstand the forces. Normal forces

and their behavior at elevated temperatures has to be understood for correct design of CLT and bonded timber joints in both ambient and elevated temperature conditions.

5.2 Design Implications

The conclusions from this study have several implications for design of timber buildings.

The first implication is that there is a threshold value of applied heat flux and mass loss rate below which self-extinction will occur. A worst-case scenario charring condition exists for defining this self-extinction. Mass loss rates reach a constant value with increasing heat flux suggesting a limit. Since the mass loss rate reaches a steady-state value during the burning process, then no matter the length of time, self-extinction will occur if the heat flux and mass loss rate are reduced below their critical levels. Beyond this limit, longer burning durations have no effect on the self-extinction characteristics of timber.

The second implication is the thermal profiles in the virgin timber are constant for design. Above 50 kW/m^2, the thermal profile is the same. The only difference between heat fluxes is the rate (charring) at which the thermal profile progress through the cross-section. This allows the designer to predict the temperature and the duration the bond line will be at a certain temperature as the pyrolysis front moves through the timber. This knowledge along with a thorough understanding of bond joint behavior can be used in design.

The third implication is the necessity to revisit standard methods to account for normal forces in design of engineered timber. The increased magnitude of the stresses in mode I as opposed to mode II along with the significant reduction in the mode I fracture energy clearly demonstrates the need. Current standards for both ambient and fire design only account for timber failure. With temperature increases reducing the adhesive properties, normal forces play an integral role in the mechanics of the joint as the failure mode shifts from timber to debonding. During debonding, the normal forces peel apart the joint beginning at local areas of discontinuity and propagating through the bond.

The final implication is the extreme importance of detailing and careful design of exposed timber. Debonding failure of CLT or any gaps in the timber product (i.e. separation between two boards allowing edge burning) allows continued burning or re-ignition of flaming combustion after the protective char and ply fall off. Since design for burnout is implicit in the fire resistance of a building, self-extinction of timber has to occur.

5.3 Future Work

This study is only the beginning in understanding the extremely complex physics and chemistry behind the combustion processes and force interactions of engineered timber. A prioritized list of future work is detailed outlining a path toward increased knowledge and higher confidence in designing safe timber buildings.

The primary goal of research on self-extinction is to design buildings with exposed timber which ceases flaming combustion after burnout of the compartment furnishings. The following bullet points outline significant areas of research:

- Self-extinction tests on different species of timber should be conducted. The values attained in this study are valid for European spruce at a specific density. The values for denser or less dense timber species could yield different results.
- The composition of the combustion gases should be measured in order to attain a limit for ignition. The study on re-ignition of the timber after delamination tends to indicate the lower flammable limit governing re-ignition while the mass loss rate governs extinction. Measurements of the gases at the surface of the timber should be captured.
- Larger specimen sizes should be tests to determine if scaling of the results is appropriate. The tests conducted are small scale samples. As the timber areas in practice are much larger, a study on the scaling effects of the data should be undertaken.
- The external incident heat fluxes applied to the timber walls in a compartment fire should be quantified and compared with the self-extinction limit. Understanding of when heat fluxes fall below the critical value for self-extinction will allow an understanding of the time constraints of timber reduction in a fire.
- Finally, full compartment tests should be conducted to study the orientation effects and distance effects of the various geometries of a room on self-extinction.

Debonding is a much wider field and in need of further research to correctly model and understand the effects of both shear and normal interfacial stresses on the overall behavior of CLT and other engineered timber. The list outlined below is by no means exhaustive and only provides several major aspects identified in this study as necessary for further research.

- Further testing of timber bond joints at both constant temperature and constant load should be conducted. The variability in the timber makes comparison of a few samples very difficult. Increasing the sample size may eliminate the scatter and reveal the true behavior of the joints.

- A thorough study on the bond length and the effective bond length for engineered timber members should be completed. Along the same lines, these effective bond length studies should incorporate temperature effects as this study has shown that increasing the temperature increases the effective bond length necessary for utilization of the bond.
- The importance of normal forces a model for timber design which included them should be formulated. The magnitude of the strains and the relative inability of the adhesive to withstand normal forces yield debonding consequences as noted in the larger CLT beam tests.
- A study should be completed to determine how best to compare results and behavior from the single-lap shear small scale tests and the larger CLT test.
- The size of the CLT beam and test samples should be increased to determine if the effects of rolling shear can be eliminated and if eliminated does debonding become the primary failure mode.
- Non-destructive crack detection methods should be researched. As the size the CLT beams increase, failure could easily occur and go unnoticed in the test. At the same time, the methods could be enhanced to measure charring as well as post-fire integrity analysis of CLT and engineered timber members.
- Constant loading CLT tests should be performed on heat flux exposed beams. The constant applied load of a percentage of the ultimate load would allow for realistic loading conditions and heating regimes.
- A combination of both loading and charring of CLT beams should be conducted to gain an understanding of the time scales involved in both processes. While the overall CLT member behavior will be a complex interaction between the two, the relative time scales and the percentage of the reduction in timber capacity could add in better design models.

References

[1] Abrahamsen, R.B. and K.A. Malo, *Structural Design and Assembly of "Treet" - A 14-Storey Timber Residential Building in Norway*, in *World Conference on Timber Engineering*. 2014: Quebec City, Canada.

[2] Timmer, S.G.C., *Feasbility of Tall Timber Buildings*, in *Civil Engineering and Geosciences-Structural Engineering*. 2011, Delft University of Technology: Delft University of Technology. p. 269.

[3] Green, M., *The Case for Tall Wood Buildings*. 2012, mgb Architecture + Design: Vancouver, Canada.

[4] Skidmore Owings & Merrill LLP, *Timber Tower Research Project*. 2013: Chicago, Illinois, USA.

[5] PLP Architecture. *PLP, Cambridge University and Smith and Walwork present timber skyscraper research to London's Mayor Boris Johnson*. 2016 [cited 2016 April 29].

[6] Wells, M., *Stadthaus, London: Raising the Bar for Timber Buildings.* Proceedings of the Institution of Civil Engineers-Civil Engineering 2011. **164**: p. 122-128.

[7] Wheeldon, D., *Knock on wood: Australian developers bet on building tall in timber.* BPN, 2012.

[8] American Society for Testing and Materials, *ASTM E119: Standard Test Methods for Fire Tests of Building Construction and Materials*. 2000, ASTM International: USA.

[9] International Organization for Standardization, *ISO 834-1: Fire-resistance tests-Elements of building construction-Part 1: General requirements*. 1999, International Organization for Standardization: Genève, Switzerland.

[10] National Fire Protection Association, *Building Construction and Safety Code NFPA 5000*. 2015, National Fire Protection Association,: Quincy, Massachusetts.

[11] Ingberg, S.H., *Tests of the Severity of Building Fires*, in *Thirty-second Annual Meeting of the National Fire Protection Association*. 1928, National Fire Protection Association: Atlantic City.

[12] Welch, S., et al., *BRE large compartment fire tests–Characterising post-flashover fires for model validation.* Fire Safety Journal, 2007. **42**: p. 548-567.

[13] Abecassis-Empis, C., et al., *Test One: The 'Uncontrolled' Fire*, in *The Dalmarnock Fire Tests: Experiments and Modelling*. 2007, School of Engineering and Electronics, University of Edinburgh: Edinburgh.

[14] McGregor, C.J., *Contribution of Cross Laminated Timber Panels to Room Fires*, in *Civil and Environmental Engineering*. 2013, Carleton University.

[15] Buchanan, A.H., B. Östman, and A. Frangi, *Fire Resistance of Timber Structures* 2014, National Institute of Standards and Technology: Gaithersburg.

[16] Barber, D., *Tall Timber Buildings: What's Next in Fire Safety ?* Fire Technology, 2015. **51**(6): p. 1279-1284.

[17] Gagnon, S., et al., *CLT: Introduction to cross-laminated timber*, in *CLT Handbook*, S. Gagnon and C. Pirvu, Editors. 2013, FPInnovations: Pointe-Claire (QC).

[18] Yates, M., M. Linegar, and B. Dujic, *Design of an 8 storey Residential Tower from KHL Cross Laminated Solid Timber Panels*, in *Techniker*. 2008: London.
[19] Gagnon, S. and M. Popovski, *Structural design of cross-laminated timber elements*, in *CLT Handbook: Canadian Edition*, FPInnovations, Editor. 2013, FPInnovations: Québec, QC.
[20] Ross, L.A., S. Gagnon, and E. Keith, *Structural design of cross-laminated timber elements*, in *CLT Handbook: US Edition*, E. Karacabeyli and B. Douglas, Editors. 2013, FPInnovations: Pointe-Claire, QC.
[21] European Committee for Standardization, *EN 1995-1-1: 2004, Eurocode 5: Design of Timber--Part 1-1: General--Common Rules and Rules for Buildings*. 2004, European Committee for Standardization: Belgium.
[22] Blass, J. and P. Fellmoser, *Design of solid wood panels with cross layers*, in *8th World Conference on Timber Engineering*. 2004: Lahti, Finland. p. 543-548.
[23] CEN, *EN 1995-1-2:2004 Eurocode 5: Design of Timber Structures-General-Structural fire design.* 2004.
[24] Frangi, A., et al. *Fire Behaviour of Cross-Laminated Solid Timber Panels*. in *9th International IAFSS Symposium*. 2006. Karlsruhe, Germany: International Association for Fire Safety Science.
[25] Dagenals, C., R.H. White, and K. Sumathipala, *Fire: Fire performance of cross-lamianted timber assemblies*, in *CLT Handbook*, FPInnovations, Editor. 2013, FPInnovations: Pointe-Claire (QC).
[26] Inghelbrecht, A., *Evaluation of the burning behaviour of wood products in the context of structural fire design*, in *Civil Engineering*. 2014, Ghent University and The University of Queensland.
[27] Aguanno, M., *Fire Resistance Tests on Cross-Laminated Timber Floor Panels: An Experimental and Numerical Analysis*, in *Civil and Environmental Engineering*. 2013, Carleton University: Ottawa-Carleton Institute of Civil and Environmental Engineering.
[28] SP Technical Research Institute of Sweden, *Fire safety in timber buildings: Technical guideline for Europe*. 2010: Stockholm, Sweden.
[29] Schaffer, E.L., *An Approach to the Mathematical Prediction of Temperature Rise Within a Semi-Infinite Wood Slab Subjected to High-Temperature Conditions.* Pyrodynamics, 1965. **2**: p. 117-132.
[30] Schaffer, E.L., *Structural Fire Design: Wood. Res. Pap. FPL 450*. 1984, U.S. Department of Agriculture, Forest Service, Forest Products Laboratory: Madison, WI.
[31] Schaffer, E.L., *State of Structural Timber Fire Endurance.* Wood and Fiber, 1977. **9**(2): p. 145-170.
[32] Schaffer, E.L., et al., *Strength Validation and Fire Endurance of Glued-Laminated Timber Beams*, in *Reseach Paper FPL 467*. 1986, U.S. Department of Agriculture, Forest Service, Forest Products Laboratory: Madison, WI.
[33] Schmid, J., J. König, and J. Köhler, *Fire-Exposed Cross-Laminated Timber–Modeling and Tests*, in *World Conference on Timber Engineering*. 2010: Riva del Garda, Italy.
[34] Smith, S.T. and J.G. Teng, *Interfacial stress in plated beams.* Engineering Structures, 2001. **23**: p. 857-871.

[35] Frangi, A., M. Fontana, and A. Mischler, *Shear behaviour of bond lines in glued laminated timber beams at high temperatures.* Wood Science and Technology, 2004. **38**(2): p. 119-126.
[36] Clauß, S., M. Joscak, and P. Niemz, *Thermal stability of glued wood joints measured by shear tests.* European Journal of Wood and Wood Products, 2011. **69**(1): p. 101-111.
[37] Craft, S., R. Desjardins, and J. Mehaffey, *Investigation of the Behaviour of CLT Panels Exposed to Fire*, in *12th International Conference and Exhibition-Fire and Materials*. 2012: San Francisco, USA
[38] Osborne, L., C. Dagenals, and N. Bénichou, *Preliminary CLT Fire Resistance Testing Report*. 2012, FPInnovations and Natural Resources Canada: Canada.
[39] Moraes, P.D., et al., *Influence of temperature on the embedding strength.* Holz als Roh- und Werkstoff, 2005. **63**(4): p. 297-302.
[40] Fernando, D., T. Yu, and J.G. Teng, *Behavior of CFRP Laminates Bonded to a Steel Substrate Using a Ductile Adhesive.* Journal of Composites for Construction, 2014. **18**(2): p. 04013040.
[41] Petrella, R.V., *The Mass Burning Rate and Mass Transfer Number of Selected Polymers, Wood, and Organic Liquids.* Polymer-Plastic Technology and Engineering, 1979. **13**(1): p. 83-103.
[42] Tewarson, A. and R.F. Pion, *Flammability of Plastics–I. Burning Intensity.* Combustion and Flame, 1976. **26**: p. 85-103.
[43] Babrauskas, V., *Ignition of Wood: A Review of the State of the Art.* Journal of Fire Protection Engineering, 2002. **12**: p. 163-189.
[44] Spearpoint, M.J. and J.G. Quintiere, *Predicting the Burning of Wood Using an Integral Model.* Combustion and Flame, 2000. **123**(3): p. 308-324.
[45] Mikkola, E. *Charring of Wood Based Materials*. in *3rd IAFSS Symposium*. 1991. Edinburgh, United Kingdom: International Association for Fire Safety Science.
[46] Drysdale, D., *An Introduction to Fire Dynamics*. 3rd ed. 2011, West Sussex, England: John Wiley & Sons, Ltd.
[47] Torero, J., *Flaming Ignition of Solids*, in *SFPE Handbook of Fire Protection Engineering*, M.J. Hurley, Editor. 2015, Society of Fire Protection Engineers: New York. p. 633-661.
[48] Reszka, P., *In-Depth Temperature Profiles in Pyrolyzing Wood*. 2008, The University of Edinburgh: The University of Edinburgh. p. 193.
[49] KLH Massivholz GmbH, *Cross-Laminated Timber* K.M. GmbH, Editor. 2013, KLH Massivholz GmbH.
[50] Delichatsios, M.A. and M.M. Delichatsios. *Critical Mass Pyrolysis Rates for Extinction of Fires over Solid Materials*. in *Fire Safety Science 5th International Symposium*. 1997. Melbourne, Australia: International Association for Fire Safety Science.
[51] Rasbash, D.J., D.D. Drysdale, and D. Deepak, *Critical heat and mass transfer at pilot ignition and extinction of a material.* Fire Safety Journal, 1986. **10**(1): p. 1-10.
[52] Delichatsios, M.A., *Piloted ignition times, critical heat fluxes and mass loss rates at reduced oxygen atmospheres.* Fire Safety Journal, 2005. **40**(3): p. 197-212.

[53] Menis, A., *Fire resistance of Laminated Veneer Lumber (LVL) and Cross-Laminated Timber (XLAM) elements*, in *Graduate School of Civil Engineering and Architecture*. 2012, Università Degli Studi Di Cagliari: Cagliari, Italy.

[54] Frangi, A., et al., *Experimental analysis of cross-laminated timber panels in fire.* Fire Safety Journal, 2009. **44**(8): p. 1078-1087.

[55] De Lorenzis, L., D. Fernando, and J.-G. Teng, *Coupled mixed-mode cohesive zone modeling of interfacial debonding in simply supported plated beams.* International Journal of Solids and Structures, 2013. **50**(14–15): p. 2477-2494.

[56] Fernando, D., *Bond Behaviour and Debonding Failures in CFRP-Strengthened Steel Members*, in *Department of Civil and Structural Engineering*. 2010, The Hong Kong Polytechnic University: Hong Kong. p. 374.